UNIVERSITÀ POLITECNICA DELLE MARCHE

Fabrication Induced Residual Strains in Thin Composite Laminates

Ilaria Poggetti

Supervisor: Dr. Jack Dyson
Prof.Valeria Corinaldesi

Corso di Dottorato in Ingegneria Industriale:
Curriculum in Ingegneria dei Materiali

This dissertation is submitted for the degree of
Doctor of Philosophy

February 2018

For me, for having the courage to dare ...

Acknowledgements

Every scientific enterprise is a complex journey through the thoughts and ambitions of the individual. No journey is complete without companions and teachers.

Looking back, I would like to recognize the incomplete student who started this walk three years ago from the perspective of a much more complete individual today. Of the many experiences and teachers that make an individual a success, there are several without whom it could never have been possible.

I would like to remember with especial regard Pierpaolo Bellacima who has supported me tirelessly for these three long years. Not a morning or night has passed during this time where he has not had to suddenly awaken and come to fix this or that at a moments beckoning. Operating silently and unknown in the backwaters, often picking up the pieces with me when things wouldn't work - I thank him sincerely for making this this possible for me.

To do a PhD, you need a home and I might add, a place to think in *peace*. There is a man at the Universita Politecnica delle Marche called Professor Gianni Albertini who gave me just that - a place to breathe and develop at my own pace. He encouraged me with kindness when I needed it and remained actively engaged in the background, solving the many administrative difficulties I have unfortunately encountered. Like Pierpaolo, without his kindenss and care, this would have been a bridge too far for me.

Life is full of reflections, and one such reflection is my year long stay at the University of Manchester in England where I was fortunate enough to have my first professional foreign experience. Much like Gianni, Professor Costantinos Soutis gave me a place where I could do more than just think, I could bring to life scientific thoughts using very expensive laboratories to see if they were true. Thanks also go to Dr Matthieu Gresil for advising on optical fibers and Neha Chandarana for assisting with the fabrication process and other laboratory work.

Climbing a mountain can be an easy task ... with the right equipment of course. There are two things I know about mountain climbing: not knowing an essential thing today can be fatal tomorrow. Climbing upto the the heights of a PhD degree is a similar experience and a good teacher and guide is therefore essential. Dr Jack Dyson of the Universita Politecnica delle Marche is an expert at showing me how to climb tall mountains. If I am here today, so is he, and that is all that needs to be said.

Abstract

The broad scope of this research is aimed at understanding experimentally and theoretically the factors that affect the formation of residual strains that are found to occur during the curing of carbon fiber composite plates of advanced layup geometry. We discuss results obtained during the manufacture of a standard test plate made of 5 harness satin woven carbon fiber sheets bonded with epoxy resin.

The phenomenon of residual strains that develop during the production of carbon fiber composites is one of the most significant problems in the industry. The necessity of high quality, large volume production lines for advanced applications demands that manufacturing processes be subject to norms of ever increasing precision and monitoring in an attempt to improve material performance and suitability.

The present study combines and extends the state of the art to include the effects of cure kinetics, internal force distributions and mold constraints present during the manufacturing process of polymer resin carbon fiber fabric sheets.

The chosen objective of this work is the investigation of residual strains in woven fabrics taking into account the modified kinetics of cure, the revised balance of internal forces, the viscoelastic behavior and the cure temperature profile specifically adapted to the practical case of a woven fabric composite like the 5 harness satin weave sheet.

Since many factors affect residual strain formation, the methodology of choice is a semi-analytical numerical simulation that extends the work of Hyer and Hahn, principally by modifying the matrices of the classical theory and integrating them with ideas from theoretical work already carried out on weave fabrics.

Using this approach, we show that the thermodynamics of woven composite fabrics can be characterized in closed form based on the mechanics and chemical kinetics of the manufacturing processes. Taking into consideration the morphology of the basic (weave) constituents these models permit accurate prediction of the composite properties expected from the global material structure.

The correspondence between the predicted and experimental values of strain shows an accurate physical understanding of the origins of the measured data for the entire thermal curing cycle used in the experiment.

Table of contents

List of figures

List of tables

Chapter 1

Introduction

1.1 Objectives and Scopes of the dissertation

Polymer composite products are increasingly applied in demanding structures in the aerospace and the aeronautical industry.

The quality and the performance of a composite part are determined by the manufacturing cycle that is accompanied mainly by the exothermal polymerization reaction of the thermoset resin. Due to the continuous variation of the resin mechanical and rheological properties, it is extremely important to ensure a uniform evolution of the cure reaction that, coupled with the heat transport conditions, can lead to exothermal peaks, thermal and chemical conversion gradients determining residual strain and gradients of the matrix mechanical properties.

Residual strain can distort the dimensions or shape of the processed part, necessitating expensive compensation through the use of shims when it is assembled into a structure. The advancement of the cure reaction implies the consolidation of the polymer resin which changes its physical state passing from a low molecular weight liquid to a rubbery solid and, then at length transforming into a glassy at the end of the processing cycle through chemical reactions of the active groups present in the system which develop progressively a denser polymeric network until reaching the so-called gel point and forming an insoluble material. Therefore, due to the continuous variation of the resin mechanical and rheological properties, it is extremely important to ensure a uniform evolution of the cure reaction that, coupled with the heat transport conditions, can lead to exothermic peaks, thermal and chemical conversion gradients determining residual strain and gradients of the matrix mechanical properties. Residual stresses and strains can distort the dimensions or shape of the processed part, necessitating expensive compensation through the use of shims when it is assembled into a structure. Liquid Composite Molding (LCM) processes are therefore the focus of this thesis, where liquid resin is injected through a textile preform. Using a distributed embedded

optical fiber sensor it has been possible to extract real time monitoring of the curing process and as a direct result the gellification of a thermo-set matrix. The aim of this work is to understand how residual strains build up during such processing. Furthermore, different modeling approaches, constitutive models and experimental techniques are investigated with the objective of understanding the various mechanisms taking place during the process and what light simple mathematical models can shed on them. A number of studies have been conducted to optimize the process cycle to objectively minimize the linear strains inside the composite materials, but it will shown that the formation of stresses and strains during manufacturing are dependent upon the quasi-liquid like composition of the composite structure before gellification and beyond that, upon solidification of the resin, the type of cooling profile that is applied.

Experimental results show in particular that the commonly held view that a variational analysis of the cooling problem for composite manufacturing can provide an optimal path over which strains are minimal during and after the cooling phase is unrealistic. Mathematically this is no surprise, since the solution to the integro-differential equations involved is possible under certain circumstances and these seem to be unphysical at best.

The experiments conducted over two different cooling schemes, one slow and the other fast, do however show that the sign of the curvature in the final cooled down plate is inverted. If the cooling problem is mathematically stable in the sense that it is a continuous function of the cool down temperature process, then the experimental results we have could be significant. That is because these results show that there must be a *real* cool-down curve as yet not specified that permits the manufacture of a plate with *zero* plate curvature but nonetheless a *constant* strain present in the composite plate at the end of manufacture. This immediately implies the existence of a suitable theoretical framework that can practically lead to optimal cooling solutions for plate curvature problems. That, be that as it may, is a future objective for both ourselves and perhaps other researchers in the field.

For about thirty years the precise effect of the liquid state resin upon optical fiber or other methods of measurement has been subject to speculation for example, and in this study we attempt to provide a simple model and experimental evidence to come the conclusion that in fabrication processes for composite materials it is highly likely that the optical fiber always measure the true strain.

The present study contributes to a better understanding of the physics of resin rheology by proposing a simple physical theory that could lead to improved composites design. A better model of resin rheology leads one directly to a precise understanding of the gellation process during the second dwell of the curing cycle and the glass transition temperature.

Subsequently this may have a significant impact upon the way the cooling cycle operates on the stresses in the relaxed structure.

Furthermore, and perhaps more significantly, we observe and explain that the presence of carbon fiber structures within a resin matrix strongly modify the rheology and hence the residual strain behavior In particular we precisely identify how this new rheology operates in terms of a physical mechanical mechanism. The originality of the substrate strain model proposed lies in the fluid-chemical action of the curing resin when it is considered as a distributed adhesive. This simple fact leads directly to a thermodynamic non extensive modification of the strain response of the composite material which is encapsulated in the pseudo-liquid state equation for connecting the solid state and liquid-state composite coefficients of thermal expansion[1].

[1]Now accepted for publication by SAGE in The Journal of Composite Materials

Chapter 2

State of Art

2.1 Composite materials

A composite is a combination of two or more component materials, with different properties and different forms through compounding processes, it not only maintains the main characteristics of the original component, but also shows new character which are not possessed by any of the original components [78]. Composite materials should have the following characteristics:microscopically it is non-homogeneous material and has a distinct interface; there are big differences in the performance of component materials and the formed composite materials should have a great improvement in performance. Composite material is a multi-phase system consisted of matrix material and reinforcing material. Reinforcing material is a dispersed phase, usually fibrous materials [78]. The fibres most frequently used are Glass, Aramid and Carbon and in some very special applications Boron fibres. These are usually in the form of long continuos filaments knows as “UD” or unidirectional tape where the fibres run in one direction only or woven into fabric, wich can be various styles of weave, weight and fibres orientation.

2.2 Matrix

The matrix is the material used to bind all the fibres together, when the resin is cured it will form a solid, and by doing this it will hold the component rigid and distribute the load by transferring it between the fibres.Based on the matrix material, the composites are classified into polymer matrix composites (PMCs), metal matrix composites (MMCs), and ceramic matrix composites (CMCs). The three types of composites differ in the manufacturing method adopted, mechanical behaviors, and functional characteristics. Since the matrix materials

undergo physical or chemical change, the processing method to be used for making the composites has a direct bearing on the matrix system used. The polymeric matrix composite are the most common. The classification of composites based on matrix material is shown in Figure 2.1.

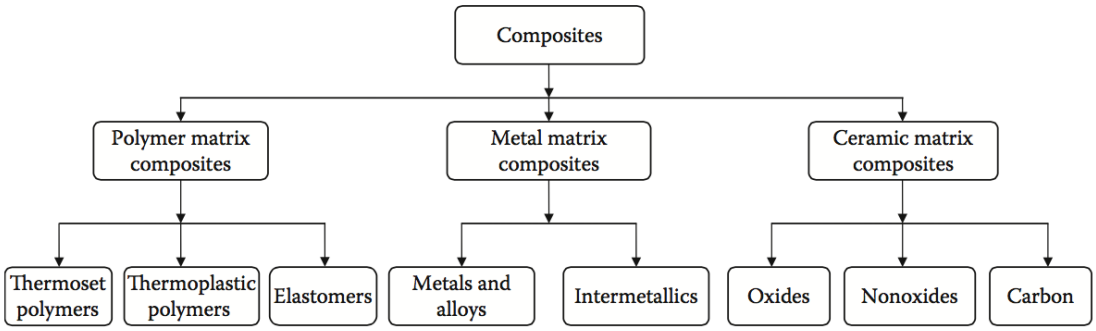

Fig. 2.1 Classification of composites based on matrix materials[6]

2.2.1 Metal matrix composites

Metal matrix composites (MMCs), as the name implies, have a metal matrix. Examples of matrices in such composites include aluminum, magnesium, and titanium. Typical fibers include carbon and silicon carbide. Metals are mainly reinforced to increase or decrease their properties to suit the needs of design. For example, the elastic stiffness and strength of metals can be increased, and large coefficients of thermal expansion and thermal and electric conductivities of metals can be reduced, by the addition of fibers such as silicon carbide.[52] Metals or metallic alloys are used as the matrix material in MMCs. Mainly lightweight metals and alloys such as, aluminum, titanium, and their alloys are used. In some special applications, heavy metals such as copper and cobalt are used. MMCs can be suitable for applications where the service tem perature is up to 1200°C. At present, short fibers or particulates are mainly used as the dispersed phase because of the processing advantage. Metals and alloys are also reinforced with continuous fibers to improve modulus and strength significantly. A major problem for the MMCs is corrosion. Most of the MMCs are still under development and only a few components are made commercially. Recent interest on MMCs has concentrated on transport applications and consequently the light metal-based MMCs, particularly aluminum and its alloy-based MMCs, have received the most attentio.[6]

2.2.2 Ceramic matrix composites

Many oxide and nonoxide ceramic materials are used as matrix materials in CMCs. CMCs are useful for high-temperature applications, where the service temperatures are above 1200°C. These materials are very expensive because most of the CMCs are processed at high temperature. In some cases, there is a need to apply high pressure at that high temperature to get a quality product.[6]

2.2.3 Polymer matrix composite

The matrix material can be a thermoset polymer, a thermoplastic polymer, or an elastomer in the PMCs. Thermoset polymers are very commonly used because of the processing advantage. Currently thermoplastic polymers are gaining importance because of their relatively high toughness values and the possibility of post-processing. To meet the specific property requirements, a wide variety of thermoplastic polymers are available. PMCs are suitable for making products, which are used at ambient temperature. There are some special polymers, which can be used up to 250°C. In any case, PMCs are not suitable for applications where the service temperature is more than 350°C. The success of PMCs, largely as replacement for metals, results from the much improved mechanical properties of the composites compared to the plastic matrix materials. The good mechanical properties of the composites are a consequence of utilizing the high-strength and high-modulus fiber reinforcement.[6] Thermoplastic flow when tey are hetated beyond a particular temperature while themoset remain in the solid state until their temperature becomes so high that degradation of the materilas takes place. The different behavior of thermosets and thermoplastics when heated arises from their chemical structures. Thermoplastic are linear polymers that in the solid state are either semicrystalline or amorphous glasses.When they are hetaed beyond the melting point of crystals or beyond the glass transition temperature polymers chains are free to move and flow takes place. On the other hand, thermosets are crosslinked polymers and they remain in the solid state as long as the covalent chemical bonds are not destroyed.[32] Due to the three dimensional network, the mechanical properties of thermosets are generally superior to those of thermoplastic materials. Moreover, thermosets possess good insulating and adhesive properties, are resistant to most chemicals and have high thermal stability. Therefore, they are commonly used as adhesive, coating or matrix for structural composites for airplanes, boats and electronic devices. Thermoplastic polymers can be melted and reformed, they have much higher strains to failure because they can undergo extensive plastic deformation resulting in singnificantly improved impact resistance.

2.2.3.1 Epoxy Resin

One of the most popular resins in use today are the epoxy resins, having the advantage of good structural strength together with the ability to withstand relatively high temperatures. Epoxy resins belong to the class of thermosetting plastics, a thermoset material cannot be melted and reformed after curing. The curing process transforms the epoxy resin into a plastic by forming a three dimensional network of covalent bonds. Curing is initiated through heat and/or curing agents hardener. The liquid resin are converted into hard brittle solid by chemical cross-linking which leads to the formation of a tightly bound three-dimensional network of polymer chains. The mechanical properties depend on the molecular units making up the network and on the length and density of cross-link. Curing can be achieved at room temperature but it is usual to use a cure schedule which involves heating at one or more temperatures for predetermined times to achieve optimum cross-linking and hence optimum properties. [39]. An epoxy is a polymer that contains an epoxide group, one oxygen atom and two carbon atoms in its chemical structure.The diglycidyl ether of bisphenol-A (DGEBA) is the most commonly used epoxy resin as it has many attractive properties such as fluidity, low shrinkage during cure and ease of processing. The cured products have good physical strength, excellent moisture, solvent and chemical resistance [44] Diglycidyl ether of bisphenol A (DGEBA) contain two epoxide groups. Hardeners are added to the epoxy prepolymers to increase the rate of polymerisation by reacting with the epoxy groups. Curing agents are organic amino or acid compounds and cross-linking is obtained by introducing chemicals that react with the epoxy and hydroxy groups between adjacent chains. The exent of cross-linking is a function of the amount of curing agent added, the curing agent become part of the epoxy structure. [12] Unreacted resins are usually referred to as A-stage resin. A partially reacted resin, usually a vitrified system below gel point is called a B- stage resin, while completely cured resin is called a C-stage resin. The essential condition to advance a thermoset resin to B-stage is vitrification prior to gelation and is achieved by keeping the reaction temperature below the curing temperature, T_c. Ease in processability is achieved by using B-stage resin. [77] An epoxy before it is fully cross-linked is said to be in stage B and in B stage an epoxy has characteristic tackiness. This B-stage resin is used to make a fiber prepreg. The type and extent of curing agent adding will control the total curing time (also called the shelf life or pot life).[12] The resins are for the most part a combination of various chemical elements. When these elements are mixed together they start a reaction that binds the molecules together and causes the resin to become solid. The speed of this reaction is dependent on two principle factors, the first of which is the mix ratio of chemical elements; the more accelerator or catalyst that is added the faster the cure will take place. It is the ratio of these elements that set the underlying “Out Life” and “Shelf life” for the prepregs. By

varing this ratio the shelf life of prepregs can be modified from six month to a year and an out of life from just a few days to six months. The second factor that controls the cure rate is the temperature. The composite industries is one of the few industries where the component is produced right at the end of the manufacturing process. In most other industries they have the raw materials at the start of manufacturing cycle and then carry out the various machining and finishing operation in order to produce the required component. The advantages that they have in this situation is that they can test the raw materials before starting the manufacturing process. If the component is not up to specification it can be rejected before any more time and effort is expended on it. But composites do not afford this luxury. When we lay our woven fabrics in the mould it is just a mass of resin and fibres that exist in the same space. Not until they are cured do we benefit from the attributes of the fibres and the resin working together with one another. In light of the above, is it clear that the manufacturing and the cure cycle process for a composite component are very delicate phases. In order to ensure that the composite material component is up to specification it is fundamental have a wide understanding of resin system and the reinforced material as well as their interaction during the manufacturing and curing process for limit and minimize the waste of components and consequently the waste of money. If the cure of the component takes place at a temperature too low the resin will not attain its full mechanical properties and the surface finish. If on the other hand the cure of the component takes place at a temperature too high the resin matrix could be degrade and it will adversely affect the strength of the component. The selection of cure cycle is essential for achieved a good quality component in term of mechanical properties and surface finish. Sometimes the composite component appears apparently very good externally but inside have a residual stresses that can affect the mechanical properties during the component life. The aim of this work will be to analyzing and understand the residual strain behavior during a complete “standard” cure and cooling cycle process and the indentification of a “special” cure and cooling cycle process that minimize the residual strain of the final composite components.

2.2.3.2 Curing Agents

In order to convert epoxy resins to hard, infusible thermoset networks it is necessary to use crosslinking agents. These crosslinkers, hardeners or curing agents as they are widely known, promote cross-linking or curing of epoxy resins. Curing can occur by either homopolymerisation initiated by a catalytic curing agent or a polyaddition/copolymerisation reaction with a multifunctional curing agent.[19] The mechanical properties of the epoxy are dependent on the type of curing agent used. Acid anhydrides and multifunctional amines are most commonly used. [40] The choice of curing agent depends on processing method,

curing conditions, i.e., curing temperature and time, physical and chemical properties desired, toxicological and environmental limitations, and cost. The epoxy group, because of its three-membered ring structure, is highly reactive and can be opened up by a variety of nucleophilic and electrophilic reagents. Curing agents are either correactive or catalytic. A catalytic curing agent functions as an initiator for epoxy resin homopolymerization, whereas the co-reactive curing agent acts as comonomer in the polymerization process. A variety of curing agents containing active hydrogen atom such as aliphatic and aromatic amines, polyamide amines, polyamides, anhydrides, dicyandiamide, isocyanate, polysulphides, mercaptans, melamine-formaldehyde, urea formaldehyde, etc. have been used. [77]

2.2.3.2.1 Amine Of the many types of curing agents, amines are most widely utilized as curing agents in epoxy matrices for high performance composites. Amine compounds are classified into primary, secondary, and tertiary amines, in which one, two, and three hydrogen molecules of ammonia (NH3) have been substituted for hydrocarbon, respectively. Amines are called monoamine, diamine, tri-amine, or polyamine according to the number of amines in one molecule. Three principal reactions take place between the amine curing agent and epoxy, the reaction is between epoxy groups and primary amine leading to the production of a secondary aminde and hydroxly group, (2) the reaction between epoxy groups and secondary amine hydrogens leading to the production of tertiary amine, (3) the etherification reactions between epoxy groups and the hydroxy group. The initial reaction of a primary amine can produce a secondary one, and the subsequent reaction leads to a tertiary amine. [47] Amines are classified into aliphatic, alicyclic, and aromatic amines according to the types of hydrocarbons involved, and the all are important curing agents for epoxy resin. Aliphatic amines yield fast cure times, whereas aromatic amines are less reactive but result in higher glass transition temperatures. [40]. Aliphatic amine rapidly reacts with epoxy resin, is a representative room-temperature curing agent.Resins that have been cured using aliphatic amines are strong, and are excellent in bonding properties. They have resistance to alkalis and some inorganic acids, and have good resistance to water and solvents, but they are not so good to many organic solvents. Aromatic amine has weaker basicity than aliphatic amine and slowly cures at room temperature due to steric hindrance by the aromatic ring. The curing virtually stops in the B-stage of a linear polymer solid due to the large difference in the reaction of primary and secondary amines. Normally, the curing of aromatic amine requires heating in two steps. The first heating is carried out at a rather low temperature of approximately 80°C so as to lessen heat generation, and the second heating is carried out at a high temperature of 150°C to 170°C. Aromatic amines are often used as curing agents in epoxy prepreg resins as well as infusion resins, including those for

resin transfer molding (RTM), vacuum assisted resin transfer molding (VARTM), resin film infusion (RFI), pultrusion, and filament winding. Cycloaliphatic amines are also used in VARTM type composite processes and specialty RTM and filament winding. Most commonly, cycloaliphatic and aliphatic amines are used as curing agents in epoxy wet-laminating resins. Shown below is a summary of some of the main advantages and disadvantages of the different classes of amine curing agents when used in epoxy systems.

2.3 Polymerization Process

Epoxy resin system are included in the group of thermosetting polymers. Starting with the initial uncured state the matrix, a mixture if resin and curing agent, undergoes a polymerization process during curing. As introduce by Flory [21] two polimerization reaction mechanism are distinguidhed: fre-radicals or ions (chain-growth polymerization) and by functional groups (step-growth polymerization) [58] . The curing of epoxy resins is associated with a change in state from a low molecular weight liquid mixture to a highly cross-linked network. The molecular mobility in the system decreases as the cure proceeds due to cross-linking of several chains into network of infinite molecular weight. [77] The molecular mobility in the system decreases as the cure proceeds due to cross-linking of several chains into network of infinite molecular weight. Figure 2.2 shows the chain-growth polymerization. In Figure 2.2 a) is shown the polymerization reaction with an initiator the unsaturated monomer molecules add onto the active site of a growing polymer chain one at time. The characteristics of step-growth polymerization are the growth throughout the matrix, whereas no initiator is necessary and the reaction between any two functional groups of monomers is stepwise. Thus, at multiple locations and at the same time similar steps are repeated throughout the reaction process as illustrated in Figure 2.2 b). In particular initiation, propagation, and termination reactions are essentially identical in rate and mechanism as shown in Figure 2.2 c). The chain length increases steadily and random growth takes place as the monomer reacts with both monomer or polymer species with equal ease until a high molecular weight polymer is obtained.[58] The transformation of low molecular weight liquid into high molecular weight amorphous solid polymer by chemical reaction is the fundamental process used in the coatings, adhesives and thermo-set industries. As the chemical reaction proceeds, the molecular weight and glass transition temperature (Tg) increase, and if the reaction is carried out isothermally below the glass transition temperature of the fully reacted system (TgINFINITO), the polymer Tg will eventually reach the reaction temperature (Tcure). During isothermal reaction below TgINFINITO, two phenomena of critical importance in thermosetting processing can occur: gelation and vitrification.[4] Gelation corresponds to the incipient formation of an infinite

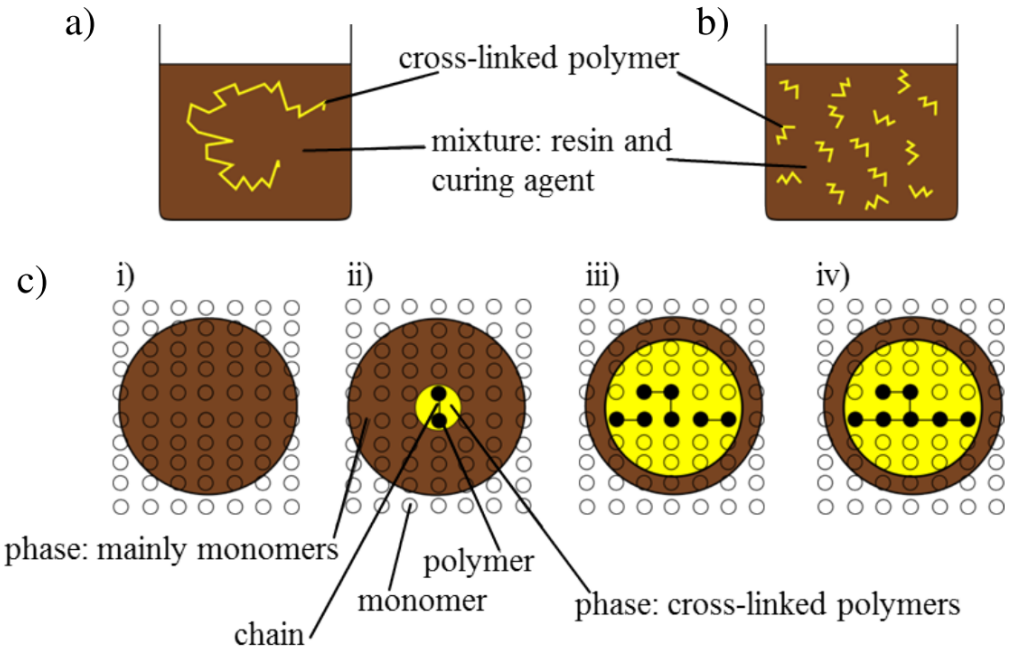

Fig. 2.2 Polymerization in thermosets: a) schematic illustration b) step-growth polymerization c) step-growth polymerization adapted to i) uncured state, ii) two monomers react, iii) state with larger chain length including dimer and trimer, iv) state where branching started. [58]

molecular network, which gives rise to long range elastic behavior in the macroscopic fluid. It occurs at a definite conversion for a given system according to Flory's theory of gelation. After gelation the material consist of normally miscible sol(solvent-soluble) and gel(solvent-insoluble) fractions, the ratio of former to the latter decreasing with conversion. Vitrification occurs when the glass transition temperature,Tg, rise to the isothermal temperature of cure. The material is liquid or rubber when Tcure>Tg; it is a glassy when Tcure<Tg. [25]

2.3.1 Cure Kinetics

Studies on the curing kinetic characterization of the thermo-set resins are important to understand the relationships between the structure of the cured resin and processing techniques, as well as the properties for high performance composites.[57] In order to investigate the cure development numerically, cure kinetics models specific to the resin system used in the composite were developed. The extent of the cure reactions is usually described by the degree of cure, α, which is quantified as the fraction of heat generated to that point relative to the total heat generated through the complete cure. The degree of cure can easily be determined using standard heat flow measurements in a Differential Scanning Calorimeter

(DSC) by integrating the exothermic DSC peak. [88] The mechanisms of the curing reaction of thermosetting resins follow the general kinetic models,namely, n-th order and autocatalytic mechanisms.[57] The reaction rate of nth-order kinetics can be expressed as:

$$\frac{d\alpha}{dt} = K(T)(1-\alpha)^n \tag{2.1}$$

The reaction rate of autocatalytic kinetics can be defined as:

$$\frac{d\alpha}{dt} = K'\alpha^m(1-\alpha)^n \tag{2.2}$$

where α is the extent of reaction, and α is given by $\alpha = \frac{\Delta H_t}{\Delta H_0}$, where ΔH_t is the partial area under a DSC trace up to time t; m and n are the reaction orders; and K' is the kinetic rate constant.

2.3.1.1 Kamal Model

According to the n-th order kinetic model, the maximum reaction rate will be observed at time t=0; according to the autocatalytic model, the reaction rate is zero or very small initially and reaches a maximum value at an intermediate conversion. The autocatalytic kinetics was expressed by Kamal, the generalized expression is:

$$\frac{d\alpha}{dt} = (K_1 + K_2\alpha^m)(1-\alpha)^n \tag{2.3}$$

where α is the cure conversion, K_1 and K_2 are the specific rate constants that are functions of temperature with two different activation energies and preexponential factors, and m and n are the reaction orders. [57] According to nth-order kinetic model, the maximum reaction rate will be observed at $t = 0$, whereas the maximum reaction rate of the autocatalytic reaction will appear at some intermediate conversion.

2.4 Matrix characterization

The exponential growth of polymer applications has led to the developmnet of several new techniques for polymer characterization, no single technique has proved more useful than thermal analysis.[76]. The standard thermal analytical techniques such as thermogravimetry (TGA), differential thermalanalysis (DTA) and differential scanning calorimetry (DSC), have been extensively used to study phase changes of materials [10]. The ability of a substance to undergo phase transitions and also the temperature intervals and heats of these transitions

can be determined from thermographic heating and cooling curves, the shape of which is different for crystalline and amorphous polymers.[27]

2.4.1 TGA

Thermogravimetry or thermogravimetric analysis is one of the most popular thermal methods. The terms are used interchangeably and often abbreviated to TG or TGA. The origins of thermogravimetric date back to 1912 when Urbain described the first equipment that could continuously heat and weigh a sample under a controlled gas atmosphere.Three years later, Honda coined the term "thermobalance" for his instrument which was also capable of reducing the heating rate when a mass change was occurring leading to a form of sample-controlled thermal analysis.Applications to polymers and pharmaceuticals blossomed after the 2nd World War and became more widespread with the introduction of commercial instrumentation beginning in th 1960s. [23]. TGA measures the amount and rate (velocity) of change in the mass of a sample as a function of temperature or time in a controlled atmosphere.The measurements are used primarily to determine the thermal and/or oxidative stabilities of materials as well as their compositional properties. The technique can analyze materials that exhibit either mass loss or gain due to decomposition, oxidation or loss of volatiles (such as moisture). It is especially useful for the study of polymeric materials, including thermoplastics, thermosets, elastomers, composites, films, fibers, coatings and paints. TGA data provide characteristic curves for a given polymer because each polymer will show a unique pattern of reactions at specific temperatures. In TGA, a sample is placed in a furnace while being suspend from one arm of a sensitive balance. The change in sample mass is recorder while the sample is maintained either at a required temperature or while being subject to a programmed heating sequence. The thermobalance can detect to 0.1 µg and calibration can be made by using standard masses.The TGA curve can be plotted as the sample mass loss as a function of temperature, or alternatively, in a differential form where the change in sample mass with time is plotted as function of temperature.

2.4.2 DTA

Differential thermal analysis (DTA) techniques permit study of thermal behavior of materials as they undergo transformations as a function of temperature. The principle of the technique is that a sample and a reference material are heated while both are monitored by thermocouples. The two thermocouples produce identical voltages when there are no thermal transformations whereas when a thermal transformation occurs there is a change in this voltage. If the change is positive there is an exothermic reaction whereas a negative

change shows an endothermic reaction. DTA thermograms plots of this voltage change as a function of the reference temperature, provide data regarding glass transition, crystallization and melting parameters. Differential scanning calorimetry (DSC) is another thermal technique similar to DTA in the type of the information available although the experiment is more reproducible due to the nature of the instrument[71]. Differential scanning calorimetry (DSC) and Differential thermal analysis (DTA) are related techniques that measure the same thermal events with different methods. DSC monitors the difference in heat flow between a sample and reference as the material is heated or cooled while DTA measures a difference in temperature. [72] DTA involves heating or cooling a test sample and an inert reference under identical conditions, while recording any temperature difference between the sample and reference. This differential temperature is then plotted against time, or against temperature. Changes in the sample which lead to the absorption or evolution of heat can be detected relative to the inert reference. Differential temperatures can also arise between two inert samples when their response to the applied heat–treatment is not identical. DTA can therefore be used to study thermal properties and phase changes which do not lead to a change in enthalpy. The baseline of the DTA curve should then exhibit discontinuities at the transition temperatures and the slope of the curve at any point will depend on the microstructural constitution at that temperature. A DTA curve can be used as a finger print for identification purposes, for example, in the study of clays where the structural similarity of different forms renders diffraction experiments difficult to interpret. The area under a DTA peak can be to the enthalpy change and is not affected by the heat capacity of the sample. DTA may be defined formally as a technique for recording the difference in temperature between a substance and a reference material against either time or temperature as the two specimens are subjected to identical temperature regimes in an enviroment heated or cooled at a controlled rate.

2.4.3 DSC

A DSC analyser measures the energy changes that occur as a sample is heated, cooled or held isothermally, together with the temperature at which these changes occur. The energy changes enable the user to find and measure the transitions that occur in the sample quantitatively, and to note the temperature where they occur, and so to characterize a material for melting processes, measurement of glass transitions and a range of more complex events. One of the big advantages of DSC is that samples are very easily encapsulated, usually with little or no preparation, ready to be placed in the DSC, so that measurements can be quickly and easily made.The main property that is measured by DSC is heat flow, the flow of energy into or out of the sample as a function of temperature or time. [22] There are two types of DSC instruments in commercial use today. One is known as a "heat flux"design while the other

is referred to as a "power compensation"instrument.While each type has its adherents, the essential information extracted by this technique is not influenced significantly by the two approaches. In essence, both heat flux and power compensated DSC's use a temperature difference between a sample and a reference as the raw data.Both types of DSC instruments convert temperature difference into a measurement of the energy per unit mass associated with the phase change that caused the temperature difference to arise. Any transition in a material that involves a change in the heat content of the material can be detected and measure by DSC.

2.4.3.1 Heat flux DSC

Heat flux DSC is of a single furnace design with a temperature sensor (or multiple sensors) for each of the sample and reference pans located within the same furnace; see FIGURE. Sample and reference pans are placed in their required positions and the furnace heated at the pre-programmed heating (or cooling) rate. When transitions in the sample are encountered a temperature difference is created between sample and reference. On continued heating beyond the transition this difference in temperature decreases as the system reaches equilibrium in accordance with the time constant of the system. It is the difference in temperature or Δt signal that is the basic parameter measured. Modern analysers are carefully calibrated so that the Δt signal is converted to a heat flow equivalent and this is displayed as a function of temperature or time. The reason a difference in temperature is created is easily understood if melting is considered. When melting of a single crystal occurs the resulting mixture of solid and liquid remains at the melting point until melting is complete, so the temperature of the sample will fall behind that of the reference. Typical heat flux DSC analysers can be used from liquid nitrogen temperatures to a maximum of around 700 °C similar to power compensation DSC, though modern high-temperature DTA analysers normally offer a calibrated DTA (heat flow) signal giving a measurement derived from the heat flux to significantly higher temperatures. [22]

2.4.3.2 Power compensation DSC

Power compensation DSC has at its heart two small identical furnaces, one for the sample and one for the reference (normally an empty pan), the reference being the right-hand furnace. These are both heated at a pre-programmed heating (or cooling) rate and power compensations are applied to either furnace as required to maintain this rate. In the resulting DSC trace the difference in energy flowing into the sample furnace is compared to the inert reference and plotted as a function of temperature or time. This design measures flow of

energy directly in mW or $J\,s^{-1}$.Therefore the raw heat flow signal can be viewed as a form of heat capacity. In practice, it reflects the changes occurring in heat capacity, and the absolute value is obtained when the method used takes into account the contribution of the empty pans and reference together with the scan rate. The small furnaces of this system can be heated or cooled at very low rates to very high rates and are ideal for a range of different techniques, particularly fast scan DSC. Power- compensated DSC also permits true isothermal operation, since under constant temperature conditions both the sample and furnace are held isothermally. The temperature range of use is from liquid nitrogen temperatures to around 730 °C. [22]

2.5 Reinforcement

In the most general case a composite material consists of one or more discontinuous phases distributed in one continuous phase, the continuous phase is called the matrix, the discontinuous phase is called the reinforcement, or reinforcing material. The geometry of the reinforcement will be characterized by its shape, its size, the concentration of the reinforcement, its disposition (its orientation), etc. [7] These charatcteristic are illustrated in Figure 2.3 The shape of the reinforcement will be schematically approximated by either spheres or

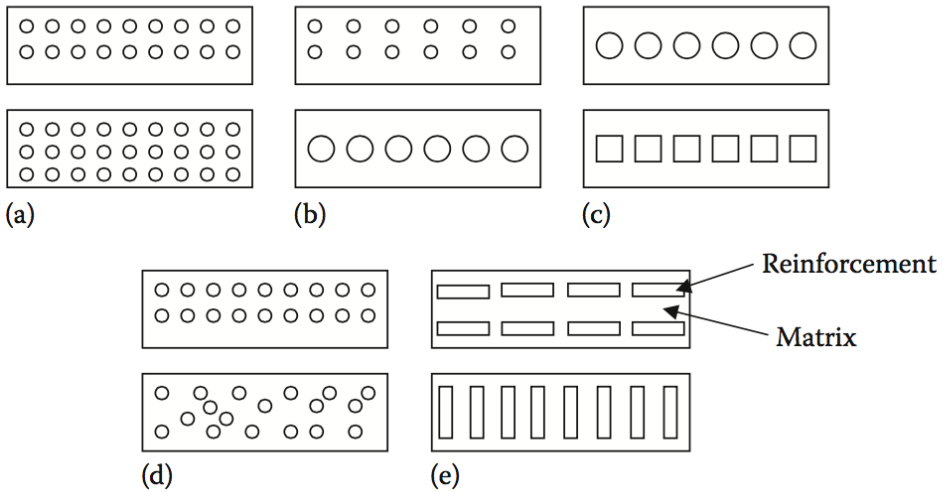

Fig. 2.3 Schematic of geometrical and spatial characteristics of reinforcements in composites: (a concentration, (b size, (c shape, (d distribution, and (e orientation.
[6]

cylinders.The concentration of the reinforcement is usually measured by the volume fraction or by the weight fraction. The concentration of the reinforcement is a determining parameter

of the properties of the composite material. The weigth fraction is relevant to fabrication and the volume fraction is commonly used in property calculations. Weight and volume fraction are related to each other through density ρ. The size of the dispersed phase also influences the properties of composites. In general, the smaller the size, the better will be the mechanical properties, because of size effect; that is, the size of defect is restricted and it should be smaller than the size of the material. The strength of any material is inversely proportional to the size of defect. The surface area of a material depends on the size and shape. For any particular volume, the smaller reinforcement has more surface area. The contact area between reinforcement and matrix increases with surface area, resulting in better properties. [6] For a given concentration the distribution of the reinforcement in the volume of the composite is also an important parameter. A uniform distribution will ensure a "homogeneity" of the material, i.e., the properties of the composite will be independent of the point of measurement. In the case of a nonuniform distribution of the reinforcement, fracture of the material will be initiated in the zones poor in reinforcement, thus diminishing the strength of the composite.In the case of composite materials in which the reinforcement is made of fibers, the orientation of the fibers determines the anisotropy of the composite material. [7] The orientation of the reinforcement in a particular direction within the matrix affects the isotropic properties of the composite. When the reinforcement is in the form of particles, the composite behaves essentially as an isotropic material. When the dimensions of reinforcement are unequal, the composite can behave as an isotropic material only when the reinforcement is randomly oriented. For example, a randomly oriented, short FRC will have isotropic properties. In some cases, the manufacturing process may induce orientation of the reinforcement and hence loss of isotropy, that is, the composite is said to be anisotropic. In components manufactured from continuous FRCs, such as unidirectional or cross-ply laminate, anisotropy may be desirable as the laminate can be arranged in such a way that the highest strength is along the direction of maximum service stress. Indeed, a primary advantage of these composites is the ability to control the anisotropy by design and fabrication.[6] Most of the properties of a composite material are a complex function of other factors. The constituents of a composite usually interact in a synergistic way to determine the properties of the composites that are not fully accounted for by the rule of mixtures. The chemical and bonding characteristics of an interface are particularly important in determining the properties of the composite. The interfacial bond strength should be sufficient for load transfer from the matrix to the fibers, and only then will the composite have better strength than the unreinforced matrix. On the other hand, if the toughness of the composite is more important than strength, then the interface should readily fail to allow toughening mechanisms such as debonding and fiber pullout to take place. The dispersed

phase can be in the form of long fibers, short fibers, whiskers, flakes, sheets, or particulates. Among these forms, fiber forms are widely used in the composites because of their superior properties and load transfer characteristics. [6]

2.6 Textile fabrics and Woven Fabric

A textile fabric is defined as a manufactured assembly of fibres and/or yarns, which has a substantial surface area in relation to its thickness and sufficient inherent cohesion to give mechanical strength to the assembly. Based on the manufacturing techniques, conventional textile fabrics can be divided into woven, non-woven, knitted and braided formations. Woven textile structures are often used as reinforcement in composite materials. Their ease of handling, low fabrication cost, good stability, balanced properties and excellent formability make the use of woven fabrics very attractive for structural applications in for example the automotive and aerospace industry. [65] Most advance composite involve the use of woven fabrics, they can be classified as two dimensional (2D) and three dimensional (3D) structures.

2.6.1 2D Woven fabrics

A typical woven fabric is made up of a number of individuals fibers drawn together into what is knows as an end or a pick. These are then interlaced in a lengthwise and widthwise fashion in order to produce a woven fabric. The fiber which run down the length of the roll form what is knows as the warp yarn and those that run across the width are known as the weft or fill yarn. The warp and the weft yarns are oriented along the length and the width of the fabric respectively.The main factor that define a particular fabric style are the warp and weft count together with the weave, the weave refers to how the warp and weft yarns are interlaced, and will determine the appearance and handling characteristics of the fabric.Depending on the repeat pattern of the interlace, 2D woven fabrics can be further classified; some examples are plain, twill and satin fabrics(Figure 2.4).[Robinson]

2.6.1.1 Plain fabrics

A plain weave is where each warp and weft yarn passes over one end or pick and under the next. This construction gives a reinforcement fabric that is widely used in general applications and can be relied upon to give laminates of predictable thickness.The plain weave is the simplest of all the available weaving patterns. This type of fabric is very stable, it is very difficult to distort. However, due to the large percentage of fibres that are twisting up and down the mechanical properties are not as good as those of unidirectional prepregs or some of

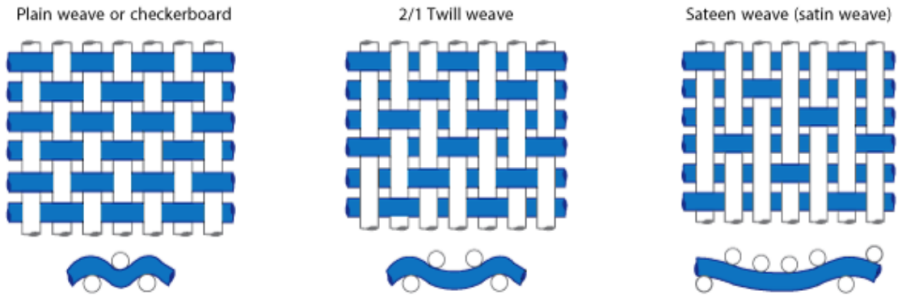

Fig. 2.4 Examples of woven fabric patterns: (a) plain weave (b) twill weave (c) 4-harness satin weave

the more open weaves. It has a high porosity which allows quick wetting out and the removal of entrapped air, its strength is equal in both the 0° and 90° fibre orientation direction.

2.6.1.2 Twill fabrics

In a twill weave the number of warp ends and weft picks that pass over each other can be varied to give twills of various construction. In the twill weave the weft yarn passes under two warp ends and then over one warp end. This pattern of interlacing gives the fabric a typical herringbone pattern. Twill weave can be identified by the diagonal lines on the face of the fabric due to warp and weft floats, depending on the direction of the diagonal lines twill can further be categorized by “S” or “Z” twill. Twill follows contours more easily than plain fabric and are easily wetted out.

2.6.1.3 Satin fabrics

In satin weave fabrics the interlacing is similar to that of the twill fabrics, though the number of ends and picks that pass over or under each other before interlacing are greater. One side of the fabric is therefore made up mainly of warp fibres while the other side is mainly weft fibres, which gives an unbalanced fabric that will tend to distortion on curing. For this reason it is necessary invert half the plies about the mid-plain of the laminate. The advantages of the satin weave are that it drapes well into double curves and because of the very flat nature of the weave it will give a good surface finish.

2.6.2 3D Woven fabrics

3D fabrics are recognised by the presence of thickness of the fabric in the Z-direction in addition to the X and Y directions. Orthogonal and angle interlock fabrics are the most renowned classes of 3D woven fabrics.

2.6.2.1 Orthogonal fabrics

In orthogonal fabrics, the straight yarns are arranged perpendicular to each other in X, Y and Z directions. The absence of crimp in the warp and weft yarns makes this structure ideal for applications where non-crimp features are required. Both isotropic and anisotropic preforms can be achieved by arranging the number of yarns in each dimension. The orthogonal fabrics can further be classified into two types, through-the-thickness orthogonal and layer-to layer-orthogonal. In orthogonal through-the-thickness fabrics, binding warp travels from one surface of the preform to the other, holding together all the layers of the preform. The orthogonal layer-to-layer is a multilayer woven fabric in which binding warps travel from one layer to the adjacent layer and back.

2.6.2.2 Angle interlock fabrics

In angle-interlock structures, the warp (or weft) yarns are used to bind many layers of weft (or warp) yarns with weft/warp yarns being straight. A third set of yarns (stuffer yarns) can also be added in angle-interlock fabrics to increase fibre volume fraction and in-plane strength. Like orthogonal fabrics, angle interlock structure can also be divided into through-the-thickness and layer-to-layer angle interlock depending on the passage of binder yarn.

2.7 Modeling of woven fabrics

The purpose of this section is describe the models use for investigate the themomechanical behavior of two dimensional orthogonal woven fabric. An orthogonal woven fabric consist of two sets of interlaced yarns. The various types of fabric can be identified by the pattern of repeat of the interlaced regions.[14] Two basic geometrical parameters can be defined to characterize a fabric n_{fg} e n_{wg}, n_{fg} denotes that a warp thread is interlaced with every $n_{\mathrm{g}} - th$ fill thread and n_{wg} denotes that a fill thread is interlaced with every $n_{\mathrm{wg}} - th$ warp thread. Here, we confine ourselves to non-hybrid fabrics and the case of $n_{\mathrm{wg}} = n_{\mathrm{fg}} = n_{\mathrm{g}}$. Fabrics with $ng \geq 4$ and where the interlaced regions are not connected are known as satin weaves. As defined by their n_{g} values, the fabrics in Figure 2.5 are termed plain weave ($n_{\mathrm{g}} = 2$), twill

weave ($n_g = 3$), 4 harness satin ($n_g = 4$), and 8 harness satin ($n_g = 8$) [43] The theoretical

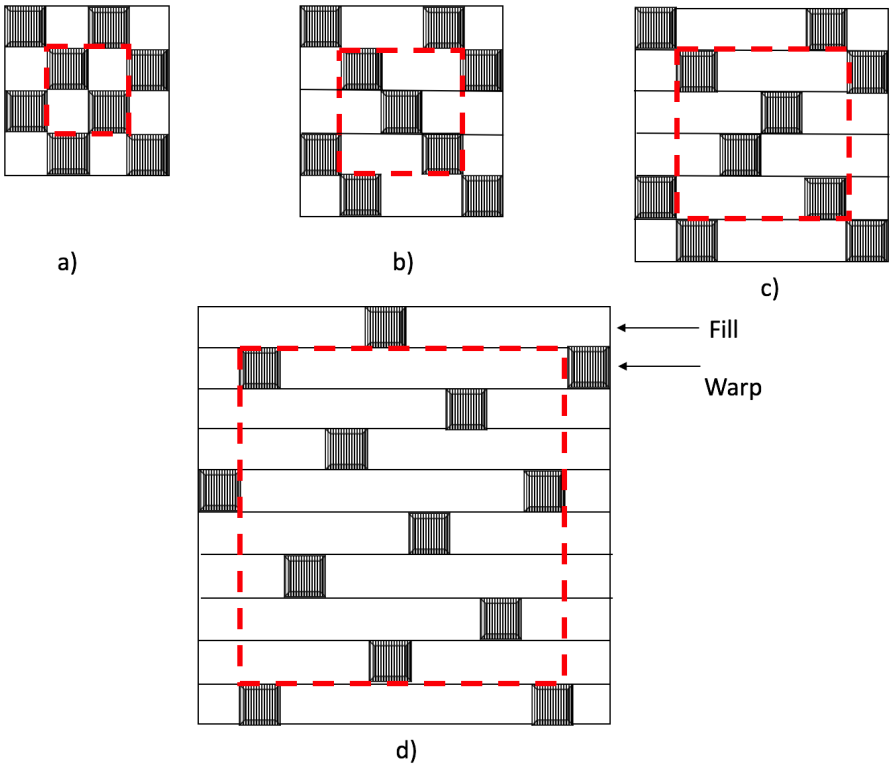

Fig. 2.5 Examples of woven fabric patterns: (a) plain weave ($n_g = 2$); (b) twill weave ($n_g = 3$); (c) 4-harness satin ($n_g = 4$) and (d) 8-harness satin ($n_g = 8$).

basis of the present analysis is the classical laminated plate theory. Under the assumptions of the Kirchhoff hypothesis, the constitutive equations are expressed in the condensed form as:

$$\begin{Bmatrix} N \\ M \end{Bmatrix} = \begin{bmatrix} A & B \\ B & D \end{bmatrix} \begin{Bmatrix} \varepsilon^0 \\ k \end{Bmatrix} \tag{2.4}$$

N and M are membrane stress resultants and moment resultants, respectively; epsilon^0 an k are the strain and curvature of the laminate geometric mid-plane, respectively. The components of the stiffness matrices A,B and D are evaluates as follows:

$$(A_{ij}, B_{ij}, D_{ij}) = \sum_{k=1}^{n} \int_{h_k}^{h_{k-1}} (\overline{Q}_{ij})_k (1, z, z^2) dz \qquad (i, j = 1, 2, 6) \tag{2.5}$$

where the reduced sirens constants $\overline{Q}_{ij}$ corresponding to the lamina defined by h_k and h_{k-1} in the thickness direction are used in the calculations. The subscript 1,2 and 6 indicate in xyz coordinate system, the x direction, the y direction , and the x-y plane, respectively. More

explicitly last equation can be written as:

$$A_{ij} = \sum_{k=1}^{n} (\overline{Q}_{ij})_k (h_k - h_{k-1}) \tag{2.6}$$

$$B_{ij} = \frac{1}{2} \sum_{k=1}^{n} (\overline{Q}_{ij})_k ({h_k}^2 - {h_{k-1}}^2) \tag{2.7}$$

$$C_{ij} = \frac{1}{3} \sum_{k=1}^{n} (\overline{Q}_{ij})_k ({h_k}^3 - {h_{k-1}}^3) \tag{2.8}$$

The inverted form is given by:

$$\begin{Bmatrix} \varepsilon^0 \\ k \end{Bmatrix} = \begin{bmatrix} A' & B' \\ B' & D' \end{bmatrix} \begin{Bmatrix} N \\ M \end{Bmatrix} \tag{2.9}$$

When the effect of temperature change is taken into account the constitutive relation and should be written as:

$$\begin{Bmatrix} N \\ M \end{Bmatrix} = \begin{bmatrix} A & B \\ B & D \end{bmatrix} \begin{Bmatrix} \varepsilon^0 \\ k \end{Bmatrix} - \Delta T \begin{Bmatrix} \widetilde{A} \\ \widetilde{B} \end{Bmatrix} \tag{2.10}$$

where:

$$\begin{Bmatrix} \widetilde{A}_x \\ \widetilde{A}_y \\ \widetilde{A}_{xy} \end{Bmatrix} = \sum_{k=1}^{n} \int_{h_k}^{h_{k-1}} \begin{bmatrix} \overline{Q}_{11} & \overline{Q}_{12} & \overline{Q}_{16} \\ \overline{Q}_{12} & \overline{Q}_{22} & \overline{Q}_{26} \\ \overline{Q}_{16} & \overline{Q}_{26} & \overline{Q}_{66} \end{bmatrix}_k \begin{Bmatrix} \alpha_{xx} \\ \alpha_{yy} \\ \alpha_{xy} \end{Bmatrix}_k dz \tag{2.11}$$

$$\begin{Bmatrix} \widetilde{B}_x \\ \widetilde{B}_y \\ \widetilde{B}_{xy} \end{Bmatrix} = \sum_{k=1}^{n} \int_{h_k}^{h_{k-1}} \begin{bmatrix} \overline{Q}_{11} & \overline{Q}_{12} & \overline{Q}_{16} \\ \overline{Q}_{12} & \overline{Q}_{22} & \overline{Q}_{26} \\ \overline{Q}_{16} & \overline{Q}_{26} & \overline{Q}_{66} \end{bmatrix}_k \begin{Bmatrix} \alpha_{xx} \\ \alpha_{yy} \\ \alpha_{xy} \end{Bmatrix}_k z dz \tag{2.12}$$

ΔT indicates a small uniform temperature change and α denotes the thermal expansion coefficients. The inverted form is given by:

$$\begin{Bmatrix} \varepsilon^0 \\ k \end{Bmatrix} = \begin{bmatrix} A' & B' \\ B' & D' \end{bmatrix} \begin{Bmatrix} N \\ M \end{Bmatrix} + \Delta T \begin{Bmatrix} \widetilde{A}' \\ \widetilde{B}' \end{Bmatrix} \tag{2.13}$$

where:

$$\begin{Bmatrix} \widetilde{A}' \\ \widetilde{B}' \end{Bmatrix} = \begin{bmatrix} A' & B' \\ B' & D' \end{bmatrix} \begin{Bmatrix} \widetilde{A} \\ \widetilde{B} \end{Bmatrix} \tag{2.14}$$

The constants $\widetilde{A}'$ and $\widetilde{B}'$ represent respectively , the in-plane thermal expansion and thermal bending coefficients. Based upon the iso-stress and iso-strain assumptions, the above constitutive equations can be used to obtain the bounds of the thermoelastic properties. The

upper bounds of compliance constants are obtained by inverting the compliance constant matrix. Similarly, the upper bounds of stiffness constant are derived from the iso-strain assumption; the lower bounds of compliance constants are then obtained by inverting the stiffness constant matrix. Three techniques for modeling the stiffness and strength properties of fabric composites. Ishikawa and Chou developed three analytical models to predict the stiffness and coefficient of thermal expansion of woven fabric composites. [1] These are the mosaic model, the crimp model (fibre undulation model) and the combination of the above two, the bridging model. [62] The mosaic model described the fabric as an assemblage of asymmetrical cross-ply laminates with no fibre undulation and gave good predictions for fabrics with few interlaced regions, such as satin fabric. The crimp model accounted for the fibre undulation using shape functions was more suitable for plain weave composites. Finally, the bridging model was developed for satin woven fabrics in order to describe the difference in properties between the straight threads region and the interlaced regions.[1]

2.7.1 Mosaic Model

The basis of idealization of the “mosaic model” can be seen from Figure 2.6. The key simplification of the mosaic model is the omission of the fiber continuity and crimp (undulation) that exist in an actual fabric. In general, a fabric composite idealized by the mosaic model can be regarded as an assemblage of pieces of asymmetric cross-ply laminates. Assuming

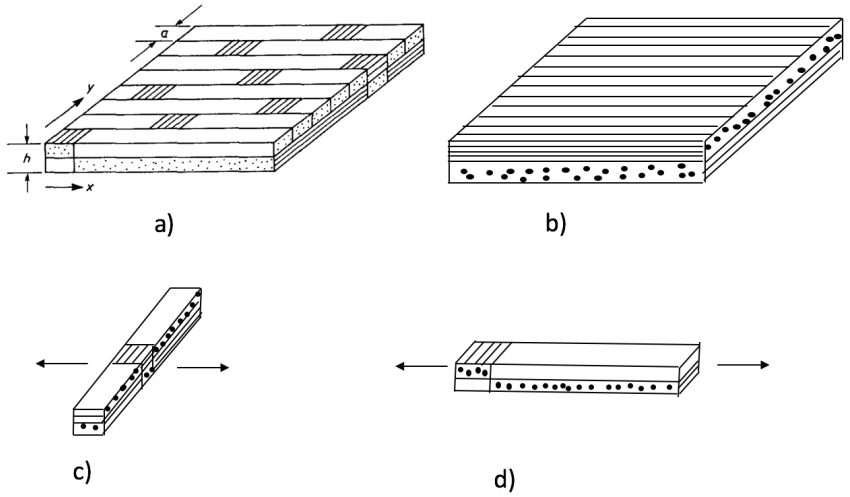

Fig. 2.6 The mosaic model:(a) repeating region in a eight-harness satin composite; (b) basic cross-ply laminate; (c) parallel model; (d) series model.

that fibers are aligned along the x direction, the stiffness constant, Q_{ij} of a unidirectional lamina, which has orthotropic symmetry in the x-y plane, are given by:

$$Q_{ij} = \begin{bmatrix} \frac{E_{11}}{D_v} & \frac{\nu_{12}E_{22}}{D_v} & 0 \\ \frac{\nu_{21}E_{11}}{D_v} & \frac{E_{22}}{D_v} & 0 \\ 0 & 0 & G_{12} \end{bmatrix} \tag{2.15}$$

where

$$D_v = 1 - \nu_{12}\nu_{21} \tag{2.16}$$

Here E_{11} and E_{22} are the Young's moduli, G_{12} is the in-plane shear modulus, and ν_{12} denotes the Poisson's ratio relating the transverse strain in the x_2 direction and the applied strain in the x_1 direction. The Q_{ij} constants are symmetrical, i.e $Q_{ij} = Q_{ji}$. The laminate is composed of two unidirectional laminae of thickness $h/2$. The total laminate thickness is h and the x-y coordinate plane is positioned at the geometrical mid-plane of the laminate, $k = 1$ and $k = 2$ define, respectively, the laminae with fibers in the y and x directions. The non-vanishing stiffness constants are:

$$\begin{aligned} A_{11} &= A_{22} = \frac{(E_{11} + E_{22})h}{2D_v} \\ A_{12} &= \frac{\nu_{12}E_{22}h}{D_v} \\ A_{66} &= G_{12}h \\ B_{11} &= -B_{22} = \frac{(E_{11} - E_{22})h^2}{8D_v} \\ D_{11} &= D_{22} = \frac{(E_{11} + E_{22})h^3}{24D_v} \\ D_{12} &= \frac{\nu_{12}E_{22}h^3}{12D_v} \\ D_{66} &= \frac{G_{12}h^3}{12} \end{aligned} \tag{2.17}$$

The extension-bending coupling costants B_{11} and B_{22} do not vanish because $E_{11} \neq E_{22}$. Also, it is understood that A_{ij}, B_{ij} and D_{ij} are symmetrical constants.

$$\begin{Bmatrix} N_{xx} \\ N_{yy} \\ N_{xy} \end{Bmatrix} = \begin{bmatrix} A_{11} & A_{12} & 0 \\ A_{12} & A_{11} & 0 \\ 0 & 0 & A_{66} \end{bmatrix} \begin{Bmatrix} {\varepsilon^0}_{xx} \\ {\varepsilon^0}_{yy} \\ {\varepsilon^0}_{xy} \end{Bmatrix} + \begin{bmatrix} B_{11} & 0 & 0 \\ 0 & -B_{11} & 0 \\ 0 & 0 & 0 \end{bmatrix} \begin{Bmatrix} k_{xx} \\ k_{yy} \\ k_{xy} \end{Bmatrix} \tag{2.18}$$

$$\begin{Bmatrix} M_{xx} \\ M_{yy} \\ M_{xy} \end{Bmatrix} = \begin{bmatrix} B_{11} & 0 & 0 \\ 0 & -B_{11} & 0 \\ 0 & 0 & 0 \end{bmatrix} \begin{Bmatrix} {\varepsilon^0}_{xx} \\ {\varepsilon^0}_{yy} \\ {\varepsilon^0}_{xy} \end{Bmatrix} + \begin{bmatrix} D_{11} & D_{12} & 0 \\ D_{12} & D_{11} & 0 \\ 0 & 0 & D_{66} \end{bmatrix} \begin{Bmatrix} k_{xx} \\ k_{yy} \\ k_{xy} \end{Bmatrix} \tag{2.19}$$

Inverting previous equation the following are obtained:

$$\begin{Bmatrix} {\varepsilon^0}_{xx} \\ {\varepsilon^0}_{yy} \\ {\varepsilon^0}_{xy} \end{Bmatrix} = \begin{bmatrix} A'_{11} & A'_{12} & 0 \\ A'_{12} & A'_{11} & 0 \\ 0 & 0 & A'_{66} \end{bmatrix} \begin{Bmatrix} N_{xx} \\ N_{yy} \\ N_{xy} \end{Bmatrix} + \begin{bmatrix} B'_{11} & B'_{12} & 0 \\ -B'_{12} & -B'_{11} & 0 \\ 0 & 0 & 0 \end{bmatrix} \begin{Bmatrix} M_{xx} \\ M_{yy} \\ M_{xy} \end{Bmatrix} \tag{2.20}$$

$$\begin{Bmatrix} k_{xx} \\ k_{yy} \\ k_{xy} \end{Bmatrix} = \begin{bmatrix} B'_{11} & -B'_{12} & 0 \\ -B'_{12} & -B'_{11} & 0 \\ 0 & 0 & 0 \end{bmatrix} \begin{Bmatrix} N_{xx} \\ N_{yy} \\ N_{xy} \end{Bmatrix} + \begin{bmatrix} D'_{11} & D'_{12} & 0 \\ D'_{12} & D'_{11} & 0 \\ 0 & 0 & 0 \end{bmatrix} \begin{Bmatrix} M_{xx} \\ M_{yy} \\ M_{xy} \end{Bmatrix} \tag{2.21}$$

In the bound approach, the two-dimensional extent of the fabric composite plate is simplified by considering two one-dimensional models where the pieces of cross-ply laminates are either in parallel or in series. In the parallel model, a uniform state of strain ε^0, and curvature k, in the laminate midplane is assumed as a first approximation. For the one dimesional repeating region of length $n_g a$, where a denotes the yarn width, an average membrane stress N_x is defined as:

$$\begin{aligned} \overline{N_x} &= \frac{1}{n_g a}\int_0^{n_g a} N_x dy \\ &= \frac{1}{n_g a}[\int_0^a (A_{11}{\varepsilon^0}_{xx} + A_{12}{\varepsilon^0}_{yy} + B_{11}k_{xx})dy + \int_0^{n_g a} (A_{11}{\varepsilon^0}_{xx} + A_{12}{\varepsilon^0}_{yy} + B_{11}k_{xx})dy] \\ &= (A_{11}{\varepsilon^0}_{xx} + A_{12}{\varepsilon^0}_{yy}) + \frac{1}{n_g a}[aB_{11}^{\mathrm{T}} + (n_g a - a)B_{11}^{\mathrm{L}}]k_{xx} \\ &= A_{11}{\varepsilon^0}_{xx} + A_{12}{\varepsilon^0}_{yy} + (1 - \frac{2}{n_g})B_{11}^{\mathrm{L}}k_{xx} \end{aligned} \tag{2.22}$$

The factor $(1-\frac{2}{n_g})$ appears because the terms B_{11}^{T} for the interlaced region and non-interlaced region B_{11}^{L} have opposite signs, namely B_{11}^{T}=-B_{11}^{L}. Other average stress resultant can be written similar for uniform mid-plane strain, ε^0 and curvature k. The moment resultant $\overline{M_x}$ for example is:

$$\begin{aligned} \overline{M_x} &= \frac{1}{n_g a}\int_0^{n_g a} M_x dy \\ &= D_{11}k_{xx} + D_{12}k_{yy} + (1 - \frac{2}{n_g})B_{11}^{\mathrm{L}}k_{xx} \end{aligned} \tag{2.23}$$

Let $\overline{A}_{ij}$, $\overline{B}_{ij}$ and $\overline{D}_{ij}$ be the stiffness constant matrices relating the average stress resultant $\overline{N}$ and the moment resultant, $\overline{M}$ with ε^0 and k. Then:

$$\begin{aligned}\overline{A_{ij}} &= A_{ij} \\ \overline{B_{ij}} &= (1-\frac{2}{n_g})B_{11}^{\mathrm{L}} \\ \overline{D_{ij}} &= D_{ij}\end{aligned} \tag{2.24}$$

These components provide upper bounds for the stiffness constants of the fabric composite based upon the one-dimensional model. IF these stiffness constants are inverted, lower bounds of the elastic compliance constants can be obtained. All the elastic stiffness constants A,B and D are computed using the basic laminate where the top layers is composed of the filling yarn. In the series model, the disturbance of stress and strain near the interface of the interlaced region is neglected. Let the model be subjected to a uniform in-plane force N_x, in the longitudinal direction. The assumption of constants stress leads to the definition of an average curvature. For instance, the average curvature, $\overline{k_{xx}}$, along the x direction is:

$$\begin{aligned}\overline{k_{xx}} &= \frac{1}{n_g a}\int_0^{n_g a} k_{xx}dx \\ &= \frac{1}{n_g a}[\int_0^{a} B'_{11}N_x dx + \int_0^{n_g a} B'_{11}N_x dx] \\ &= \frac{1}{n_g a}[a{B'_{11}}^{\mathrm{T}} + a(n_g-1){B'_{11}}^{\mathrm{L}}N_x \\ &= (1-\frac{2}{n_g}){B'_{11}}^{\mathrm{L}}N_x\end{aligned} \tag{2.25}$$

The terms B'_{11} for interlaced region ${B'_{11}}^{\mathrm{T}}$ and non-interlaced region ${B'_{11}}^{\mathrm{L}}$ are equal and opposite in sign. Let $\overline{A'_{ij}}$, $\overline{B'_{ij}}$ and $\overline{D'_{ij}}$ be the compliance constant matrices relating the average mid-plane strain,ε^0 , and curvature $\overline{k}$, with the stress resultant N, and moment resultant M, thus:

$$\begin{aligned}\overline{A'_{ij}} &= A'_{ij} \\ \overline{B'_{ij}} &= (1-\frac{2}{n_g}){B'_{ij}}^{\mathrm{L}} \\ \overline{D'_{ij}} &= D'_{ij}\end{aligned} \tag{2.26}$$

Last equations give the upper bounds for the composite compliance constant and, after inversion, the lower bounds for stiffness constants. Both upper and lower bounds for elastic stiffness and compliance constant can be obtained from the mosaic model. Bidirectional

composites are represented by the limiting case of $\frac{1}{n_g} \longrightarrow 0$ ($n_g \longrightarrow \infty$) and the upper and lower bounds of the elastic constants coincide with each other.

2.7.2 Crimp Model

The crimp model is developed in order to consider the continuity and undulations of fibers in a fabric composite. Although the formulation of the problem developed in the following is valid for all n_g values, the crimp model is particularly suited for fabrics with low n_g values. The crimp model also provides the basis of analysis for the bridging model. Figure 2.7 depicts the geometry of the model where the undulation shape is defined by the parameters $h_1(x)$, $h_2(x)$ and a_u. The parameters $a_0 = \frac{(a-a_u)}{2}$ and $a_2 = \frac{(a+a_u)}{2}$ are automatically determined by specifying a_u, which is geometrically arbitrary in the range from 0 to a. Because a pure

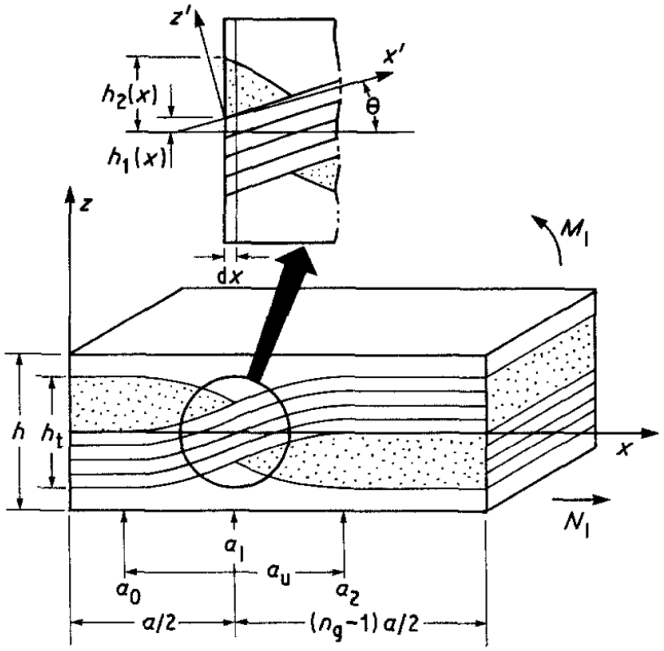

Fig. 2.7 Fibre undulation model.
[43]

matrix region appear in the model, the "overall" fiber volume fraction, V_f, can be different from that in the yarn region. To simulate the actual configuration, the following form of

crimp is assumed for the filling:

$$h_1(x) = \begin{cases} 0 & 0 \le x \le a_0 \\ \left[1 + sin\left\{(x - \frac{a}{2})\frac{\pi}{a_u}\right\}\right]\frac{h_t}{4} & a_0 \le x \le a_2 \\ \frac{h_t}{2} & a_2 \le x \le \frac{n_g a}{2} \end{cases} \tag{2.27}$$

The sectional shape of the warp yarn is expressed by

$$h_2(x) = \begin{cases} 0 & 0 \le x \le a_0 \\ \left[1 - sin\left\{(x - \frac{a}{2})\frac{\pi}{a_u}\right\}\right]\frac{h_t}{4} & a_0 \le x \le \frac{a}{2} \\ \left[1 + sin\left\{(x - \frac{a}{2})\frac{\pi}{a_u}\right\}\right]\frac{h_t}{4} & \frac{a}{2} \le x \le a_2 \\ -\frac{h_t}{2} & a_2 \le x \le \frac{n_g a}{2} \end{cases} \tag{2.28}$$

It is assumed that the laminated plate theory is applicable to each infinitesimal piece of the model along the x axis. Thus, A_{ij}, B_{ij} and D_{ij} are expressed as function of x ($0 \le x \le \frac{a}{2}$) by:

$$\begin{aligned} A_{ij}(x) &= \int_{-\frac{h}{2}}^{h_1(x)-\frac{h_t}{2}} Q_{ij}^{\mathrm{M}}\,dz + \int_{h_1(x)-\frac{h_t}{2}}^{h_1(x)} Q_{ij}^{\mathrm{F}}(\theta)dz + \int_{h_1(x)}^{h_2(x)} Q_{ij}^{\mathrm{W}}\,dz + \int_{h_2(x)}^{\frac{h}{2}} Q_{ij}^{\mathrm{M}}\,dz \\ &= Q_{ij}^{\mathrm{M}}[h_1(x) - h_2(x) + h - \frac{h_t}{2}] + Q_{ij}^{\mathrm{F}}(\theta)\frac{h_t}{2} + Q_{ij}^{\mathrm{W}}\,[h_2(x) - h_1(x)] \\ B_{ij}(x) &= \frac{1}{2}Q_{ij}^{\mathrm{F}}(\theta)[h_1(x) - \frac{h_t}{4}]h_t + \frac{1}{4}Q_{ij}^{\mathrm{W}}\,[h_2(x) - h_1(x)]\,h_t \\ D_{ij}(x) &= \frac{1}{3}Q_{ij}^{\mathrm{M}}\left\{[h_1(x) - \frac{h_t}{2}]^3 - h_2^3(x) - \frac{h^3}{4}\right\} + \frac{1}{3}Q_{ij}^{\mathrm{F}}(\theta)[\frac{h_t^3}{8} - \frac{3h_t^2 h_1(x)}{4} + \frac{3h_t h_1^2(x)}{2}] \\ &\quad + \frac{1}{3}Q_{ij}^{\mathrm{W}}\,[h_2^3(x) - h_1^3(x)] \end{aligned} \tag{2.29}$$

where superscripts F,W, and M signify the filling yarn, warp yarn and matrix, respectively. Similary expression can be written for $\frac{a}{2} \le x \le \frac{n_g a}{2}$. The local stiffness of the filling yarn, $Q_{ij}^{\mathrm{F}}(\theta)$, in the above equations is calculated as function of the local off-axis angle, $\theta(x)$, which is defined as:

$$\theta(x) = arctan\left(\frac{dh_1(x)}{dx}\right) \tag{2.30}$$

Consider a filling yarn composed of parallel fibers. The fiber direction is denoted as the 1 direction, the 2 and 3 directions are perpendiculare to the fiber and they define the transversely isotropic plane. Then, from the Young's moduli ($E_{11}, E_{22} = E_{33}$), shear moduli ($G_{12} = G_{13}, G_{23}$) and Poisson's ratio (ν_{12}) of the filling yarn, the elastic constants of the filling yarn

with respect to the xyz axes can be defined. The angle between the 1 and x axes is θ:

$$\begin{aligned}
&\frac{1}{E^{\mathrm{F}}_{xx}(\theta)} = \frac{cos^4\theta}{E_{11}} + \left(\frac{1}{G_{12}} - \frac{2\nu_{21}}{E_{22}}\right) cos^2\theta sin^2\theta + \frac{sin^4\theta}{E_{22}} \\
&E^{\mathrm{F}}_{yy}(\theta) = E_{22} = E_{33} \\
&\frac{1}{G^{\mathrm{F}}_{xy}(\theta)} = \frac{cos^2\theta}{G_{12}} + \frac{sin^2\theta}{G_{23}} \\
&\nu^{\mathrm{F}}_{yx}(\theta) = \nu_{12}cos^2\theta + \nu_{32}sin^2\theta
\end{aligned} \tag{2.31}$$

It is also understood from the assumption of transverse isotropy of the filling yarn that $\nu_{12} = \nu_{13}$, $\frac{E_{11}}{\nu_{12}} = \frac{E_{22}}{\nu_{21}}$, $\nu_{23} = \nu_{32}$ and $G_{23} = \frac{E_{22}}{2(1+\nu_{23})}$. Thus the local stiffness constants of the undulated portion of the filing yarn, referring to the xyz coordinates axes, are given as functions of the fiber orientation angle θ.

$$Q^{\mathrm{F}}_{ij}(\theta) = \begin{bmatrix} \frac{E^{\mathrm{F}}_{xx}(\theta)}{D_v} & \frac{E^{\mathrm{F}}_{xx}(\theta)\nu_{yx}{}^{\mathrm{F}}(\theta)}{D_v} & 0 \\ \frac{E^{\mathrm{F}}_{xx}(\theta)}{\nu^{\mathrm{F}}_{yx}(\theta)} D_v & \frac{E^{\mathrm{F}}_{yy}(\theta)}{D_v} & 0 \\ 0 & 0 & G^{\mathrm{F}}_{xy}(\theta) \end{bmatrix} \qquad (i,j = 1,2,6) \tag{2.32}$$

where

$$D_v = 1 - \frac{(\nu_{yx}{}^{\mathrm{F}}(\theta))^2 E^{\mathrm{F}}_{xx}(\theta)}{E^{\mathrm{F}}_{yy}(\theta)} \tag{2.33}$$

The local compliance constants, $A'_{ij}(x)$,$B'_{ij}(x)$ and $D'_{ij}(x)$ are obtained by inverting the stiffness constants $A_{ij}(x)$,$B_{ij}(x)$ and $D_{ij}(x)$.Define the average in-plane compliance of the model under a uniformly applied in-plane stress resultant by

$$\overline{A'_{ij}}^{\mathrm{C}} = \frac{2}{n_g a} \int_0^{\frac{n_g a}{2}} A'_{ij}(x)dx \tag{2.34}$$

where the superscript C signifies the crimp model. Since $A'_{ij}(x)$ is a constant within the straight yarn portion of Figure 2.7, last equation can be rewritten as:

$$\overline{A'_{ij}}^{\mathrm{C}} = \left(1 - \frac{2a_u}{n_g a}\right) A'_{ij} + \frac{2}{n_g a} \int_{a_0}^{a_2} A'_{ij}(x)dx \tag{2.35}$$

where A'_{ij} in the first term on the right-hand side denotes the compliance of the straight portion of the yarns, namely a cross-ply laminate, and is indipendent of x. The other average

compliance coefficients $\overline{B'_{ij}}^{\mathrm{C}}$ and $\overline{D'_{ij}}^{\mathrm{C}}$ are obtained in a similar manner.

$$\overline{B'_{ij}}^{\mathrm{C}} = \left(1 - \frac{2}{n_g}\right) B'_{ij} + \frac{2}{n_g a} \int_{a_0}^{a_2} B'_{ij}(x)dx \tag{2.36}$$

$$\overline{D'_{ij}}^{\mathrm{C}} = \left(1 - \frac{2a_u}{n_g}\right) D'_{ij} + \frac{2}{n_g a} \int_{a_0}^{a_2} D'_{ij}(x)dx \tag{2.37}$$

In the case of $n_g = 2$, $\overline{B'_{ij}}^{\mathrm{C}}$ vanishes because $B_{ij}(x)$ is an odd function with respect to $x = \frac{a}{2}$, the center of undulation, due to the assumed form of $h_1(x)$. The final results of the average elastic stiffness $\overline{A_{ij}}^{\mathrm{C}}$, $\overline{B_{ij}}^{\mathrm{C}}$ and $\overline{D_{ij}}^{\mathrm{C}}$ for entire strip can be reached by the inversion of $\overline{A'_{ij}}^{\mathrm{C}}$, $\overline{B'_{ij}}^{\mathrm{C}}$ and $\overline{D'_{ij}}^{\mathrm{C}}$. If this procedure is applied in the warp direction, balanced properties such as $\overline{A_{11}}^{\mathrm{C}} = \overline{A_{22}}^{\mathrm{C}}$ can be realized.

2.7.3 Bridging model and experimental confirmation

The crimp model which is based upon a single fiber yarn has led to the concept of a bridging model for general satin composites. Such a model is desiderable because the interlaced regions in a satin weave are often separated from one another. The hexagonal shape of the repeating unit in a satin weave, as shown in Figure 2.8 is modified to a square shape Figure 2.8 b) for simplicity of calculation. A schematic view of the bridging model is shown in Figure 2.8 c) for a repeating unit which consist of the interlaced region and its surrounding areas. This model is valid only for satin weaves where $n_g \geq 4$. The four regions labeled I,II,II,IV and V consist of straight filling yarns, and hence can be regarded as pieces of cross-ply laminates of thickness h_t. Region III has an interlaced structure with an undulated filling yarn. Although the undulation and continuity in the warp yarns are ignored in this model, their effect is expected to be small because the applied load is asssumed to be in the filling direction. The in-plane stiffness in region III, where $n_g = 2$, has been found to be lower than that of a cross-ply laminate. Therefore, regions II and IV carry bigger loads than region III; all three of these regions act as bridges for load transfer between regions I and V. It is also assumed that regions II, III and IV have the same average mid-plane strain and curvature. Then, the average stiffness constants for the regions II, III and IV are:

$$\begin{aligned}
\overline{A_{ij}} &= \frac{1}{\sqrt{(n_g)}}(\sqrt{(n_g)} - 1)A_{ij} + A_{ij}^{\mathrm{C}}] \\
\overline{B_{ij}} &= \frac{1}{\sqrt{(n_g)}}[(\sqrt{(n_g)} - 1)B_{ij} \\
\overline{D_{ij}} &= \frac{1}{\sqrt{(n_g)}}[(\sqrt{(n_g)} - 1)D_{ij} + D_{ij}^{\mathrm{C}}]
\end{aligned} \tag{2.38}$$

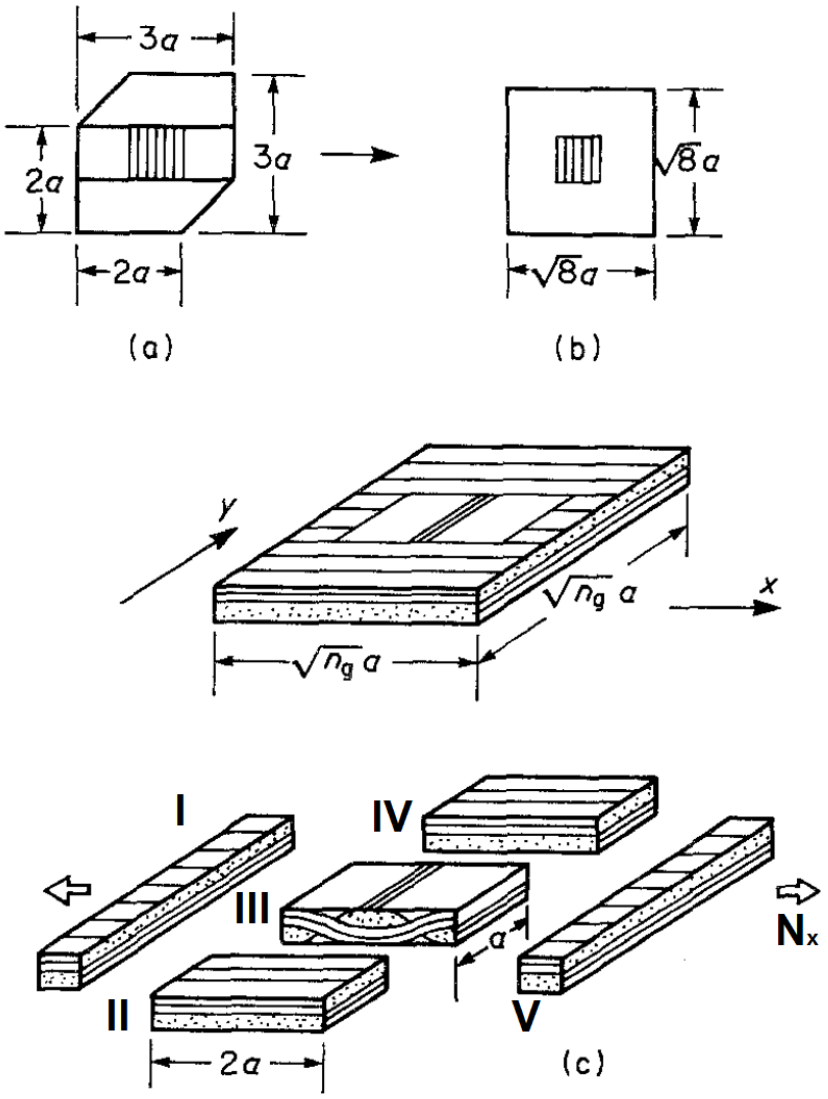

Fig. 2.8 Concept of the bridging model: (a) shape of the repeating unit of eight-harness satin; (b) modified shape for the repeating unit of eight-harness satin; (b) modified shape for the repeating unit; (c) idealization for the bridging model.

The total in-plane force carried by regions II,III, IV is equal to that by region I or V. Then the following average compliance constants are derived:

$$\begin{aligned}
\overline{A'_{ij}}^{S} &= \frac{1}{\sqrt{(n_g)}}[2\overline{A'_{ij}} + (\sqrt{(n_g)} - 2)A'_{ij}] \\
\overline{B'_{ij}}^{S} &= \frac{1}{\sqrt{(n_g)}}[2\overline{B'_{ij}} + (\sqrt{(n_g)} - 2)B'_{ij}] \\
\overline{D'_{ij}}^{S} &= \frac{1}{\sqrt{(n_g)}}[2\overline{D'_{ij}} + (\sqrt{(n_g)} - 2)D'_{ij}]
\end{aligned} \tag{2.39}$$

The superscripts S denotes properties of the entire satin plane. Finally $\overline{A_{ij}}^{S}$,$\overline{B'_{ij}}^{S}$ and $\overline{D_{ij}}^{S}$ can be obtained by inverting last equation. The fiber crimp model is effective for plain weave composites whereas the bridging model is valid for satin weave composites. This is because there are no strainght yarn regions surrounding an interlaced region in the plain weave. Therefore, no bridging effect is expected in plane weave composites, and the analysis based on the fiber undulation model provides a reasonable prediction of the behavior of plain weave composites.

2.8 Composite manufacturing processes

The manufacturing of polymers and development of new technologies for their composites have contributed a lot in the composite manufacturing science. In this section a review of currently available manufacturing processes methods for FRPs has been presented. The recent developments in each technology area are surveyed and various new applications and advantages/disadvantages have been discussed.

2.8.1 Autoclave

The maximum performance of thermoset composite materials can be achieved by autoclave process. During autoclave process the material is subject to elevated pressures and temperatures. The autoclave is basically a very large, internally heated pressure vessel, with internal connections for vacuum hoses and sensors such as thermocouples. The autoclave is usually computer controlled, and often pressurized with nitrogen or carbon dioxide to reduce the risk of an internal fire. [5] In the autoclave, a composite is laid up and enclosed in a vacuum bag and the pressure in the vacuum bagging is equal to one bar and to increase pressure to more than one bar, additional external pressure is required. A full or partial vacuum is drawn within the bag and the bag is kept inside the autoclave chamber where the pressure is kept at more than one bar, usually pressures is rise up to 5 7 bar, this extra pressure is added on the exterior of the bag. Simultaneously the temperature is raised which results in reduction in viscosity of the polymer.

2.8.2 Out-of-autoclave (OoA) methods

Autoclave cure is commonly used for high-performance aerospace composites. In this cure method, high pressure is applied in an autoclave to suppress void formation and to obtain appropriate fiber volume fraction and thickness. However, because the autoclave uses facilities for high heat and large pressures in the curing stage, substantial installation costs

are incurred with composite fabrication.[90] Furthermore, structural sizes are limited by an autoclave size even though manufacturers are seeking integral molding for large-scale structures to reduce product weight and manufacturing cost. Out-of-autoclave (OoA) methods are attractive alternatives to the conventional autoclave method. Researchers and industries have developed several OoA methods in the past few decades (e.g. resin transfer molding, pultrusion, etc,). [75]

2.8.2.1 Hand layup

Hand layup is an oldest open-mold process used for the composite manufacturing. This process is simple, and it is a low-volume and labor-intensive process. Large components, such as boat hulls, can be prepared by this technique. Reinforcing mat or woven fabric or roving is placed manually in the open mold, and resin is poured, brushed, or sprayed over and into the glass plies. Squeegees or rollers are used to remove the entrapped air manually to complete the laminated structure. The most commonly used matrixes are polyesters and epoxies that can be cured at room temperature. The time of curing depends on the type of polymer used for composite processing. For example, for epoxy-based system, normal curing time at room temperature is 24–48 h. A catalyst and accelerator are added to the resin, which enables room-temperature curing of the resin. In order to get high- quality part surface, a pigmented gel layer is first applied on the mold surface. Hand layup is the most commonly preferred process for the manufacture of polymeric composites. [45]

2.8.2.2 Pultrusion

Pultrusion process generally involves pulling of continuous fibers through a bath containing resin, mixed with a catalyst, and then it is passed through a preforming fixture followed by a heated die. The excess resin is removed and the component is partially pre-shaped while passing through the performing fixtures. The sectional geometry and finish of the product are determined by a heated die. Further curing is often required for a good quality product. The strength and weight of the profiles produced by this process compete with the traditional metal profiles made of steel and aluminum. The composite sandwich panels are designed, pultruded, tested, and evaluated for their mechanical performance in relation to the panels, which are manufactured from vacuum-assisted resin transfer molding (VARTM). Pultruded panels show significant advantages over VARTM panels, including increased tensile strength and stiffness, increased bending stiffness at panel level, and reduction in material and production costs. [45]

2.8.2.3 Liquid composite molding process

In liquid composite molding (LCM) processes, a premixed liquid thermoset resin is injected into a dry fiber perform in a closed mold. As the liquid spreads through the preform, it coats the fibers, fills the space between the fibers, expels air, and finally as it cures, it transforms into the matrix. This section describes two LCM processes, namely RTM, VARTM and VARI.

2.8.2.3.1 Rtm Resin transfer molding (RTM) is a low-pressure closed molding process for moderate- and high-volume production, it shows in Figure 2.9.

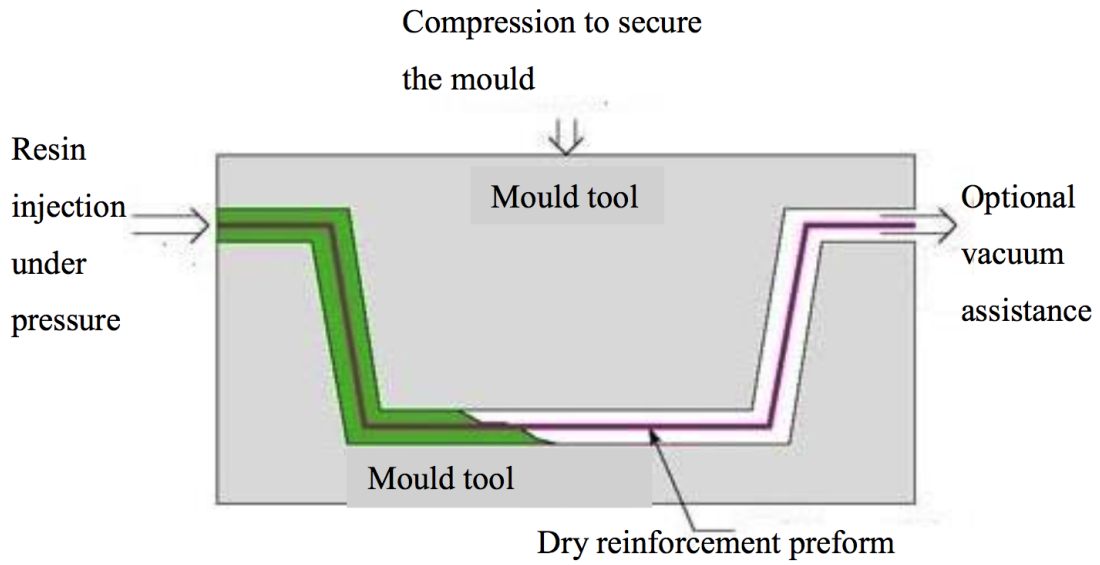

Fig. 2.9 RTM Process

This process basically involves placement of the dry reinforcement in the bottom part of the mold, and then the other half is clamped over the bottom mold. For complex shapes, preforms are used. After closing the mold, a low-viscosity liquid resin containing catalyst is pumped in, which displace the air through strategically located vents. The resin/catalyst ratios are controlled by metered mixing equipment and injected into the mold. The resin is injected into the closed mould to impregnate the reinforcement. The commonly used matrix resins include polyester, vinyl ester, epoxy, and phenolics. Both injection and curing can take place at either ambient or elevated temperature. In order to have optimum surface finish, a gel coat is applied to the mold surface prior to molding. High-quality parts such as automotive body parts, bathtubs and containers are produced by this method. [45]

2.8.2.3.2 Vacuum Assisted Resin Infusion Moulding RTM process is modified by using vacuum for efficient resin transfer and impregnation. VARIM (Vacuum Assisted Resin Infusion Moulding) has become synonymous with a cost-effective process for producing high-quality large-scale composites. The VARTM process comprises three steps: constructing a vacuum package, resin filling, and curing. In the first step, to prepare the vacuum package, a chemical agent was applied to the mold surface and left to dry. After that, a dry preform is covered with a peel ply and distribution medium, and then enclosed by a vacuum bag with a sealant. [78] Both the chemical agent and peel ply were applied to prevent the adhesion of the final CFRP fabric to the mold and/or other components. Infusion mesh was put on top the peel ply. In the VARTM process, the infusion mesh is used to promote resin flow through the reinforcement, facilitating the ability of the vacuum pump to draw resin into any voids before resin curing. The inlet for infusion, composed of a rubber connecter and a segment of spiral tube, was positioned on the distribution medium. The vent for air and excess resin elimination was positioned on the other side of the inlet. Because the inlet and vent are considered critical points in the entire process, they are tightly sealed with sealant tape. The entire package was enclosed in a vacuum bag and sealed with gum tape. Finally, two external hoses were connected to the inlet and vent. The first hose connected the inlet to the resin source, and the second hose connected the vent to the vacuum pump through a catch pot with a pressure gage. Because the sealing, using sealant tape, is very sensitive and any small leakage will lead to failure of the entire process, a sealing test was made before resin filling. In this test, the inlet was closed and the vacuum pump was turned on to draw the air trapped inside the mold; then, the vent line was closed and the vacuum pump switched off, and the mold was left for some hours. Then, the line was opened and any movement of the pressure gage indicator indicates leakage, and thus the need for an additional check-up to seal the leak. After establishing the vacuum, degassed resin was infused from the inlet.[2] Curing and demoulding steps follow the impregnation process to finish the product. A diagram of the process is illustrated in Figure 2.10 The main steps of the process are [28]:

1. Dry fabric or preform and accompanying materials such as release films, peel plies are laid on tool surface.

2. The preform is sealed with a vacuum bag and the air is evacuated by a vacuum pump.

3. Liquid resin with hardener from an external reservoir is drawn into the component by vacuum.

4. The liquid resin with hardener is infused into the preform until complete impregnation.

5. Curing and de-moulding steps follow the impregnation to finish the product.

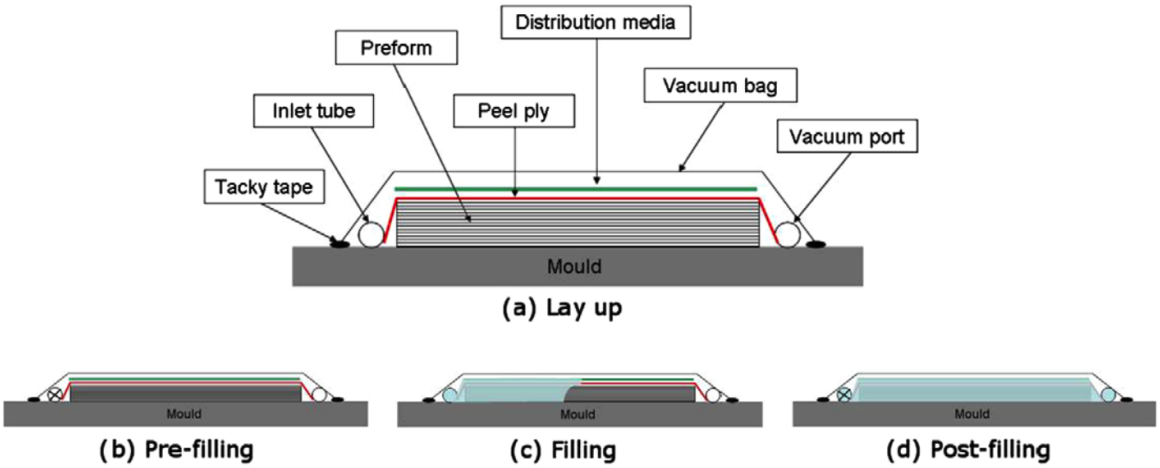

Fig. 2.10 VARIM Process: (a) lay-up, (b) pre-filling, (c) filling, (d) post filling. [30]

2.9 Residual deformation after manufacturing

The mechanical properties of a molded part and their variations from part to part depends on many factors, including the quality of raw materials, the degree of cure, and the presence of molding defects in the part. Many of the molding defects can be either eliminated or reduced by proper part and mold designs as well as by controlling the various process parameters described in the earlier sections. Since complete elimination of all molding defects is not possible, it is important that the quality of the molded parts be inspected regularly for critical defects that can cause premature failure in a part during its service. The criticality of a defect or a group of defects is established through extensive testing at the prototype development stage. The quality inspection techniques and the part acceptance criteria are also established at the prototype development stage.[59]

2.9.1 Raw materials

Among the raw materials, the two most important candidates for close quality inspection are fibers and resin. Measurements of tensile strength and modulus are the primary screening methods for continuous fibers. For the resin, curing agents, or diluents, the standard quality inspection items are the density, viscosity, color, and moisture content. Additional tests recommended for the incoming resin and other components are (1) wet chemical analysis to determine the amount of functional groups (such as epoxide groups in epoxies or acid numbers in polyesters) in the material, (2) infrared (IR) spectroscopy or nuclear magnetic resonance (NMR) spectroscopy to fingerprint the chemical structure and impurities, and (3) liquid chromatography or gel permeation chromatography (GPC) to determine the weight-

average molecular weight and molecular weight distribution of the resin molecules.[59] The average molecular weight and molecular weight distribution are two very important characteristics of a resin that control its viscosity and mechanical properties. Raw materials are often purchased by the part manufacturer in the form of prepreg rolls. The prepreg characteristics that influence its moldability as well as its mechanical properties are resin content, volatile content, filament count, filament diameter, gel time, and resin flow. The gel-time and resin-flow tests can indicate cure advancement in the B-staged resin, which in turn is related to the tackiness and drapability of the prepreg as well as to the fluidity of the resin during the molding process. Proper tack is required to (1) adhere the prepreg to the mold surface as well as to the preceding ply and (2) release the backup film without separating the resin from the prepreg. The prepreg should also be sufficiently drapable to conform to the contour of the mold surface. The gel-time and resin-flow tests are inadequate to detect variations in resin formulation. To improve the quality assurance of the B-staged resin in the prepreg, chemical and rheological tests, such as liquid chromatography, differential scanning calorimetry (DSC), and dynamic mechanical analysis (DMA), should be adopted.[59]

2.9.2 Cured composite part

Quality inspection of cured composite parts includes both destructive and nondestructive tests (NDT). Examples of routine destructive tests are burn-off tests for checking the fiber weight fraction and tension tests on specimens cut from the finished parts for checking their strength and modulus values. Performance tests on randomly selected parts are also recommended. Simple NDT include thickness measurements, visual inspection for surface defects, and proof tests. In proof tests, each part is loaded to predetermined stress levels, which are usually lower than the design stress level. A cured composite part may contain a multitude of internal defects, such as voids, delaminations, fiber misorientations, and nonuniform fiber distribution. Some of these internal defects may act as or grow into critical flaws during the service operation of a part and severely affect its performance. During a production process, these defects are detected by NDT, and parts are either accepted or rejected on the basis of defect quality standards developed earlier at the prototype development stage. In the event of service failure, the NDT records can also serve a useful purpose in analyzing the cause of failure. At the present time, both ultrasonic and radiographic tests are performed on structural composites used in aircraft or aerospace applications. Other NDT methods, such as the acoustic emission test, thermography, and the acousto- ultrasonic test, are used mostly as research tools to monitor damage development during mechanical tests of composite specimens. A common problem with all these tests, including ultrasonic and radiography,

is the lack of standards that can be used to distinguish between critical and noncritical defects.[59]

2.9.3 Structural health monitoring in composite

As the use of fiber reinforced polymer matrix composites increases in applications ranging from aerospace and military field to those in civil infrastructure, the need for ensuring a high level of quality control is also increased. Simultaneously, there is a need to ensure that products and systems respond as required over extended periods of time. Thus, while there is a continuing need for methods of non-destructive evaluation (NDE), especially those capable of rapidly detecting even smaller sized defects, there is also a need to go further than just detection to the assessment of the effect of the defect on performance and life. This extension of NDE which includes the steps of diagnosis and prognosis is often known as structural health monitoring (SHM). [51] Structural health-monitoring systems can be classed as two types of systems: passive and active sensory smart structures. The passive sensory smart structure contains only sensors and electronics, with a communication mechanism and potentially some storage and processing capability, which is capable of processing the sensor data in such a way that will provide the operator with structural condition information. These systems are passive to the extent that the sensors are using the structural in-flight loads to detect/monitor structural damage. Active sensory systems contain both sensors and actuators. In this case, the actuators provide a well-defined (known) excitation and the response is monitored by the sensors. This sensing system can be used on demand by the operator, for example, at the beginning or end of each flight. Current approaches to ensure aircraft integrity for metallic components rely simply on measuring fatigue consumption, achievable through the use of usage monitoring techniques. However, when this approach is combined with continuous damage detection it is called a health and usage monitoring system (HUMS) or structural health monitoring (SHM). This approach can eliminate or drastically reduce the need for inspection. The ability to detect damage is particularly important for composite structures that are susceptible to impact damage and disbond damage in secondary bonded joints. Here, SHM systems will enable the detection and characterization of this type of insidious damage. The introduction of SHM-based structures may allow less stringent certification requirements, thus reducing the cost of certification of composite structures and possibly reducing certification concems with secondary bonded structures. Using smart sensor concepts, damage and damage growth in the airframe and other structural life-related problems would be continuously monitored on-board the aircraft to provide real-time damage assessment. This technology could permit a reduction in inspection and regular maintenance costs with substantial impact on the through-life costs. The overall goal is for the

structural health monitoring system to form a sub- system of a total integrated vehicle health monitoring system (IVHMS).To achieve this goal, significant progress needs to be achieved in the areas of structural health monitoring sensors, data/information processing, diagnostic and prognostic algorithm development, and data dissemination and storage. Current SHM programs are concentrating on the demonstration of various sensor systems, such as optical fiber and piezotransducer systems, through civil flight- testing and the development of design guidelines for incorporation of sensors into composite manufacturing processes. [5]

2.9.4 Methods of Non-Destructive Techniques

There are varieties of methods to evaluate materials or components and non-destructive methods are an important category of them with many applications. The field of Non-Destructive Evaluation (NDE) or Non-Destructive Testing (NDT) involves the identification and characterization of damages on the surface and interior of materials without cutting apart or otherwise altering the material.[69] Traditional NDE technologies are based on the detection of damage or defects (often caused during the manufacturing process or intrinsic in the raw constituent materials) which in the case of composites can range from air bubbles, voids, and blisters, fiber/fabric misalignment and/or wrinkling, fiber failure, matrix crazing and cracking, resinrich or poor sites, layer separation and delaminations, as well as to aspects such as bond failures, crush ing of cores and core shear. [51] The basic types of NDT methods include contact and non-contact methods and both of them have their specific applications in testing and evaluating the composites. Most NDT techniques require good contact between the sensor and tested composite surface to obtain reliable data. Contact methods are traditional ultrasonic testing, eddy current testing, magnetic testing, electromagnetic testing, and penetrant testing. Another approach to speed up the data collection process is to eliminate the need for physical contact between the sensor and tested structure. Non-contact methods are through transmission ultrasonic, radiography testing, thermography, shearography, and visual inspection. Optical methods (e.g. thermography, holography or shearography) are mostly non-contact. [69] Since the presence of defects in reinforced plastics, either "ab initio" or as a consequence of damage in service, is to some extent inevitable, it follows that manufacturers and users need sensitive techniques for the detection of these defects and damage. Much of the technology previously developed for metallic engineering materials and structures has been transferred across, with appropriate modifications, for use with fibre composites. Some of these techniques are more useful than others, and it is often good practice to use a back-up technique where possible rather than to rely on a single method. Brief details of some of these NDT tools are given below.

Chapter 3

The experimental and model methodologies

In this chapter the epoxy resin will be analyzed through the experiment with DSC the resin, the fiber-optic resin and fiber-optic resin and woven structure will be modeled. This analysis is intended to understand what corresponds to the strain value recorded by a distributed optical fibre sensor embedded in an epoxy carbon fibre panel. There is a detailed description of the composite model strain to understand the strain value recorded by an optical sensor distributed during the liquid-gel phase curing stages into a composite plate using the VARIM manufacturing process.

3.1 Experimental Set-up

3.1.1 Resin System characterization

Differential Scanning Calorimetry (DSC) is used to investigate the curing performance of the resin. Measurements are made of the energy absorbed or released by a sample as it is heated, cooled and/or held on an isotherm. Thus DSC measures the heat flow from or into the sample provides information about the endothermic or the exothermic nature of resin system reactions. DSC measurements can be divided into two types of tests, isothermal measurements and dynamic measurements. Isothermal scanning measurements involve keeping the sample at a fixed temperature up to some fixed time. Dynamic scanning measurements (non isothermal) involve heating the sample at a fixed temperature gradient over a desired temperature range. All the DSC experiments in this study were carried out using a DSC Q100 analyzer from TA Instruments. The commercial epoxy resin system LY564/HY2954 is commonly used for the manufacturing of a wide range of industrial composites and has been chosen as

the resin system for the present manufacturing experiments. The resin system supplied by Huntsman consist of two components: Araldite LY564 the epoxy matrix and its hardener Aradur HY2954.

3.1.1.1 Preparation

The resin and the hardener were well mixed using a resin to hardener mixing ratio of 100:35 (by weight), then the resin system was degassed at room temperature in a vacuum chamber for 20 minutes. After mixing and degassing the neat resin system (unreinforced) was enclosed in aluminium pans, then were measured the weights of resin system samples and the samples weights were between 5 and 10 mg. The cure kinetics of the epoxy system samples were characterized by differential scanning calorimetry (DSC) in both isothermal and non-isothermal conditions.

3.1.1.2 Experiments

To carry out the DSC investigation, dynamic scans were performed by loading the samples at 25 °C, holding at 25 °C for five minutes to assure equilibrium between the samples and reference temperatures, then heating them at a rate of 5 °Cmin^{-1}, 10 °Cmin^{-1} and 15 °Cmin^{-1} to 320 °C, until no further exotherm was observed. A dynamic DSC trace of sample at a heating rate of 10 °Cmin^{-1} is shown in figure 3.1. The total heat of reaction of the epoxy resin system LY564/ HY2954 is the area under this curve which has been measured to be 409 Jg^{-1}, comparing well with the value of 409.5 Jg^{-1} reported by Lee and Wei [55] analysing an identical resin system at the same heating rate of 10 °Cmin^{-1}.

$$H_{\mathrm{u}} = \int_0^{\infty} \dot{Q}\, dt \tag{3.1}$$

Integration of the exothermic peak was carried out by determining and subtracting the instrument baseline followed by a simple integration of the peak itself (see figure 3.1):

3.1.1.3 Isothermal DSC Experiments

The isothermal DSC experiments were conducted at 80 °C, 100 °C and 140 °C. All samples were loaded into the DSC at 25 °C. After loading the samples the DSC was quickly driven to the desired temperature, then data acquisition was begun and the samples were kept at constant temperature for 120 minutes. The heat released up to some time t is $H(t)$ was determined by:

$$H(t) = \int_0^{t} \dot{Q}\, dt \tag{3.2}$$

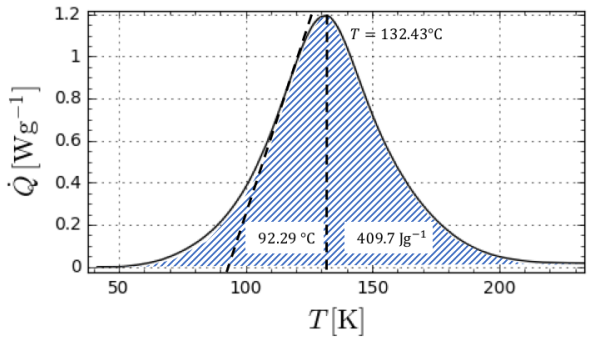

Fig. 3.1 DSC dynamic scan at a heating rate of 10 °Cmin^{-1}.

These values were subsequently used to derive the degree of cure over the isotherm and characterise the resin completely.

3.1.2 Panel manufacture experiment

A Vacuum Assisted Resin Infusion Moulding (VARIM) composite processing methods based on the impregnation of a dry layers reinforcement by liquid thermoset resin driven under vacuum environment was used to manufacture:

1. one 5-harness satin (5HS, see figure 3.25) weave carbon fibre with an epoxy resin system LY564/HY2954 composite panel 450 mm x 200 mm. The non isothermal temperature curing cycle used in the first manufacturing experiment is shows in 3.2. [70]

2. one 5-harness satin weave carbon fibre with an epoxy resin system LY564/HY2954 composite panel 200 mm x 200 mm. The non isothermal temperature curing cycle used in the second manufacturing experiment is shows in 3.3

3. one 5-harness satin weave carbon fibre with an epoxy resin system LY564/HY2954 composite panel 200 mm x 200 mm. The non isothermal temperature curing cycle used in the third manufacturing experiment is shows in 3.4

The first and the second panel follows a standard cure cycle suggested by the resin system supplier.The third pannel have a different cure cycle, the cooling phase is different.At the end of cure process in the case of the first and second panel the oven is turned off and the cooling phase follows Newton's Law of Cooling, then the cooling process is very slow. In the third panel at the end of cure, the oven is opened and the hot air is expelled out of the

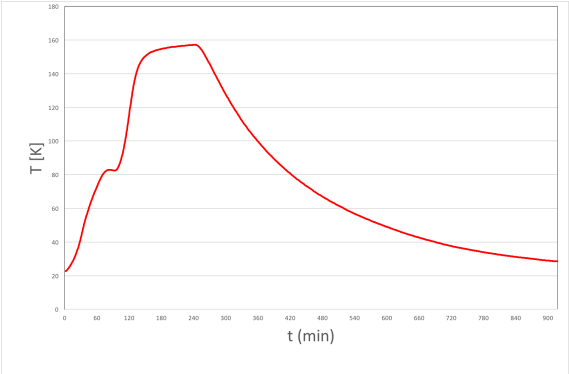

Fig. 3.2 The non isothermal temperature curing cycle used in the first manufacturing experiment.

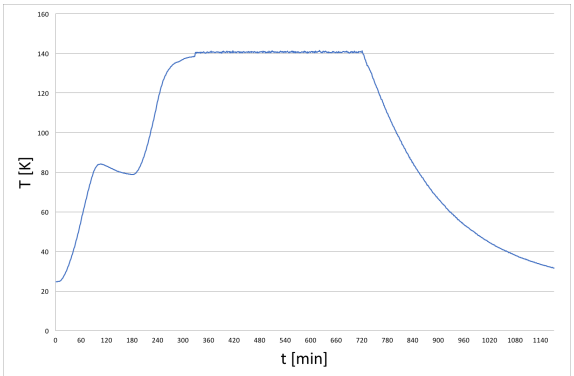

Fig. 3.3 The non isothermal temperature curing cycle used in the second manufacturing experiment.

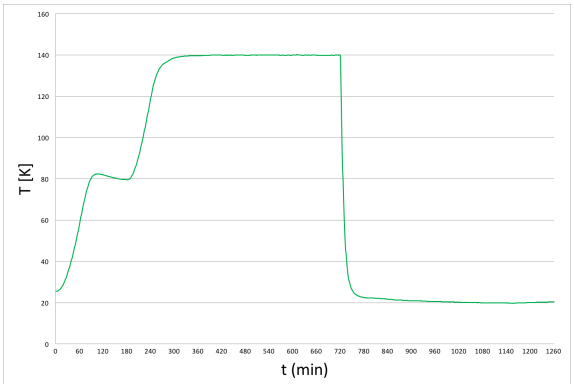

Fig. 3.4 The non isothermal temperature curing cycle used in the third manufacturing experiment.

oven quickly. Each panels has been manufactured using the following steps manufacturing processing and are presented in the next subsections.

3.1.2.1 Preparation of Materials: Woven fabric reinforcement

The first step of all the manufacturing process was to decide and establish the preform dimensions (size and number of layers) having in mind that the mould and hence the bagging and working space available was of 60 cm x 60cm.[70] Once defined the final dimensions of the first test specimen (a 6-layered CFRP rectangular shape test coupon of 42cm x 15cm), six 45cm x 20cm layers of woven carbon fibre sheets were cut and kept separately, exceeded dimensions were left for later trimming to obtain the previously established sample dimensions. [70]. The dimension of the second and third test specimens are the same, 6-layered CFRP square shape 20cm x 20cm. Once defined the dimension of the layers the flash tape is positioned on top of the fabric for delimitate the dimension decided and to avoid the fibre losing by the layers as shown in figure 3.5. With the help of a marker and a ruler, the individual cutting points are identified and straight lines are drawn to locate the layer's sides. The fabric were cut with a fabric's cutter and positioned in a safe place.

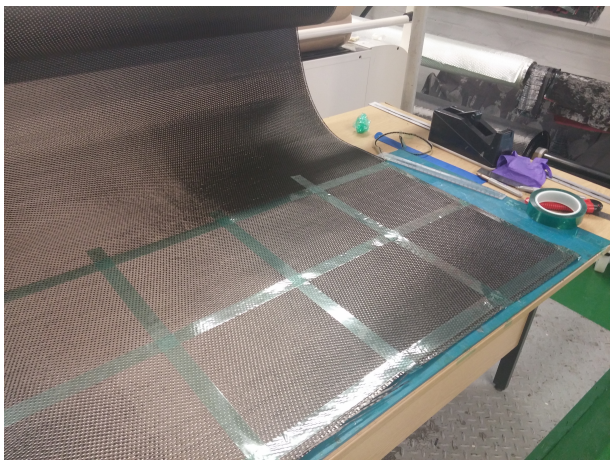

Fig. 3.5 The green flash tape placed along the fabric's edges.

3.1.2.2 Preparation of Materials:Mould surface preparation

After remouve resin residual on the mould from previous formation of composite with a spatula it was spread all over the mould plate a mould cleaner. The cleaner is used to dissolve and clean a stainless steel flat mould from surface contamination of resin residues (about 3 coatings were used for better results). After preparing the mold surface a chemical release

system was applied uniformly on the mould surface (about 5 coatings were used for better results) to eventually release the product after manufacture and to obtain a smooth surface finish. The clean and release operation took about 2 hours, when the mould surface is dried up, the carbon fibre fabric were stacked on the mould.

3.1.2.3 Embedded the OrFDR in the woven fabric and set-up LUNA ACQUISITION SYSTEM

In order to acquire strain and temperature data while monitoring the infusion and curing processes, and later during mechanical testing of the composite sample, the optical fibre sensor was needed to be conditioned for a more accurate sensing operation. Due to the nature of this type of sensor to be sensitive against strain and/or temperature changes along the optical fibre (both at the same time if no stress-free condition is present), it was proposed to isolate some sections of the optical sensor with PTFE capillary jackets (Figure 3.1.2) (10 mm long each). By doing this, the protected segments of the optical fibre are then intended to be only sensitive to temperature changes, achieving an almost free-strain condition. On the first fibre layer, eight protective jackets were equally spaced positioned one from each other and slightly glued, serving as a guideline for the optical sensor along the plate (Figure 3.1.3). A similar proceeding was done for the third and fifth layers. The fibre optic sensor was carefully passed through the six reinforcement layers so that the end tip of the sensor (which reflects the light back to the interrogator) would stay at the bottom of the plate, leaving the input on the top side, while making it possible to trace two semi-circular loops to change the sensor's direction between layers (Figure 3.1.4). Once the optical sensor was passed through the layers and the already glued jackets with the final configuration, the jackets' ends were sealed with epoxy adhesive, impeding resin to fill inside them during infusion, avoiding with this any stress propagation throughout the resin to the optical sensor and therefore obtaining a total of 24 temperature probes uniformly distributed over the plate. Just have to point out that the inlet of the sensor into the carbon fibre plate constitutes the 24th temperature sensor and was used as temperature reference probe since the PTFE protection covers the sensor fibre from the connector to the inlet at the plate. In the end, the sensor remained on top of the first, third and fifth layers (Figure 3.1.5).Regardless of the optical sensor positioned between the carbon fibre layers, three K- type thermocouples were also placed on top of the stack with each sensing tip allocated closely to the different levels of the optical sensor. During this process dry fabrics with embedded OFDR (optical frequency-domain reflectometry), peel plies and a knitted infusion mesh are placed onto the tool surface and a plastic vacuum bag is placed on top of the assembly. The one-sided mold is connected with a resin source and the air inside that vacuum bag is evacuated by a vacuum pump. The peel plies are placed

on the top of the dry fabric, which is porous layer and allows the vacuum to bleed trapped air and volatile materials out of the laminate assembly. The resin system flow through the dry fabric is entirely assisted by the vacuum pressure. A highly permeable layer called the "resin distribution medium" is placed on the top of the preform spreads the resin quickly over the lateral extent of the part. The resin front moves both in the planar as well as thickness direction [91]. When the part is completely wetted out, the infusion lines are closed and the part is put inside the oven and curing started. Curing and demolding steps follow the impregnation process to finish the product and the vacuum is maintained until the end of cure [37, 29]. To monitor most of the composite panel with the optical fibre sensor, the lay-up and the sensor embedding designed in such a way that strain information from along, across and through different layers could be acquired together with a single optical sensor in a continuous measurement. A polyimide coated silica glass optical fibre sensor 2-m long, 250 μm diameter, single-mode, low-bend-loss was embedded symmetrically across three of six 400 x 200 mm plies of 5HS satin carbon fibre. The optical fibre position required careful insertion between the composite layers. With help of a common pin, the optical sensor could be safely attached and positioned where desired without using glue or any bonding aid initially (bonds to the resin afterwards). In this way the overall properties of the finished part remain in tact and the presence of the sensor does not influence mechanical or chemical properties especially since it is parallel to the weave direction [54]. In the first pannel the optical fibre embedding was performed in this way from the top layer down to the bottom later in the shape of an "S", so that the input side ended on the top lamina as in figure 3.6. Each sensing region is 50mm apart, separated from each other and from the panel edges; its

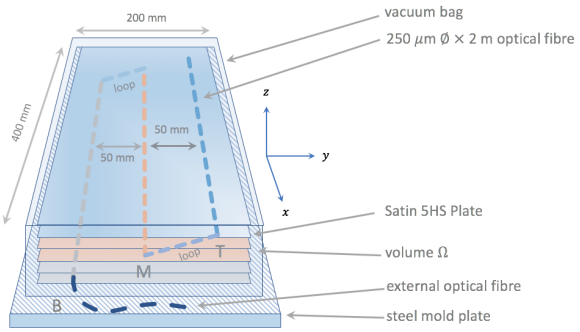

Fig. 3.6 Embedded optical sensor and composite panel geometry.

length is about 300 mm, holding 460 sensors with a gauge length of 1.25 mm. The portion of the OFS embedded in the panel was completely bare fibre, allowing it to fully interact with the composite and its changes during the manufacturing process. At the end of the sensor

embedding within the stack, a 10 mm portion of the protective sleeve was pushed through the top carbon fibre lamina, ensuring a safe insertion of the sensor, since it becomes very easy to break the optical fibre right at its panel exit location. Special care was taken for the placement of the sensors across the sealant tape to avoid air leaks and assure a steady vacuum environment for the composite manufacture. Also, the PTFE jacket was sealed from the inserted end to block any resin flowing inside the tube, which makes the sensor assembly very brittle and unmanageable. Distributed stress data was acquired from the sensor via an OFDR based interrogator from LUNA Technologies, ODiSI B model. In addition to this, temperature measurements recorded with K Type thermocouples as in figure 3.13. Three thermocouples were also embedded, each close to the sensing sections of the optical fibre. This gave information about the resin distribution during infusion and the thermal behavior at each level of the composite while in the curing oven [70]. The second and third pannel were made with the same 5hs fabric and with the same resin system of the first one, but the cure cycle and the distribution of optical sensor were not the same of the first one. The optical sensor distribution is shows in the figure3.7.

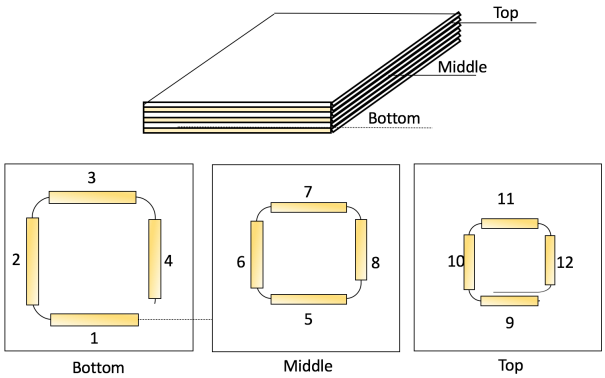

Fig. 3.7 Embedded optical sensor and composite panel geometry.

3.1.2.4 Bagging process and vacuum application

To remove the air under the bag, a vacuum pump is used and a pressure of one atmosphere is applied to achieve the consolidation of the laminate. Having all the reinforcement layers stacked together, with the optical fibre sensor and thermocouples embedded, the next step was to place the bagging materials (resin infusion mesh, peel-ply, bagging film, bag sealing tape, etc.) in order to enclose the carbon fibre feature and create a vacuum environment while performing the resin infusion, subsequently placing the inlet and outlet spiral tubes for the

resin flow (Figure 3.1.6) Here it was needed to look after the sensor inlet which needed to be connected from the outside of the vacuum bag without letting any pressure drop to take place (no air should get into the bag), guiding the fibre sensor out of the mould and sealing its pass through the bag with bag sealing tape (tacky tape). After performing a vacuum test inside the bagged mould and verified that there were no air leaks using a vacuum meter and making a very close inspection, then the mould was ready for the resin infusion.

3.1.2.5 Resin System preparation and degassing

Depending on the sample's dimensions and the volume fraction desired, the amount of resin and hardener needed is calculated. For and aim in volume fraction about 60% fibres and 40% resin within the sample prepared, an estimated thickness of 0.28 mm was used for each fibre layer in order to obtain the total volume of the composite sample (with the previously stated length and width dimensions). Once calculated the previous and obtained the volume of resin (including hardener) it was then converted in terms of weight by employing the resin and hardener's density found in the product's spec sheet, stating also de amount of each substance according to the mixing ratio (35 parts of hardener per 100 parts of resin, by weight). An extra amount of resin mixture (50% more) was added to the calculated total due to losses by preparation and the resin that remains inside the feeding tube. This also helps to not run out of resin during infusion. The amount of each component was weighed with an accurate scale and together mixed properly, ensuring homogeneity, watching out for crystals and impurities. After a few minutes of mixing, the resin was introduced in a vacuum chamber to remove entrapped air within. The degassing process took around 50 minutes, making sure that no spillage would take place due to the rising foam by letting some air to come inside the vacuum chamber every time resin was about to come out the cup containing it. It is important to notice that everything is already set up for the infusion process before preparing the resin, because once it is ready after degassing, infusion must be performed almost immediately to avoid an advanced curing stage of the resin, increasing its viscosity and making it hard to flow inside the tubes and the sample itself, resulting in a non-homogeneous or in an incomplete infusion, possibly having to start again all the set up.

3.1.2.6 Infusion process

The main purpose of the resin infusion process is to first remove all the air present between the carbon fibre laminate and then fill in the stack with resin by means of a vacuum assisted resin injection. After this, the carbon fibre layers will be strongly bonded together within an epoxy resin matrix. To achieve the previous, it is important to keep the vacuum inside the

bag of the preform during the infusion, and later the curing, processes. A couple of clamps were used to help keeping closed the inlet and outlet tubes, for example, after testing the bag for any air leaks after the preform preparation and the bagging process. Right after degassing the resin, infusion took place. With the inlet tube clamped and the outlet tube connected to a vacuum pump already working, the end of the inlet tube was immersed at the bottom of the resin cup and finally unclamped to let the resin flow into the mould (Figure 3.1.7). The infusion process should not last too long due to the curing of the resin taking place, but the vacuum must still be present all along this manufacturing step. After noticing that the top surface of the stack was fully wet with resin, the pump was left to operate a little bit more to ensure that also the layers beneath were also filled with resin. Afterwards, both tubes, inlet and outlet, were again clamped and the pump disconnected. One important thing to take into account for resin infusion is the room temperature at which the process is being held. Low temperature (below 18°C) will rise the viscosity of the resin, making it harder to flow first, into the mould, and then, inside the fibre layers. If infusion is going to be performed at a low temperature, it is then recommended to pre-heat the resin (around 25°C) for better results and easiness. Resin flow inside the mould was monitored with the optical fibre following the change in strain, with a baseline set after only vacuum with no resin was applied.

3.2 Resin characterisation model

3.2.1 The Kamal Model application on resin system

Once the values of $H(t)$ and H_u are known, the degree of cure $\alpha(t)$ at some time t in minutes can be calculated using the following relation:

$$\alpha(t) = \left(\frac{1}{H(120)} - \frac{1}{H_u} \right) H(t) \tag{3.3}$$

which corrects for post cure exothermic release. Several researchers have modeled the curing kinetics a of thermoset resin and an overview on the models is given by Halley [33]. The thermoset curing reaction rate can be described by kinetic phenomenological models which relate the measured conversion in equation 3.3 to chemical kinetic parameters that determine the reaction rate. The LY564/HY2954 resin system is described well by the Kamal model [46] differential equation:

$$\frac{d\alpha}{dt} = (K_1 + K_2\alpha^m)(1-\alpha)^n \tag{3.4}$$

$$K_1 = A_1 \exp^{-E_1/RT} \tag{3.5}$$

$$K_2 = A_2 \exp^{-E_2/RT} \tag{3.6}$$

Here K_1 and K_2 are Arrhenius rate constants that take into account the autocatalytic nature of the cure process, K_1 equation 3.5 takes into account the catalytic effect of the groups initially present in the formulation, while K_2 equation 3.6 is related to the effect of the hydrolysis groups formed by the epoxide-amino addition reaction [64]. The constants A_1 and A_2 are the pre-exponential factors, E_1 and E_2 are the activation energies, R is the universal gas constant, and T is the absolute temperature. It should be noted that the Kamal model does not account for partial polymerization of a thermoset cured resin, where typically, the degree of cure is less than one. This is because the reaction ends before consumption of the reactants is complete. It is therefore important to take into account the maximum degree of cure by introducing the maximum degree of cure α_{max} achieved by the polymer system during isothermal cure. The Kamal equation 3.4 then becomes:

$$\frac{d\alpha}{dt} = (K_1 + K_2\alpha^m)(\alpha_{\max} - \alpha)^n \tag{3.7}$$

This equation is fitted to the data obtained from equation 3.3 to extract the relationship of its parameters $K_1, K_2, m, n, \alpha_{max}$ as functions of the isothermal temperature T through linear interpolation as shown in figures 3.8, 3.9 and 3.10. Table 3.1 lists these graphical

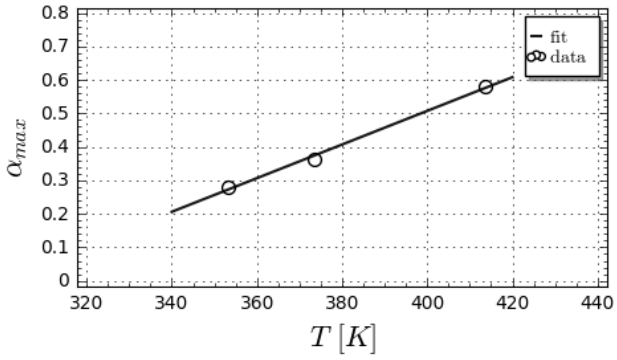

Fig. 3.8 The maximum degree of cure, α_{max} fit and data values.

relationships as a temperature parameterisation of the Kamal model for the LY564/HY2954 resin system. The parameterisation in table 3.1 can be extrapolated to obtain the *complete* model of the resin in the T, α and T, t planes. The parameterisation in T shows good linearity for the most part and extrapolation can be expected to give reasonable results. A simple extension across all α values for $\dot{\alpha}$ is the total Kamal model of isothermal kinetics for the LY564/HY2954 resin used in panel manufacture. This is shown as a rate surface in

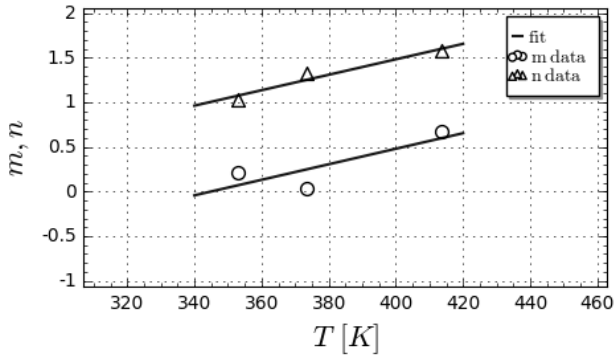

Fig. 3.9 The m, n fit and data values as a function of temperature.

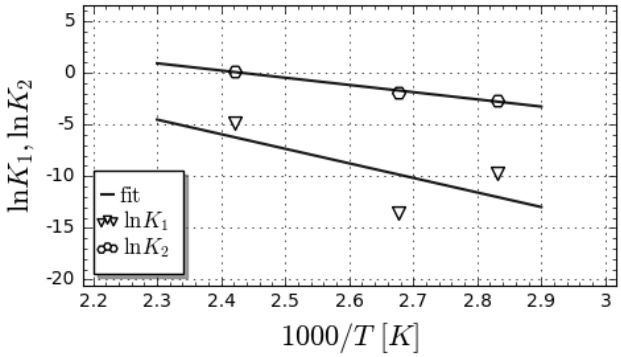

Fig. 3.10 The rate constant logarithms $\ln K_1, \ln K_2$ as a function of inverse temperature.

figure 3.11. The extrapolation was derived from the linear temperature parameterisation of the Kamal model at three different temperatures permitting a complete knowledge of the resin kinetics for use in the structural models. Integrating figure 3.11 produces all the isotherms generated by the parameterisation in table 3.1. The thermokinetic behaviour of the LY564/HY2954 resin system is therefore completely described by the interpolation relationships derived in table 3.1. The relationships provide a description of the resin at every temperature and every state of cure during isolated isothermal processes which allows the prediction of curing development when the temperature profiles are *not* isothermal as in the case of the panel manufacture experiment. The line in bold in figure 3.12 is the line integral of equation 3.3 computed using the applied temperature profile during panel manufacture as shown in figure 3.13. This curve in provides the variation of α as a function of time which describes the thermomechanical and thermochemical behaviour of the composite during cure and is important for predicting the glass transition temperature. Figure 3.12 shows both the α surface for isothermal processing of the isolated resin system as well as the integral

Table 3.1 Parameterisation for equation 3.4

Parameter	Relationship	N
$\ln K_1$	$27.85074 - 14.08090 \times (1000/T)$	1
$\ln K_2$	$16.94357 - 6.971903 \times (1000/T)$	2
m	$0.00870T - 3.00221$	3
n	$0.00865T - 1.98177$	4
$\alpha_{\max}$	$0.00502T - 1.50208$	5

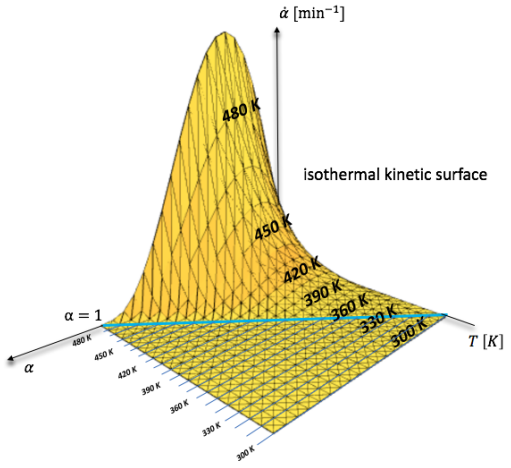

Fig. 3.11 The LY564/HY2954 resin system thermo-kinetic surface derived from the DSC measurements. Note how the maximum cure triangle rate limits the chemical reaction.

curve of the same resin system during the a non-isothermal process. Clearly the solutions differ in their thermodynamic efficiency. The qualitative picture of the non-isothermal line suggests that non-isothermal processes produce a faster and more complete manipulation of the reaction rate in the panel volume during manufacture, which will be seen to have mechanical consequences for the rate at which strain is generated during the manufacturing process (see equation 3.63).

3.2.2 Panel manufacture experiments

The physics of an immersed optical fibre during VARIM composite manufacture is a complicated phenomenon. The composite assembly, during manufacture, moves from a liquid to fully amorphous or glassy state at the glass transition temperature, during which many physical and chemical phenomena need to be accounted for. In this section we apply and

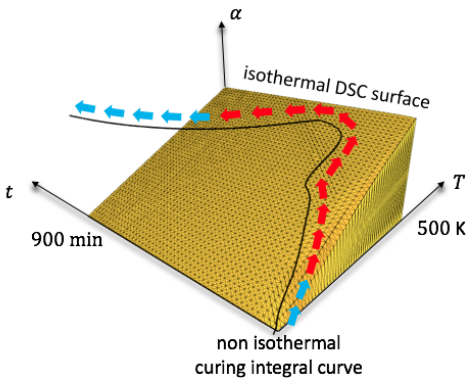

Fig. 3.12 The isothermal and non-isothermal LY564/HY2954 resin system curing parameter variation derived from the DSC measurements.

combine several thermodynamic, chemical and mechanical effects to develop a theoretical model of the curing process inside the panel during manufacture.

3.2.3 Static fluid expansion

We develop and solve a reacting fluid model compatible with conditions inside the panel during the early stages of cure. We will assume that the vacuum infusion process has been completed, the average velocity of fluid particles inside the volume is zero and that the pressure distribution inside the panel volume is uniform as cure is about to begin. Further, the resin system is assumed to be fully penetrated into the carbon fibre 5HS weave and then subjected to the curing profile in figure 3.13. The Newtonian hypothesis has been theoretically shown to be a complete first-order correction to the theory of perfect fluids in the limit where all gradients are small [34]. Thus Newtonian fluids should approximate the behavior of many real fluids in the limit of very slow motion. Various authors [18] confirmed this to be the case through numerical calculations of slow fluid motion through porous substrates. Therefore, for considerations of thermally and chemically driven fluid motion inside the pressurised and confined panel volume Ω, we impose that the highly viscoelastic resin fluid behaves like a Newtonian fluid. In other words, we consider flow dynamics where shear effects are potentially much larger than inertial ones. This is the regime of the slow moving fluid with Reynolds number lower than 5. As will be shortly seen,

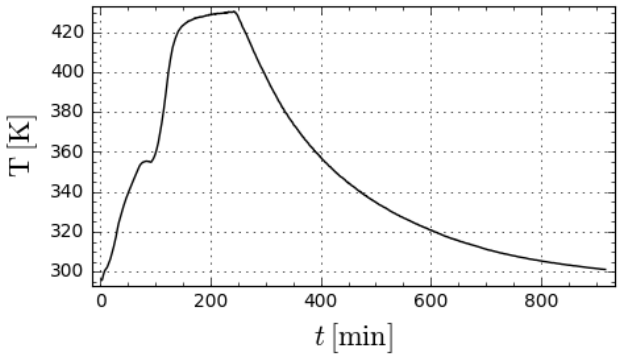

Fig. 3.13 The non isothermal temperature curing cycle used in the manufacturing experiment.

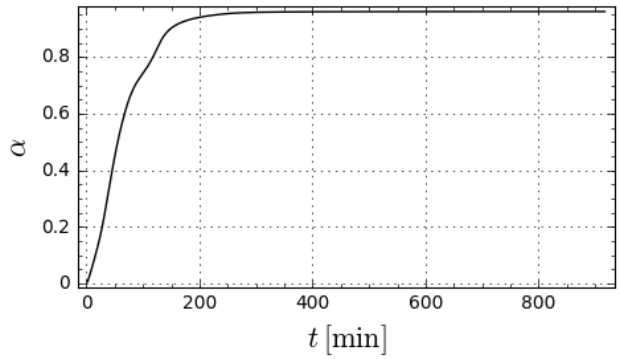

Fig. 3.14 The non isothermal α curing parameter derived as a function of time from the isothermal DSC experimental Kamal model of the LY564 epoxy resin used in manufacturing the panel.

the resulting Navier-Stokes equations can be solved for *non*-shearing flows which seem to largely characterise the curing process.

3.2.4 General theory of reacting fluids

To develop a physical model of the low viscosity cure phase we use the idea that the two components of the mixed epoxy resin are to be treated as interpenetrating continua [34, 3]. The two component chemical species are entirely miscible and that there is no change of phase during reaction. In the mixture we let the suffix i denote the physical properties of the i^{th} chemical species where $i = 1,2,3$ and only one chemical reaction (the creation of cured epoxy resin) is significant. Let $i = 3$ denote the cured resin product, $i = 1$ be the LY564 epoxy compound and $i = 2$ the HY2954 hardner compound. The volume Ω is the thin flat plate region containing the entire composite structure and its continuous boundary is $\partial\Omega$. Inside

Ω the three resin components occupy a total volume $V^{(1)}$. The mass balance of the resin chemical mixture at any point in Cartesian space is described by the integrated conservation of chemical masses over arbitrary volumes giving the Lagrangian or substantial derivative of a differential volume in motion:

$$\frac{d\rho}{dt} + \rho \nabla \cdot \mathbf{v} = 0 \tag{3.8}$$

where ρ is the mass per unit volume of the entire mixture and $\mathbf{v}$ is the mean velocity of the mixture. These two quantities are related to the the individual reacting species by the following combination laws:

$$\rho = \sum_i \rho_i \tag{3.9}$$

$$\rho \mathbf{v} = \sum_i \rho_i \mathbf{v}_i \tag{3.10}$$

where the densities are stoichiometric (defined over the same volume). Assuming a single stoichiometric reaction over the two chemical species where the temperature gradient vanishes over Ω , the balance of linear momentum gives:

$$\rho \frac{d\mathbf{v}}{dt} = -\nabla p + \sum_i \rho_i \mathbf{F}_i + \nabla \cdot \mathbf{P} \tag{3.11}$$

This is the Navier-Stokes equation of the fluid resin reaction where p is the total fluid pressure and the $\mathbf{F}_i$ are the external forces per unit mass acting on each chemical species. The quantity $\mathbf{P}$ is the viscous stress tensor given for a Newtonian fluid of bulk viscosity λ and shear viscosity η by:

$$\mathbf{P} = \lambda \nabla \cdot \mathbf{v}\mathbf{I} + \eta(\nabla \mathbf{v} + \nabla \mathbf{v}^*) \tag{3.12}$$

The viscous stress tensor contributes to the the irreversible work done against viscosity by the fluid motion. Here the rates of reaction have been neglected as having little impact on the composition of the stress tensor and indeed this is commonplace in such general calculations [3]. Since the resin system is reacting chemically, the total energy balance of the reacting system must be considered. The total energy of the reacting fluid is the sum of its kinetic and internal energies. The energy used in internal chemical interactions is not available for mechanical work. Let the total heat flux vector be the sum of the diffusion of heat energy (symbol $\mathbf{q}$) and the heat transport by chemical species mass flux (symbol $\mathbf{j}$). If the specific

enthalpy of a species is h_i then the total heat flux is just:

$$\mathbf{j}_i = \rho_i(\mathbf{v}_i - \mathbf{v}) \tag{3.13}$$

$$\mathbf{j}_q = \mathbf{q} + \sum_i h_i \mathbf{j}_i \tag{3.14}$$

Denoting the specific internal energy by e and the total heat flux vector by $\mathbf{j}_q$ the first law of thermodynamics for a fluid gives:

$$\rho \frac{de}{dt} = -\nabla \cdot \mathbf{j}_q + \sum_i \mathbf{j}_i \mathbf{F}_i + \mathbf{P} : \nabla \mathbf{v} - p \nabla \cdot \mathbf{v} \tag{3.15}$$

where the penultimate term is the total irreversible dissipation of energy by viscous forces and the last term represents reversible dissipation of strain energy by viscous forces. The second term is the net work done by externally acting body type forces. This term will contain the effect of external body and traction forces acting on the panel such as the mold constraint. Defining the species concentration c_i:

$$c_i = \frac{\rho_i}{\rho} \tag{3.16}$$

means that:

$$h = \sum_i c_i h_i \tag{3.17}$$

The specific enthalpy is related to the specific internal energy:

$$e = h - \frac{p}{\rho} \tag{3.18}$$

Using these relationships in the energy balance equation above removes the unknown internal energy and casts the equation in a more useful form:

$$\rho \frac{dh}{dt} + \nabla \cdot \sum_i h_i \mathbf{j}_i = -\nabla \cdot \mathbf{q} + \frac{dp}{dt} + \sum_i \mathbf{j}_i \cdot \mathbf{F}_i + \mathbf{P} : \nabla \mathbf{v} \tag{3.19}$$

The enthalpy of the mixture is thermodynamically related to the temperature, pressure and the mixture composition. This equation can therefore be further reduced by differentiating the individual species concentrations:

$$\frac{dh}{dt} = \sum_i c_i \frac{dh_i}{dt} + h_i \frac{dc_i}{dt} \tag{3.20}$$

Using the conservation of mass, the second term can be reduced to:

$$\sum_i h_i \frac{dc_i}{dt} = \rho^{-1} \sum_i (h_i r_i - h_i \nabla \cdot \mathbf{j}_i) \tag{3.21}$$

where:

$$r_i = \alpha_i m_i r \tag{3.22}$$

The quantity r_i is the specific rate of creation of species i measured as mass created per second per unit volume, α_i is the stoichiometric coefficient of the species and r is the total specific rate of reaction measured as moles per second per unit volume. Thus r has a direct relationship to the quantity α measured in the DSC experiments:

$$\alpha(t) = \frac{V^{(1)} \alpha_3 m_3}{\sum_i m_i} r = \frac{V_3}{V^{(1)}} \tag{3.23}$$

The term $\rho^{-1} \sum_i h_i r_i$ is just the specific rate at which heat $-\dot{Q}$ is created by the reaction, where the dot denotes the total derivative with respect to time. This quantity is measured in heat created by the reaction per second per unit volume. Differentiating the second term $\sum_i c_i dh_i/dt$ can be rewritten thermodynamically:

$$\sum_i c_i \frac{\partial h_i}{\partial T} \frac{dT}{dt} + \sum_i c_i \frac{\partial h_i}{\partial p} \frac{dp}{dt} + \sum_{i,j} c_i \frac{\partial h_i}{\partial c_j} \frac{dc_j}{dt} \tag{3.24}$$

Noting that h is an extensive quantity and that $\rho h = \sum_j \rho_j h_j$ where h_j does not depend upon ρ_j. This means:

$$\rho h = \sum_j \rho_j \frac{\partial \rho h}{\partial \rho_j} \tag{3.25}$$

The ρh can be differentiated as a formal product and written in terms of the species concentrations:

$$\frac{\partial \rho h}{\partial \rho_j} = h_j + \sum_i c_i \frac{\partial h_i}{\partial c_j} \tag{3.26}$$

and then the second term has to vanish [3]. This is equivalent to saying the enthalpies of each species are related only to the density of their own species. The partial derivative sum of h_i with respect to pressure is proportional to density : $\rho l + 1$ where l is like a latent heat of reaction. Lastly writing:

$$c_p = \sum_i c_i \frac{\partial h_i}{\partial T} \tag{3.27}$$

the thermodynamics of the reaction simplifies to:

$$\rho c_p \frac{dT}{dt} + \sum_i \mathbf{j}_i \cdot \nabla h_i = -\nabla \cdot \mathbf{q} + \rho l \frac{dp}{dt} + \frac{dQ}{dt} + \sum_i \mathbf{j}_i \cdot \mathbf{F}_i + \mathbf{P} : \nabla \mathbf{v} - p \nabla \cdot \mathbf{v} \tag{3.28}$$

3.2.5 Reduction of the fluid model

The general model of the reacting species derived in the previous section can be further simplified upon the basis of conditions pertaining to the present experiments. The mixture of reactants $1,2$ in $V^{(1)}$ is assumed to be homogeneous. Further on, this will have important consequences for how mechanical energy is distributed during the cure process. Once the resin fluid is completely permeated through the carbon fibre reinforcement, thus occupying completely a volume $V^{(1)}$ in the vacuum bag, any further displacements in Ω are due only to thermal strains. Physically, the constant atmospheric pressure and restricted movement in the vacuum bag means that the thermal displacements of the resin volume will occur slowly (thus a low Reynolds number). Mathematically, the thermal expansion of a body is approximately a linear isotropic expansion of the space $\Omega \to \Omega'$. In Cartesian coordinates a linear transformation Θ represents the thermal expansion of the resin product 3:

$$\Theta : (x,y,z,t) \to (bx,by,bz,t) \tag{3.29}$$

where $b = \sum b_i$ is the linear isotropic expansion coefficient of the entire reaction. The coefficient of expansion represents the total expansion of *all* three chemicals in $V^{(1)}$. We assume that below the glass transition temperature all three chemicals remain slow moving or creep flowing liquids (with differing fluid properties) at the same applied pressure p. The total *measured* thermal strain is driven by the expansion of the reacted resin product 3. Reactants $1,2$, that is the LY564 epoxy and HY2954 hardener, even though they have a coefficient of thermal strain around one order of magnitude greater than that of the resin product [36], will *not* contribute to to the measured total strain in this experiment for reasons that will be seen in the next sections. Due to this $b_1 = b_2 = 0$. Mathematically, we seek the solution to the Navier-Stokes equation for such an isotropic creep flow. This is of importance in establishing the resulting flow of the resin enclosed by a vacuum bag in a pressured environment. The thermal creep flow (TCF) solution for expansion in the context of the Navier-Stokes equation will lay the basis for a thermo-mechanical model of the expansion of the entire composite during cure making it possible to explain the strain observations made by the optical fibre during the experiment. Theoretically the most important result will be that

such a flow is significantly different to the normal motion of a fluid inside a thick, convective cavity. Further, because of equation 3.29, a TCF is thermodynamically reversible. This fact separates the work done by the thermal strains from the chemical enthalpies involved in the curing reaction. The large aspect ratio of the composite plate justifies the assumption of zero thermal gradient inside Ω. Therefore :

$$T(x,y,z,t) = T(t) \tag{3.30}$$

$$\mathbf{F}_i = \mathbf{0} \tag{3.31}$$

where the second relationship follows from the fact that the plate is thin and on a gravitational equipotential plane. The material volume of the vacuum bag and its accessories is much smaller and more flexible than the composite panel in Ω which permits the simplification that the vacuum bag is a frictionless, light container and exerts no pressure penalty upon the expanding composite. Further we shall (perhaps inaccurately) assume any surface traction arising from contact of the resin structure with the mould surface is negligible. With these assumptions it is possible to find a formal solution for the thermal expansion of a trapped fluid inside $V^{(1)}$ in the following manner: the TCF expansion of the trapped resin fluid system in equation 3.29 necessarily implies that there is physically no sliding between resin fluid layers during such isotropic flows. Using these simplifications in the general fluid model immediately reduces the momentum and energy equations 3.11, 3.28 to:

$$\nabla \cdot p\mathbf{I} = -\rho \frac{d\mathbf{v}}{dt} + \nabla \cdot (\mathbf{P}) \tag{3.32}$$

$$\rho c_p \frac{dT}{dt} = \frac{dQ}{dt} + \lambda \nabla \cdot \mathbf{v}\mathbf{I} : \nabla \mathbf{v} - p\nabla \cdot \mathbf{v} \tag{3.33}$$

These coupled equations can describe the thermal creep of the slowly expanding viscoelastic resin inside the vacuum bag. The momentum balance equation can be rewritten as:

$$\nabla \cdot \bar{\sigma} = -\mathbf{f} \tag{3.34}$$

where $\bar{\sigma}$ is the mean stress tensor of an isotropic solid and $\mathbf{f}$ acts like a body force per unit volume throughout Ω accelerating the volume element dV [34]. Equation 3.8 describes the mass kinetics of the all the reactants in the fluid mixture:

$$\frac{d\rho}{dt} = -\nabla \cdot \mathbf{v}\rho \tag{3.35}$$

To be compatible with equation 3.29 the velocity divergence must produce a reversible mechanical transformation in volume (total mass is immutable) and therefore sources the

thermal creep flow of the fluid:

$$\nabla \cdot \mathbf{v} = 0 \tag{3.36}$$

where c is the volumetric thermal strain coefficient of the resin system. A simple solution of this equation is isotropic thermal velocity field which can be written down in Cartesian form as:

$$\mathbf{v} = \frac{c}{3}\frac{dT}{dt}\begin{bmatrix}1\\1\\1\end{bmatrix} \tag{3.37}$$

From equation 3.30:

$$b = \sum_i b_i = \frac{c}{3} \tag{3.38}$$

Insertion of equation 3.36 into equations 3.12, 3.32 and 3.33 gives the irreversible energy dissipation term:

$$\mathbf{P} : \nabla \mathbf{v} = 0 \tag{3.39}$$

which solves the Navier-Stokes problem for a general reversible thermal fluid expansion: since the temperature is assumed to be uniform in equation 3.30 the mean stress in Cauchy's momentum balance (equation 3.34) becomes the actual stress:

$$\nabla \cdot \boldsymbol{\sigma} = \mathbf{0} \tag{3.40}$$

where $\boldsymbol{\sigma} = p\mathbf{I}$. This expression is just the Cauchy stress equation for an isotropic *solid* and it implies that the motion of the liquid during thermal creep flows is exactly that of a rigid body with the essential difference of not being able to support shear stresses [34]. The energy balance now takes the form:

$$\rho c_p \frac{dT}{dt} = \dot{Q} \tag{3.41}$$

These are the decoupled differential equations of a thermally expanding, incompressible solid incapable of supporting shear stresses in the volume $V^{(1)}$. Equations 3.40 and 3.41 show that for thermal creep flow the liquid resin can be treated as a thermally expanding *solid* body. In the next section we discuss the chemical interaction of the resin product with

its substrate inside Ω. The result will be an applicable thermo-chemical curing theory that allows the analysis of both the measurement thermal strains during the cure stages below the glass transition temperature.

3.2.6 Adhesive clustering and polymer condensation

The DSC and panel manufacture experiments use the epoxy resin system LY564/HY2954, where the LY564 component is the base resin of the epoxy prepolymer diglycidyl ether of bisphenol-A (DGEBA) and the curing agent HY2954 is the hardener of 3,3-di-methyl-4,4-diamino-dicyclohexyl methane(3DCM), see figure 3.15.

The reaction between bisphenol A (BPA) and epichlorhydrin (ECH) occurs in three suc-

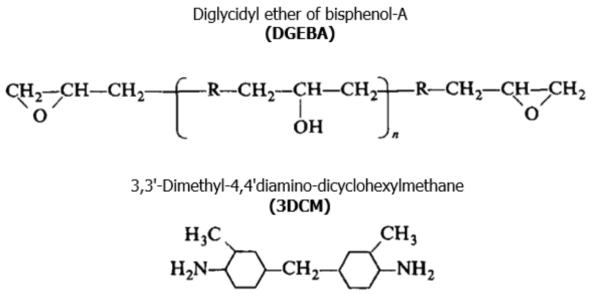

Fig. 3.15 Epoxy DGEBA/3DCM system.

cessive stages and leads to the formation of the (DGEBA) type resin product [8]3.16. The bifunctional resin is made up of two terminal epoxy groups. The aromatic bisphenol A rings provide good thermal properties and mechanical strength even at high temperatures, while the hydroxy and aliphatic chains provide respectively adhesive properties and flexibility. At the extremes of the DGEBA chain there are the reactive groups to which the hardening agents are linked. The presence of such efficient reactive groups outside the chain determines the *high adhesion* and cohesiveness of this type of resin. The curing agent influences the viscosity, the reactivity of the mixture and the type of bonds that are formed and lead to high crosslinking rates. During the cross-linking process, this catalysis emits energy that in turn generates heat and accelerates the process itself. To initiate the crosslinking process, the epoxy resins must be mixed with the curing agent and the mixture must be dosed in the correct proportions. The epoxy resin system was prepared by blending DGEBA and the curing agent at a 100:35 weight ratio so that $\alpha_1 = 1$ and $\alpha_2 = 0.35$. The stoichiometry of the epoxy-hardener system affects the properties of the cured material. Employing different types and amounts of hardener tends to control the overall cross-link density. Initially, below the glass transition temperature, the mixture of the resin and hardener is in liquid form and

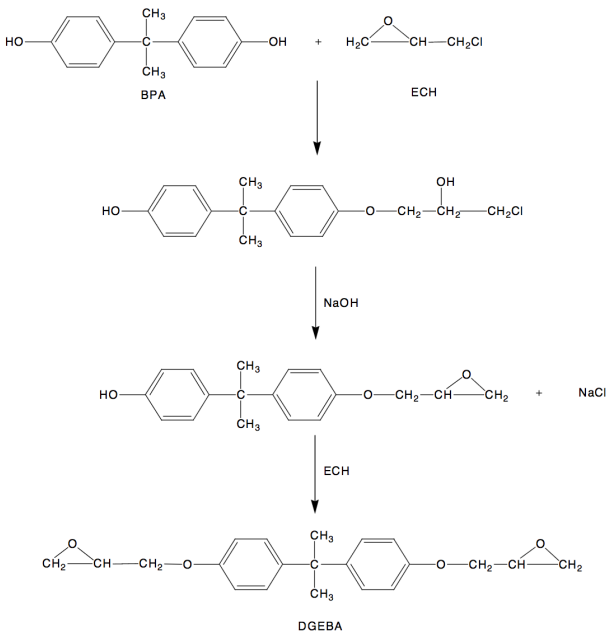

Fig. 3.16 DGEBA synthesis reaction.

the resin system is characterized by low viscosity at room temperature and low molecular mass. The transformation during cure from liquid to gel is characterized by a rapid increase of molecular weight resulting from the progress of the linking reaction between the chains which marks the beginning of a network formation. The onset of this irreversible transformation from a viscous liquid to elastic gel is the gel point. As the cure progresses more crosslinks are formed and thermosetting resins become infused and insoluble by exothermic chemical reactions (irreversible polyaddition reactions). The resulting material is an infinite three-dimensional *solid* network and it involves conversion of the polymer into an insoluble, highly crosslinked material. The crosslinking reaction in an epoxy resin takes place in a condensed phase and, at the beginning, the kinetics are controlled by the chemical reaction of the functional groups (see K_1, K_2 in equation 3.3). As the viscosity of the medium increases, the kinetics are controlled by the diffusion of the reactants[1], the degree of conversion levels off and the system becomes a glass. The degree of conversion increases due to the growing and crosslinking of the chains [60]. In the context of the panel manufacturing experiments therefore, the epoxy resin polymerization may be characterised as one which leads to gelled, or insoluble, products provided that the reaction is carried far enough, where the reactants are functionally capable of producing indefinitely large three dimensional molecules. Since

[1]Considered to be unknown in equation 3.28. Nevertheless, these can be accounted for to a certain extent through the inclusion of the $\alpha_{\max}$ in equation 3.7.

gelation occurs only when there is the possibility of unlimited growth in three dimensions, the conclusion is that it is the result of the formation of infinitely large molecules. Flory and Carothers [11] point out that when one intermolecular linkage has been formed per initial monomeric molecule, all of the polymerizable material must be bound into one gigantic molecule until possibilities for further intermolecular reaction are exhausted. The quantity of reactable material however is found to be determined through one other factor called the reaction extent. If a reactant exhausts all its linkage possibilities, the polymerization should then stop. For smaller extents of reaction this indicates that polymerization may not actually occur. Carothers [11], however, has shown that that indefinitely large molecules might still continue to be formed even at lower extents of reaction if a small fraction of the reactable units with further intermolecular reaction extent unite to form more infinite polymer molecules, while any remaining units would then develop as comparatively small molecules. Thus the concept of a size distribution of molecular chains during polymerization is a natural consequence of the reaction extent or reaction entropy between the reactants. Gelation, may be possible before all the available molecules have been linked up [68] and interspersed with networks of the large molecules and as a result there would be many smaller molecules of varying size. Common experience shows that gelation occurs in three dimensional polymerizations long before all of the material is bound together in one infinitely large molecule and gelation actually occurs when a critical number of intermolecular linkages has been exceeded [11, 68]. The molecular size distribution during polymerization is an important phenomenon during the curing process in a confined space of resin, reinforcement fiber fabric and mould. However, a related and equally important concept is the distribution of reactive sites: for epoxy resin systems the reactions occur in the form of molecular bonds or linkages between amine (hardener) sites and the epoxy molecule itself [68]. The molecular weight of converted resin increases as a function of the number of bonds between the hardener and the resin material. Naturally, larger molecules occupy more physical space and if gelation actually starts before the theoretical limit of total linkage is reached then it is reasonable to assume the spatial distribution of such large converted molecular chains will follow on average that of the interspersed amine sites in the mixture volume. Assuming that the hardener and resin are uniformly mixed, and the temperature distribution in the composite panel is uniform, it follows that the rate of production of large molecular adhesive chains is uniform throughout the volume $V^{(1)}$. One might visualise this as volumes around the amine sites [68] that are reasonably far apart developing independently of one another until they are close enough to be linked and merge into one larger polymer molecule - a process of polymer condensation. If the mean radius of a large molecular volume is $\langle r \rangle$ and there are n molecululular structures

in all, then it is easy to show that for a smooth size distribution:

$$\langle r \rangle \sim \left(\frac{V^{(1)} \alpha}{n^2} \right)^{1/3} \tag{3.42}$$

where n is the number of large molecular regions uniformly distributed in $V^{(1)}$ (or a control volume Γ, see figure 3.17). At the beginning of the reaction n is very large, α is small and as a consequence $\langle r \rangle$ is vanishingly small. However, as the reaction completes, and the temperature approaches the glass transition then $n, \alpha \to 1$ and the volume occupied by the reacted resin approaches $V^{(1)}$. Such reacted molecules are of course also an epoxy adhesive which are also commonly used as strong industrial adhesives. Any cured resin product that comes into contact with substrates will therefore tend to bond to it strongly [73], fixing the resin to the substrate surface ($b_1 = 0, b_2 = 0$ in equation 3.38). More precisely, the region of the interphase between substrate and matrix is critical for determining the mechanical properties of the composite material. Two of the most commonly accepted mechanisms for interphase formation are [73] (a) the preferential absorption of curing agent on the fiber surface and (b) the diffusion of curing agent into epoxy-rich volumes. Both of these mechanisms lead to stoichiometric imbalances that are frozen in as the system vitrifies and contact with substrate materials such as the reinforcement fibres or optical fibres will attach them strongly to those structures as curing progresses. Summarising, the cured resin expands into spaces between the carbon fibres and around the optical fibres approximately in accordance with equation 3.42 which can explain the deposition or *condensation* of cured resin product onto substrate as a function of time. We use the Navier-Stokes solutions for thermal creep flow, equations 3.40 and 3.41, together with equation 3.42 to treat the strain development in each of two substrates interacting with the matrix: The first is the experimental strain gauge in the form of the embedded optical fibre and the second is the reinforcement carbon fibre weave structure itself.

3.3 Resin-Embedded optical fibre characterisation model

Consider a single straight cylindrical optical fibre passing from one end of $V(1)$ to the other at time $t = 0$. The optical fibre is surrounded by a distribution or suspension of freely expanding small cured resin product ($i = 3$) spheres as shown in figure 3.17 I. The spheres are suspended in unreacted LY564/HY2954 fluid ($i = 1, 2$) deposited around *uniformly distributed* HY2954 amine sites as shown. As cure progresses equation 3.42 implies that at some time $t > 0$, these spherical droplets of *still liquid* epoxy adhesive grow until they begin to enclose one another

and condense onto the optical fibre as in figure 3.17 II. Proximity creates new possible

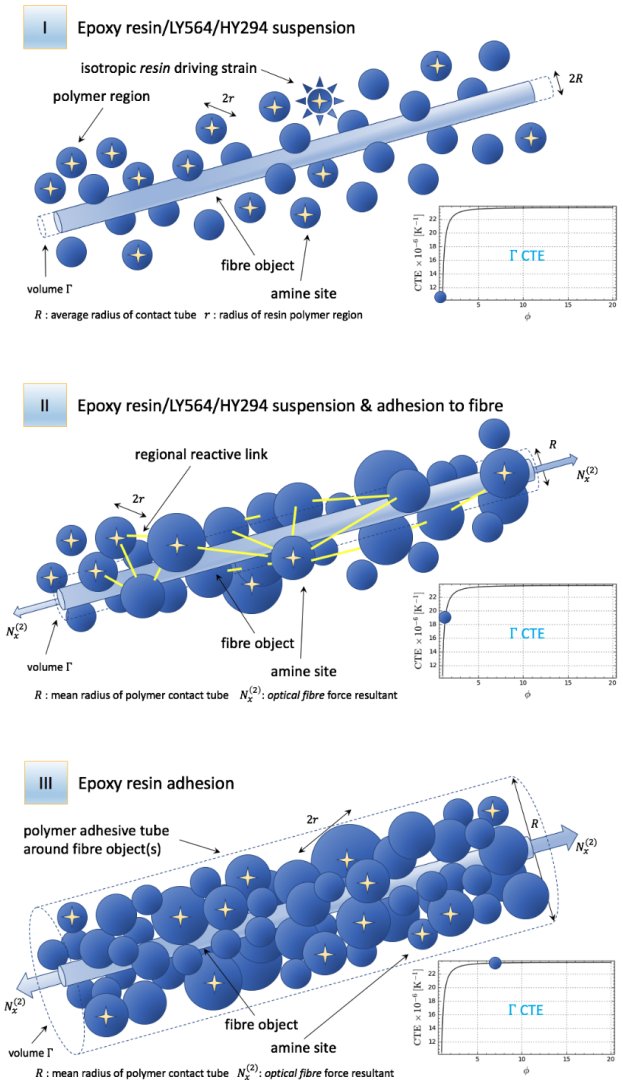

Fig. 3.17 The optical fiber inside the resin system, I resin system suspension, II resin system suspension and adhesion, III resin system adhesion.

reaction pathways for the resin clusters to follow and these are illustrated graphically by the yellow connecting rods from droplet to droplet. If the average radius of the condensed droplets around the axis of the optical fibre is $R(t)$ then an equivalent mechanical picture is that the entire optical fibre is surrounded by and fixed to a concentric cylindrical tube of condensed epoxy adhesive of radius $R(t)$. This creates a composite mechanical system made of condensed resin and optical fibre along the length l of the panel. As time progresses, due to equation 3.42,the radius $R(t)$ becomes larger and further adhesive condenses onto

the embedded optical fibre as shown in figure 3.17 III. Applying the Navier-Stokes stress equation 3.40 in cylindrical polar coordinates:

$$\left(\frac{1}{r}\frac{\partial r p_r}{\partial r}, \frac{1}{r}\frac{\partial p_\theta}{\partial \theta}, \frac{\partial p_z}{\partial z}\right) = \mathbf{0} \tag{3.43}$$

to the volume Γ enclosed by the cylinder of radius $R(t)$ we may solve the equilibrium problem for the embedded optical fibre (region 2 or substrate) and cured resin (region 1) cylinders in the composite panel: Mathematically, the stress tensor in region 1 is isotropic with constant fluid pressure so that $p_r = p_\theta = p$. In particular for an incompressible *solid material* (the Young modulus of optical fibres of various types is $\sim 16-67\,\text{GPa}$) the usual constituitive relationship is (see [41]):

$$\begin{bmatrix}\sigma_x\\ \sigma_\theta\\ \sigma_r\end{bmatrix} = \begin{bmatrix}C_{11} & C_{12} & C_{12}\\ C_{12} & C_{22} & C_{23}\\ C_{12} & C_{23} & C_{22}\end{bmatrix}\begin{bmatrix}\varepsilon_z - c\Delta T\\ 0\\ 0\end{bmatrix} \tag{3.44}$$

where the x coordinate runs along the optical fibre axis as in figure 3.6. Solutions of the stress equations for the optical fibre surrounded by the resin in each region are therefore given:

$$\sigma_x^{(1)} = C_{11}^{(1)}(\alpha)(\varepsilon_x^{(1)} - c^{(1)}\Delta T) \tag{3.45}$$

$$\sigma_x^{(2)} = C_{11}^{(2)}(\varepsilon_x^{(2)} - c^{(2)}\Delta T) \tag{3.46}$$

Equation 3.43 implies that the integrated force of the expanding resin structure over both concentric cylinders must vanish in a Cauchy equilibrium:

$$\begin{aligned}\pi(R(t)^2 - r_0^2)C_{11}^{(1)}(\alpha)(\varepsilon_x^{(1)} - c^{(1)}\Delta T)\\ +\pi r_0^2 C_{11}^{(2)}(\varepsilon_x^{(2)} - c^{(2)}\Delta T) = 0\end{aligned} \tag{3.47}$$

implying therefore that as the resin structure expands over the surface of the optical fibre, it works against both the optical fibre elasticity and its intrinsic free thermal expansion. Since the cured resin is a strongly bonded adhesive:

$$\varepsilon_x^{(1)} = \varepsilon_x^{(2)} \tag{3.48}$$

Solving the Cauchy equilibrium with this requirement over the embedded optical fibre yields:

$$\varepsilon_x^{(2)} = \left[\frac{(\phi^2 - 1)C_{11}^{(1)}(\alpha)c^{(1)} + C_{11}^{(2)}c^{(2)}}{(\phi^2 - 1)C_{11}^{(1)}(\alpha) + C_{11}^{(2)}} \right] \Delta T \tag{3.49}$$

$$\phi = \frac{R(t)}{r_0} \tag{3.50}$$

Equation 3.49 is thus a simple strength of materials argument that relates the net expansion of the optical fibre to the quantity of resin surrounding it. It also presents a recurrent theme in the rest of this article in its simplest mathematical form and has been usefully employed as an inset to illustrate the effects of equation 3.42 in figures 3.17 and 3.18. Figure 3.19 shows a plot of equation 3.49 in the form of thermal strain coefficient against ϕ for current experimental data. For $\phi \sim 1$ the measured strain is the pure optical fibre thermal strain

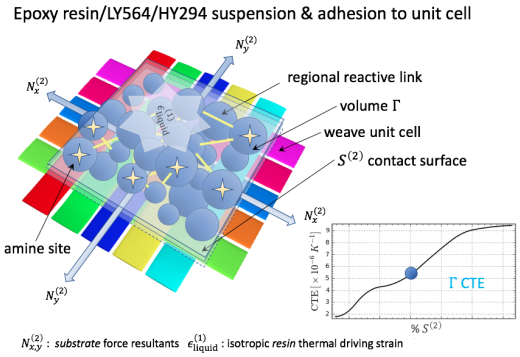

Fig. 3.18 The mathematical representation of the CTE of control volume Γ. The rapid rise of this curve indicates that very little time is needed before there is enough cured resin enveloped around the optical fibre to curtail its intrinsic mechanical contribution.

of the assembly while for values of ϕ beyond 2, the measured strain approaches the true strain of the surrounding resin cylinder Γ. In practice, for less then ideal setups, equation above can therefore be employed usefully to correct the *experimental* strain measured during cure once the interaction geometry is known. If the weave fabric is close to the optical fibre (here $\phi = \phi_0 \sim 3$ will cause volume Γ to intersect parts of the 5HS fabric weave), then condensation occurs on the two substrates simultaneously and in equation 3.49 the quantity $C_{11}^{(1)}(\alpha)$ is therefore potentially the viscoelastic constituitive coefficient for both the weave *and* cured resin (resin structure) at once. In that case, $C_{11}^{(1)}(\alpha)$ can have an appreciable value even when the resin is in a liquid state. Mathematically, $C_{11}^{(1)}(\alpha)$ is estimated to be $\sim V^{(1)}\alpha\beta_T^{-1} + V^{(2)}E_{11}^{5HS}$ for the panel manufacture experiment, where $V^{(2)}$ is the volume occupied by the 5HS weave. Here β_T represents the isothermal compressibility of the cured

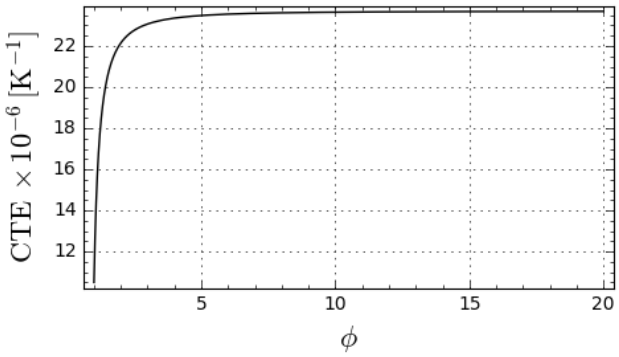

Fig. 3.19 The embedded mean optical fibre infusion strain at $t = 0$ (top line, black) undergoes a near constant downward shift in each section by the end of the manufacturing process. The original strain signal including noise is in gray.

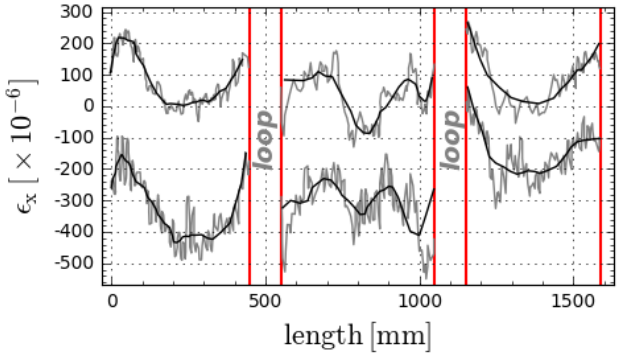

Fig. 3.20 The optical fiber inside the resin system. Inset shows the Γ control volume CTE as a function of surface condensation in a unit cell of 5HS homogenised laminate. It is the equivalent of figure 3.17 for a plate substrate geometry.

resin volume and has a typical value ~ 1 GPa^{-1}. In contrast to the dynamic and rather complicated $C_{11}^{(1)}(\alpha)$, the optical fibre $C_{11}^{(2)}$ is a fixed quantity throughout curing and for this experiment it has a value of around 16 GPa with it's protective coating applied. Clearly, the nonlinearity of equation 3.49 indicates that the thermally expanding resin is put into compression by the mechanical resistance of the optical fibre very early on, and in these experiments an important quantity is the value of $t = t_0$ when $\phi = \phi_0$. From equation 3.23 since $\alpha = V_3/V^{(1)}$ then:

$$\alpha(t_0) = \alpha_0 = \frac{\pi \phi_0^2 r_0^2 l}{V^{(1)}} \tag{3.51}$$

which for the panel manufacture experiment gives a value of $\alpha_0 \sim 10^{-4}$. Referring to figure 3.13 we see that the resin is in state α_0 in the first few minutes of cure. Thus it is fair to say that the embedded optical fibre measures the strains associated with the resin structure faithfully during the entire manufacturing process. These arguments are supported by results obtained during the panel manufacture experiment due to the distributed nature of the optical fibres themselves: electronic snapshots of the distributed strain, at $t = 0$ and at the end of cure when $t \sim 900$ min along the entire length of the embedded optical fibre are given in figure 3.20. To a good approximation, excluding the loop regions (see figure 3.6), the two lines are shifted down by a constant value at every point of the optical fibre. The strain in the embedded optical fibre at the beginning of cure, due to the resin infusion stress [91], is preserved through a downward constant shift in each section of the embedded optical fibre to the end of the manufacturing process implying that the initial strain distribution in the optical fibre is (approximately) an invariant during the curing process. Physically, the optical fibre sections are not therefore free to move as the resin structure strains *uniformly* around them. Instead they are constrained to move *with* the panel as it strains in response to the forces of cure - as predicted by equations 3.49 and 3.51 above.

3.4 Resin-Embedded optical fibre- 5HS substrate characterisation model

The cylinder model of the last section analyses the slow motion of a pure resin liquid about a single fibre. However valuable that might be to providing an insight as to what happens when a fibre is embedded into a reacting liquid resin under pressure, it falls short of a complete description of reversible thermal expansion stress in the fluid as the resin cures. It is important to differentiate that while the concentric cylinder model is accurate for an isolated optical fibre in a resin tube, it is however not a satisfactory description for properties of the surrounding resin structure. The reinforcement fibres are in close contact with one another (see figure 3.18) where $R \sim r_0$ in equation 3.49. This immediately suggests that the resin strain is the thermal strain of the reinforcement carbon fibre grid which is contrary to experimental observation, due to the fact that resin condensation takes place on a substrate with a completely different geometry. To treat the displacement of the surrounding fluid resin structure, a different physical model is therefore required as shown in this section. In mathematical terms, the geometry of the manufacturing process (see figure 3.6) holds the entire composite plate assembly flat on a steel backing mold under vaccum pressure p. Equation 3.40 says that the thermal expansion of the mold, reinforcement fibres and

the cured component of the liquid resin interact together as a single solid entity. As cure progresses, equation 3.42 implies that more and more substrate surface is covered over by epoxy adhesive regions which become interconnected into one volume over time (see figure 3.18). We define this to to be equivalent to the filling of a control volume Γ covering a control surface $S^{(2)}$ of a 5HS weave unit cell and figure 3.18) . When expanding thermally, such regions do mechanical work against all substrates they are connected to in accordance with equation 3.40. In effect this means that the volumetric strain of the condensed resin *drives* the expansion of the substrate. Physically, the constituitive relation for such resin structure geometries can be approximated by one of several flavours of composite laminate or mean-field homogenization theories(CLT) with the shearing force terms removed. For a viscoelastic 5HS lamina without planar shear strains:

$$\mathbf{0} = \mathbf{A}(\alpha)\varepsilon_{\text{solid}}(\alpha,t) - \mathbf{A}_{\otimes}(\alpha)\begin{bmatrix} c_1 \\ c_2 \end{bmatrix}\Delta T \tag{3.52}$$

where $\mathbf{A}$ and $\mathbf{A}_{\otimes}$ are the composite lamina and thermal stiffness "A" matrices calculated exactly as for a solid, with a known viscoelastic dependence on the curing parameter α. The quantities $(c_1, c_2)^T$ are the linear thermal strain coefficients of a single 5HS weave sheet bonded to the LY564/HY2954 resin system where directions $1,2$ are local to the lamina (see figure 3.18). The thermal shear term is ignored by assumption. The overall *free* thermal expansion strain of one lamina of the composite panel should be given by the CLT adapted for a weave which solves the Cauchy equilibrium in equation 3.40:

$$\varepsilon_{\text{solid}}(\alpha,t) = \mathbf{A}^{-1}(\alpha)\mathbf{A}_{\otimes}(\alpha)\begin{bmatrix} c_1 \\ c_2 \end{bmatrix}\Delta T \tag{3.53}$$

where the directional coefficients of thermal expansion of the composite structure $(c_1, c_2)^T$ will *drive* the thermal strain of the resin structure. Equation 3.53 is the 5HS weave substrate analog of equation 3.49. This expression is derived for a fully cured composite and does not take into account the increasing surface coverage of the epoxy adhesive as a function of α. To better understand the relationship of strain production below the glass transition temperature we recourse to equation 3.41 noting that it was derived for reacting resin *by itself* embedded into Ω or its equivalent, the control volume Γ, without reference to interaction with the substrate. Since the actual structure present in the volume is in fact an amalgam of uncured and reacted resin together with the highly dense structure of reinforcement fibres (in this experiment the fibre fraction is equivalent to that of a 61% unidirectional composite plate), aspects of the energy balance equation need reinterpretation when the weave material

is included. In general, for variable densities:

$$\dot{Q} = H_u \frac{d\rho\alpha}{dt} \tag{3.54}$$

Since the temperature is assumed constant throughout Ω (see equation 3.30), the curing rate is spatially uniform. If in addition we assume that the density of the structure is constant during reactions (that is, chemical shrinkage is ignored for the present) then the energy balance equation is thermodynamically reversible and is written:

$$\rho c_p \frac{dT}{dt} = H_u \rho \frac{d\alpha}{dt} \tag{3.55}$$

Expanding and rearranging:

$$\int_{T_0}^{T} c_p(T,t)dT = H_u \alpha(t) \tag{3.56}$$

This expression details the rate at which reacted resin is produced. Using equation 3.23 and the assumption of homogeneous cured resin production in Ω, the increment in the cured resin product volume dV_3 produces a related increase in surface coverage of the weave fabric substrate (region 2). The adhesive contact between resin product (region 1) and the substrate surface area does mechanical work on the unit cell during thermal expansion of the resin. Homogenising the substrate and cured resin product as a CLT structure:

$$\varepsilon^{(2)}(\mathbf{r},t) = \varepsilon^{(1)}(\mathbf{r},t) = \varepsilon_{\text{liquid}}(\mathbf{r},t) \tag{3.57}$$

we have as in equation 3.48 made the region 1 and region 2 strain fields equal due to adhesive condensation. If the total strain imposed upon the substrate by thermal expansion *at* the glass transition temperature is $\varepsilon_{\text{liquid}}$ and $\varepsilon_{\text{solid}}$ is the strain calculated in equation 3.52, then the thermomechanical resin conversion process necessarily requires a strain field that accounts for increasing surface strain up to some dimensionless, unknown factor $f(\alpha)$:

$$\varepsilon_{\text{liquid}}(\mathbf{r},t) = \varepsilon_{\text{solid}}(\mathbf{r},t) f(\alpha) \tag{3.58}$$

Since the liquid resin product does work expanding the unit cell thermally by $dV^{(1)}_{\text{strain}}$ against some *bulk* pressure $p^{(2)}(\mathbf{r},t)$ exerted by the substrate surface $S^{(2)}(t)$, then this is equal to the

total strain energy in the homogenised control volume Γ in figure 3.18:

$$\int_0^{V^{(1)}_{\text{strain}}(t)} p^{(2)} dV^{(1)}_{\text{strain}} = \int_\Gamma \varepsilon_{\text{liquid}} \mathbf{A}_\otimes \varepsilon_{\text{liquid}} dV \tag{3.59}$$

where the integration on the left measures deformation whereas on the right hand side we have a summation of volumes. Using equations 3.58, 3.59 and 3.57 together with the mean value theorem:

$$\alpha \langle p V^{(1)}_{\text{strain}} \rangle = f^2(\alpha) \langle \varepsilon^{(\mathbf{1})}_{\text{solid}} \mathbf{A}_\otimes \varepsilon^{(\mathbf{1})}_{\text{solid}} \rangle V_\Gamma \tag{3.60}$$

The averaged energies are equal so that:

$$f(\alpha) = \sqrt{\alpha(t)} \tag{3.61}$$

Therefore:

$$\varepsilon_{\text{liquid}}(\mathbf{r},t) = \varepsilon_{\text{solid}}(\mathbf{r},t)\sqrt{\alpha(t)} \tag{3.62}$$

below the glass transition temperature. Equation 3.53 is therefore modified or corrected for surface strain in equation 3.59:

$$\varepsilon_{\text{liquid}}(t) = \mathbf{A}^{-1}(\alpha)\mathbf{A}_\otimes(\alpha) \begin{bmatrix} c_1 \\ c_2 \end{bmatrix} \sqrt{\alpha}\Delta T \tag{3.63}$$

For thermodynamic chemical curing processes under constant pressure before the glass transition temperature of the resin, the in liquid thermal expansion coefficient differs from its solid value by a factor $\sqrt{\alpha}$. A comparison of the strain curves from different theories against the actual liquid state distributed mean field strain measured during the experiment can be seen in figure 3.21. The standard solid polymer CLT of equation 3.53 produces a straight (dashed gray) line as expected. The modified fluid CLT develops a a better match (heavy curved black line) to the actual data measured. The straight line in black is the thermal mass corrected strain for a portion of the fibre *outside* composite panel (see figure 3.6). An interesting result of equation 3.63 is that the resin-carbon structure below the glass transition point can be regarded as a *pseudo*-fluid that exhibits both solid mechanical and fluid properties at the same time. It is then of a certain degree of significance in this context that for a free standing sample of resin without vacuum pressure or embedded carbon-fibre substrate - as in the DSC machine experiments - the thermal strain is known to vary [36] as α. The behaviour of the resin during VARIM manufacture is therefore significantly different

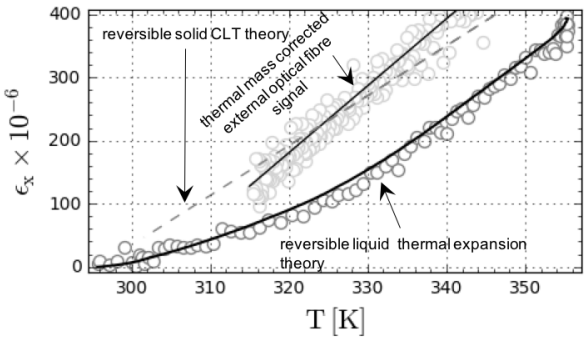

Fig. 3.21 A comparison of standard Ishikawa CLT equation 3.99 with the modified Ishikawa CLT of equation 3.100 with embedded optical fibre strain signal during panel manufacture.

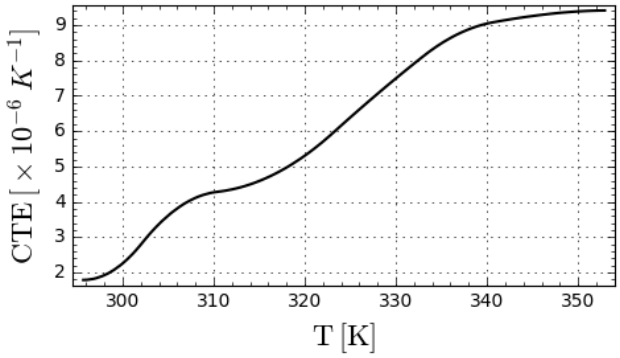

Fig. 3.22 The CTE of the resin structure derived from figure 3.21 as a function of temperature. This the equivalent of figure 3.21 for a 5HS unit cell *surface* control volume Γ. See figure 3.18.

.

to when in isolation. Summarising, this model solves the Navier-Stokes derived thermal expansion equilibrium (see equation 3.40) for a curing resin while actively condensing onto embedded carbon-fibre substrate from its liquid state. The results are useful in explaining the experimental data of the panel manufacturing carried out in section "Panel Manufacture Experiment" and serves to complete the description of the apparent physical processes in the composite panel present while the composite panel is cured below the glass transition temperature.

3.4.1 Ishikawa viscoelastic CLT

The mathematical model of the reaction kinetics is incomplete without a discussion of how the quantities $\mathbf{A}$ and $\mathbf{A}_{\times}$ and their equivalents are to be determined for a viscoelastic 5HS weave lamina or laminate. The physical thermal strain field theory permits the direct application of the *solid* viscoelastic stiffness theory to the pseudo-fluid resin state through the mathematical transformation:

$$(\text{thermal fluid strain}) = (\text{solid strain}) \times \sqrt{\alpha} \tag{3.64}$$

In so doing we afford a correction to the fluid term for an embedded fibre process over cure temperatures below the glass transition temperature. It must be clear that what is meant by a "solid strain" in the above idealisation is a phenomenological model of rigid body viscoelasticity. Equally in the term "thermal fluid strain" there is no traditional fluid dynamics involved in the description as such and the elements of the theory (due to equation 3.40) still rely on physical manipulations of the *solid* constitutive relationships between fibres and resin to compute interpolated stiffnesses at every stage of cure including the pseudo-fluid phase. The standard phenomenological model of viscoelasticity adopted by White and Gopal [87, 83, 26] and others is modified here using a parameterisation appropriate for the Satin 5HS weave as described by Ishikawa [42] instead of a uni-directional formulation. The main methodology describes the reaction process without considering the reaction of the individual species as in the sections above or as developed by White and Hahn [87]. The reason for this has already been given, namely that the adhesive action of the cured resin volume upon the reinforcement fibres is assumed to fix them together to the condensing resin. Mechanical moments cannot be supported by such a structure since the resin is still a liquid and the chemical reactions are far from completed, yet the action of the rigid mould (see figure 3.6) promotes a solid like thermal creep stress equilibrium in the vacuum bag (see equation 3.40) elastically deforming the embedded substrates (see equation 3.59). The mechanical properties of the composite material change viscoelastically as the curing progresses. In particular, the transverse compliance, $S_{22}(t)$, undergoes a substantial change with time during cure, see [81, 26]. This behaviour is modeled by a power law of the form:

$$S_{22}(\alpha,t) = S_{22i}(\alpha) + D(\alpha)a_T(\alpha,t)^{-q(\alpha)} \tag{3.65}$$

where D the transverse creep coefficient, a_T the shift factor and q is the transverse creep exponent. The creep parameters D and q are found from experiment. The initial compliance initial elastic response of the resin structure. The creep parameters D, q, and a_T can be

represented as linear functions of α:

$$D(\alpha) = D_i + \alpha(D_f - D_i) \tag{3.66}$$

where D_i is the initial transverse creep coefficient, D_f the cured transverse creep coefficient, q_i the initial transverse creep exponent and q_f is the cured transverse creep exponent [87]. The initial transverse modulus of elasticity E_{22} is initially ($\alpha < \alpha^*$):

$$E_{22i} = E^* \tag{3.67}$$

and when α passes the resin gel point ($\alpha \geq \alpha^*$):

$$E_{22i} = a_0 + a_1\alpha + a_2\alpha^2 \tag{3.68}$$

where E_{22i} is the initial transverse modulus, E^* the very low value of the uncured transverse modulus for the resin structure, $\alpha^* \approx 0.82$ is the degree of cure at the resin gel temperature and a_0, a_1 and a_2 are modelling parameters. The value of E^* is around the same value as β_T used earlier in before section. The longitudinal modulus of elasticity E_{11} and major Poisson ratio v_{12} are also modelled as linear functions of α:

$$E_{11}(\alpha) = E_{11i} + \alpha(E_{11f} - E_{11i}) \tag{3.69}$$

$$v_{12}(\alpha) = v_{12i} + \alpha(v_{12f} - v_{12i}) \tag{3.70}$$

where E_{11i} is the uncured longitudinal modulus, E_{11f} the fully cured longitudinal modulus, v_{12i} is the uncured major Poisson ratio and v_{12f} is the fully cured major Poisson ratio. The 5HS fabric can be approximated for the purposes of the present calculations as an amalgam of unidirectional laminae and specialised bridge element stiffness matrices of the fill direction see [42]. These are the two elements in the calculation of what is known as the Ishikawa *bridge* model. In what follows, we adapt the static bridge model to one that permits viscoelastic curing evolution in the phenomenological sense defined above. The starting point is the curing model for simple unidirectional laminates pervading so much of the literature see [87, 26]. The α dependent linear interpolation of the engineering constants permit the α dependent engineering constants above to be converted to compliances through

the usual CLT equation set to be modified for viscoelastic changes during manufacture:

$$S_{22i}(\alpha) = \frac{1}{E_{22i}(\alpha)} \tag{3.71}$$

$$S_{11}(\alpha) = \frac{1}{E_{11}(\alpha)} \tag{3.72}$$

$$S_{12}(\alpha) = \frac{-\nu_{12}(\alpha)}{E_{11}(\alpha)} \tag{3.73}$$

where $S_{ij}(\alpha)$ are now the cure dependent compliances. The formal unidirectional *unrotated* lamina stiffness matrix follows immediately:

$$Q_{11}(\alpha,t) = \frac{S_{22}(\alpha,t)}{S_{11}(\alpha)S_{22}(\alpha,t) - S_{12}(\alpha)^2} \tag{3.74}$$

$$Q_{22}(\alpha,t) = \frac{S_{11}(\alpha)}{S_{11}(\alpha)S_{22}(\alpha,t) - S_{12}(\alpha)^2} \tag{3.75}$$

$$Q_{12}(\alpha,t) = \frac{-S_{12}(\alpha)}{S_{11}(\alpha,t)S_{22}(\alpha,t) - S_{12}(\alpha)^2} \tag{3.76}$$

where the Q_{ij} are elements of the CLT reduced material response matrix $\mathbf{Q}(\alpha,t)$. The bridge element matrices will be seen to be more specialised integrated compliances that operate over the bridge structure in a 5HS composite fabric. These stiffness corrections to the standard unidirectional CLT call for a modification of the above scheme presented by Hahn to the one suggested by Ishikawa and Chou in their papers [42]. The logical assumptions of continuum mechanics are extended by Iskhikawa and Chou [42] to give the CLT mean field constituitive theory a pointwise validity. The effect of this is that a simple flat plate relationship will hold everywhere in the symmetric weave during curing. In the analysis that follows, we will follow Ishikawa and drop the transverse y dependence. The undulatory inverse compliance of the 5HS weave at some point x in the undulatory direction in figure 3.23 has to be computed by the summation of fill, warp and resin CLT material stiffness contributions along the 5HS unit cell [42] . This splits the pointwise matrix $\mathbf{A}^{-1}(x)$ into three standard CLT integrals

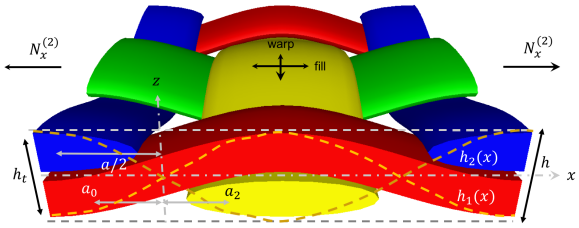

Fig. 3.23 Undulation unit cell for an Ishikawa one dimensional weave model with idealised h_1 $h_2$shape functions.

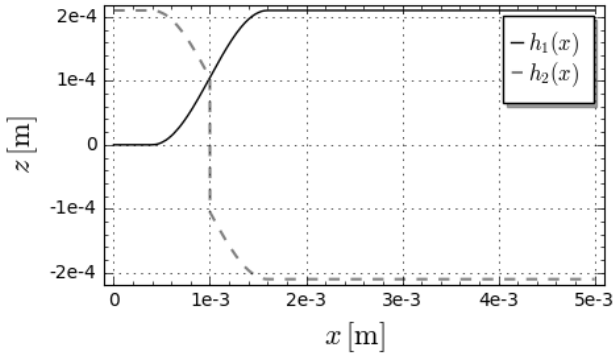

Fig. 3.24 The real $h_1(x)$ and $h_2(x)$ shape functions used in calculating the Ishikawa unit cell for the 5HS weave used in the experiment.

along z:

$$\begin{aligned}\mathbf{A}(x) = \mathbf{Q}^M(h_1(x) - h_2(x) + h - h_t/2) \\ + \mathbf{Q}^F(\theta)h_t/2 + \mathbf{Q}^W(h_2(x) - h_1(x))\end{aligned} \tag{3.77}$$

The height field or shape function quantities $h_i(x)$ define the limits of integration of particular fabric structure zones along the z coordinate. These are geometric in nature and will depend upon the exact weave type being used (see figure 3.23). The structural contributions to the overall pointwise inverse compliance matrix take the form of the $\mathbf{Q}^{M,F,W}$ CLT response matrices which are briefly explained below. The "M" matrix contribution is given by the

resin isotropic CLT lamina stiffness:

$$\mathbf{Q}^M = \begin{bmatrix} \frac{E^M(\alpha)}{D_\nu^M(\alpha)} & \frac{\nu^M(\alpha)E^M(\alpha)}{D_\nu^M(\alpha)} & 0 \\ \frac{\nu^M(\alpha)E^M(\alpha)}{D_\nu^M(\alpha)} & \frac{E^M(\alpha)}{D_\nu^M(\alpha)} & 0 \\ 0 & 0 & G^M(\alpha) \end{bmatrix}$$

$$D_\nu^M(\alpha) = 1 - [\nu^M(\alpha)]^2 \tag{3.78}$$

where E^M and ν^M are the Young modulus and Poisson ratio of the pure resin respectively. The fill stiffness describes the loss of rigidity of the axially oriented fibres over the warp angle $\theta(x)$:

$$\frac{dh_1}{dx} = \tan\theta \tag{3.79}$$

This variation is geometric in nature, redefining the associated "F" CLT stiffness matrix as follows:

$$\mathbf{Q}^F = \begin{bmatrix} \frac{E_{11}^F(\alpha,\theta)}{D_\nu^F(\alpha,\theta)} & \frac{\nu_{21}^F(\alpha,\theta)E_{22}^F(\alpha,\theta)}{D_\nu^F(\alpha,\theta)} & 0 \\ \frac{\nu_{21}^F(\alpha,\theta)E_{22}^F(\alpha,\theta)}{D_\nu^F(\alpha,\theta)} & \frac{E_{22}^F(\alpha,\theta)}{D_\nu^F(\alpha,\theta)} & 0 \\ 0 & 0 & G_{12}^F(\alpha,\theta) \end{bmatrix}$$

$$D_\nu^F(\alpha) = 1 - [\nu_{21}^F(\alpha,\theta)]^2 \tag{3.80}$$

The elements of the matrix can be computed in terms of engineering constants as follows:

$$E_{11}^F(\alpha,\theta) = [A + B + C]^{-1}$$

$$A = \frac{l(\theta)^4}{E_{11}^F(\alpha)}$$
$$B = \left(\frac{1}{G_{13}^F(\alpha)} - \frac{2\nu_{31}^F(\alpha)}{E_{11}^F(\alpha)}\right) l(\theta)^2 m(\theta)^2$$
$$C = \frac{m(\theta)^4}{E_{33}^F(\alpha)}$$

$$\nu_{21}^F(\alpha,\theta) = \nu_{31}^F(\alpha) l(\theta)^2 + \nu_{23}^F(\alpha) m(\theta)^2$$
$$G_{12}^F(\alpha,\theta) = G_{12}^F(\alpha) l(\theta)^2 + G_{23}^F(\alpha) m(\theta)^2$$
$$E_{22}^F(\alpha,\theta) = E_{22}^F(\alpha) = E_3^F(\alpha)$$

where l and m are the cosine and sine of θ respectively. The constant quantities E^F, G^F, ν^F are the usual fixed engineering constants in the standard CLT model for a flat lamina. What is seen here is a mixing of of the properties of the lamina due to the varying incline $\theta \neq 0$. To complete the list of contributions to the stiffness model we note that the response of the non axial fibre plane is close to the standard transverse unidirectional CLT stiffness matrix:

$$\mathbf{Q} = \begin{bmatrix} \frac{E_{11}^W(\alpha)}{D_\nu^W(\alpha)} & \frac{\nu_{21}^W(\alpha) E_{22}^F(\alpha)}{D_\nu^W(\alpha)} & 0 \\ \frac{\nu_{21}^W(\alpha) E_{22}^F(\alpha)}{D_\nu^W(\alpha)} & \frac{E_{22}^W(\alpha)}{D_\nu^W(\alpha)} & 0 \\ 0 & 0 & G_{12}^W(\alpha) \end{bmatrix}$$

$$D_\nu^W(\alpha) = 1 - [\nu_{21}^F(\alpha)]^2 \tag{3.81}$$

the elements of which are defined by equations (whatever) above. Since the warp direction is orthogonal to the fill direction, this matrix is rotated through $\pi/2$ radians:

$$\mathbf{Q}^W = \mathbf{R}^{-1}(\pi/2)\mathbf{Q}\,\mathbf{R}(\pi/2) \tag{3.82}$$

where $\mathbf{R}$ is a rotation operator about z. This formalism modifies the CLT theory for application to a 5HS weave structure by developing a pointwise $\mathbf{A}(x)$ matrix in the axial direction of the unit cell. The pointwise response next needs to be averaged to provide a mean field strain that can be used to calculate the observed response of the weave under actual experimental conditions. Specifically, noting equation 3.52, for some applied load distribution or membrane

stress $\mathbf{N}(x)$ in the unit cell, for one single 5HS unit cell and the following must hold from point to point:

$$\mathbf{N}(x) = \mathbf{A}(x)\boldsymbol{\varepsilon}(x) \tag{3.83}$$

where $\mathbf{A}(x)$ is total stiffness contribution of the resin structure *in the fill direction* and $\boldsymbol{\varepsilon}(x,y)$ is the associated strain field at the point x on the midplane. Write the reduced undulatory force equation as:

$$\sum_k \boldsymbol{\varepsilon}(x+k\delta x)\delta x = \sum_k \mathbf{A}^{-1}(x+k\delta x)\mathbf{N}(x+k\delta x)\delta x \tag{3.84}$$

Taking the limit $\delta x \to 0$ on both sides and noting the overall strain:

$$\langle \boldsymbol{\varepsilon}_{\text{solid}} \rangle = \langle \mathbf{A}^{-1} \rangle \langle \mathbf{N} \rangle \tag{3.85}$$

so that:

$$\langle \mathbf{A}^{-1}(x) \rangle = \frac{1}{l}\int_0^l \mathbf{A}^{-1}(x)dx \tag{3.86}$$

where l is the length of one side of a square of composite. This relationship is an extension of the "springs in series rule" and we can use it to work out the overall stiffness of the plate in the fill direction. Equation (11) in Ishikawa does something similar in the undulation model:

$$\langle \mathbf{A}^{-1} \rangle = \frac{2}{n_g a}\int_0^{n_g a/2} \mathbf{A}^{-1}(x)dx \tag{3.87}$$

The best way to work out the average compliances is through numerical integration.. However the total response of the fill direction needs to be amalgamated with that of the warp direction *over the length of a defined unit cell* of 5HS fabric weave. To achieve that we use Ishikawa's bridge concept together with the cure evolution in the engineering constants to develop a manufacturing model for the 5HS fabric *bridge unit cell*. The approximately square shape of the repeating unit in a satin weave, as shown in figure 3.25 is a repeating unit approximation to a satin weave structure which consists of the interlaced region and its surrounding areas. The four regions labelled by A, B, D and E consist of straight fill threads, and hence can be regarded as pieces of cross-ply laminates of thickness h_t. Region C has an interlaced structure with an undulated fill thread. Although the undulation and continuity in the warp threads can be ignored since the error is expected to be small because the applied load is considered in the fill (x) direction. The in-plane stiffness in region C can be shown to be much lower than

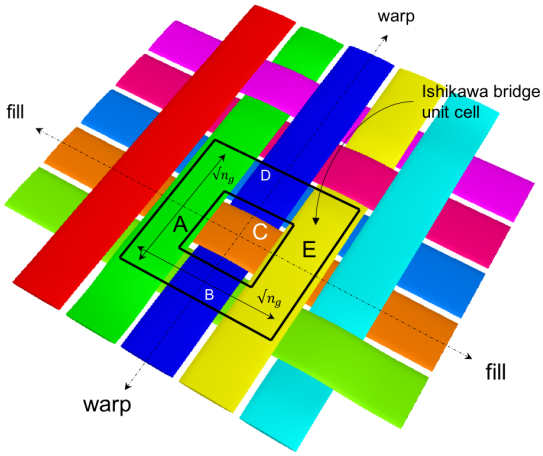

Fig. 3.25 Unit cell for an Ishikawa one dimensional bridge structure.

that of a cross-ply laminate [42]. Therefore, as a consequence, regions B and D carry higher loads than region C and act as *bridges* for load transfer between regions A and E. The bridge model is therefore a normal unidirectional laminate, with a square section missing in the center. In place of the uni-directional square section is the undulation (see figure 3.23) and thus the Ishikawa bridge model can be summarised as being a simple strength of materials calculation applied to stiffnesses. If this is so then the averaged stiffness matrix for this single unit cell with loads applied in the fill direction is for a single 5HS weave lamina is:

$$\langle \mathbf{A} \rangle(\alpha,t) = \frac{\sqrt{n_g}-1}{\sqrt{n_g}}\mathbf{A}^{CP} + \frac{1}{\sqrt{n_g}}\langle \mathbf{A}^{U} \rangle \tag{3.88}$$

where $\mathbf{A}^{CP}$ is the stiffness calculated for the standard CLT crossply or unidirectional sections A, B, D and E and $\langle \mathbf{A}^{U} \rangle$ is the undulatory contribution of section C. Given that the this total stiffness matrix is essentially one dimensional, an easy improvement can be made to the stiffness model of the unit cell cross-plying it with another identical one rotated by $\pi/2$ radians creating a balanced symmetric arrangement as in the panel manufacture experiment:

$$\langle \mathbf{A}^{\Sigma} \rangle(\alpha,t) = \frac{\sqrt{n_g}-1}{\sqrt{n_g}}\mathbf{A}^{2\times CP} + \frac{1}{\sqrt{n_g}}\langle \mathbf{A}^{2\times U} \rangle \tag{3.89}$$

where:

$$\mathbf{A}^{2\times CP} = \sum_{i\in S_{CP}} \frac{h_t}{2}\mathbf{R}_i^{-1}\mathbf{Q}\mathbf{R}_i \tag{3.90}$$

and:

$$\mathbf{A}^{2\times U} = \sum_{i\in S_U} \mathbf{R}_i^{-1}\langle \mathbf{A}^U\rangle \mathbf{R}_i \tag{3.91}$$

where $S_{CP} = \{0, \pi/2, \pi/2, 0\}$ and $S_U = \{0, \pi/2\}$. Here, as already established:

$$\langle \mathbf{A}^U\rangle = \langle \mathbf{A}^M\rangle + \langle \mathbf{A}^F\rangle + \langle \mathbf{A}^W\rangle \tag{3.92}$$

where $\langle \mathbf{A}^M\rangle$, $\langle \mathbf{A}^F\rangle$ and $\langle \mathbf{A}^W\rangle$ are given:

$$\begin{aligned}
\langle \mathbf{A}^M\rangle &= \left[\frac{2}{l}\int_0^l [\mathbf{Q}^M(h_1(x) - h_2(x) + h - h_t/2)]^{-1}dx\right]^{-1} \\
\langle \mathbf{A}^F\rangle &= \left[\frac{2}{l}\int_0^l \left[\mathbf{Q}^F(\theta(x))\frac{h_t}{2}\right]^{-1}\right]^{-1} \\
\langle \mathbf{A}^W\rangle &= \left[\frac{2}{l}\int_0^l [\mathbf{Q}^W(h_2(x) - h_1(x))]^{-1}dx\right]^{-1}
\end{aligned}$$

Equation 3.52 gives the Cauchy equilibrium of equation 3.40:

$$\mathbf{0} = \langle \mathbf{A}^\Sigma\rangle(\alpha,t)\langle \varepsilon_{\text{solid}}\rangle - \langle \mathbf{A}^\Sigma_\otimes\rangle(\alpha,t)\begin{bmatrix} c_1 \\ c_2 \end{bmatrix}\Delta T \tag{3.93}$$

where $(c_1, c_2)^T$ are *linear* coefficients of thermal expansion *local* to the top ply. The thermal stiffness matrix $\langle \mathbf{A}^\Sigma_\otimes\rangle(\alpha,t)$ can be calculated by repeating the symmetric balanced summation technique above:

$$\langle \mathbf{A}^\Sigma_\otimes\rangle(\alpha,t) = \frac{\sqrt{n_g}-1}{\sqrt{n_g}}\mathbf{A}^{2\times CPT} + \frac{1}{\sqrt{n_g}}\langle \mathbf{A}^{2\times UT}\rangle \tag{3.94}$$

where:

$$\mathbf{A}^{2\times CPT} = \sum_{i\in S_{CP}} \left(\frac{h_t}{2}\right)\mathbf{R}_i^{-1}\mathbf{Q} \tag{3.95}$$

and:

$$\mathbf{A}^{2\times UT} = \sum_{i\in S_U} \mathbf{R}_i^{-1}\langle \mathbf{A}^U\rangle \tag{3.96}$$

The thermal strain equation for a symmetric laminate of 5HS weave is given:

$$\langle \varepsilon_{\text{solid}} \rangle = [\langle \mathbf{A}^{\Sigma} \rangle(\alpha,t)]^{-1} \langle \mathbf{A}^{\Sigma}_{\otimes} \rangle(\alpha,t) \begin{bmatrix} c_1 \\ c_2 \end{bmatrix} \Delta T \tag{3.97}$$

or:

$$\varepsilon_{\text{solid}} = \mathbf{K}^{-1}(\alpha,t)\mathbf{K}_{\otimes}(\alpha,t) \begin{bmatrix} c_1 \\ c_2 \end{bmatrix} \Delta T \tag{3.98}$$

where the mean fields are now implied. This equation is the 5HS fabric unit cell equivalent of the cross-ply CLT at curing time t for temperatures *above* the glass transition temperature. Note however that these equations do not take into account the substrate surface strain discussed in previous section. The major contribution to curing comes not from the inherent stiffness or viscoelastic properties of the fluid resin, but rather the evolution of the surface strain of the substrate as it cures as seen earlier. We have also assumed that there is no chemical shrinkage is absent. This is to some extent justified for this experiment since the first dwell time in figure 3.14 is small. The only effects taken into account are the cure boundary and Ishikawa contributions to the CTE. The CTE can easily be computed for 5HS fabrics by differentiating equation 3.98 :

$$\mathbf{CTE}_{\text{solid}} = \mathbf{K}^{-1}(\alpha,t)\mathbf{K}_{\otimes}(\alpha,t) \begin{bmatrix} c_1 \\ c_2 \end{bmatrix} \tag{3.99}$$

and using equation 3.62:

$$\mathbf{CTE}_{\text{liquid}} = \mathbf{CTE}_{\text{solid}} \sqrt{\alpha} \tag{3.100}$$

The values of the thermal expansion coefficients $(c_1, c_2)^T$ are determined by considering the standard CLT estimate (see Hyer, [41]) in local lamina coordinates:

$$c_1 = \frac{c_{11}^{(2)} V^{(2)} E_{11}^{(2)} + b V^{(1)} E^{(1)}}{V^{(2)} E_{11}^{(2)} + V^{(1)} E^{(1)}} \tag{3.101}$$

$$c_2 = b + (c_{22}^{(2)} - b) V^{(2)} \tag{3.102}$$

$$+ \frac{E_{11}^{(2)} \nu^M - \nu_{11}^{(2)} E^M}{V^{(2)} E_{11}^{(2)} + V^{(1)} E^{(1)}} (b - c_{11}^{(2)}) V^{(1)} V^{(2)} \tag{3.103}$$

where $b = b_3$ in equation 3.38 since $b_1 = b_2 = 0$ as they have no adhesive action. To

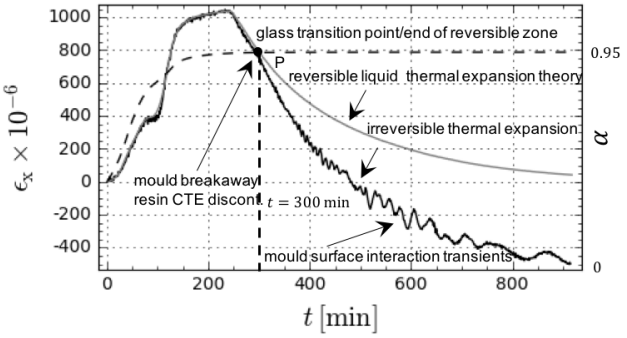

Fig. 3.26 Tri-curve determination of the glass transition temperature.

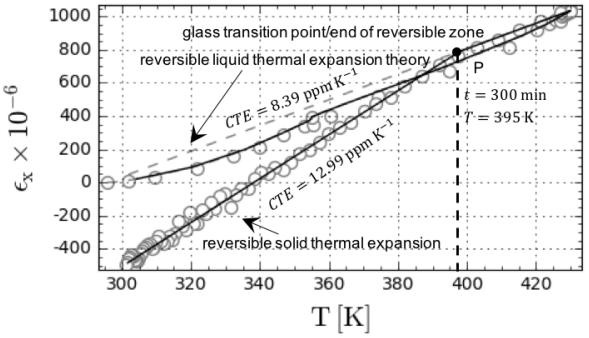

Fig. 3.27 Comparison of the complete panel manufacture strain-temperature optical fibre data and equation 3.99.

use the theory, we obtained the non-isothermal variation of $\alpha(t)$ extracted from the DSC experiments (see figures 3.12 and 3.14) for working out the viscoelastic matrix $\mathbf{KK}_{\otimes}^{-\mathbf{1}}$ in equation 3.99. The Huntsman datasheet values for cured LY564/HY2954 resin are $b \approx 75\,\text{ppm}\,\text{K}^{-1}$ at the glass transition temperature and for the 5HS weave sheet we set $c_{11}^{(2)} \approx -0.4\,\text{ppm}\,\text{K}^{-1}$. The volume ratio is decided in terms of a unidirectional laminate equivalent where $V^{(1)} : V^{(2)} \approx 39 : 61$. For the actual manufactured 5HS composite unit cell this equates to about $60 : 40$ [24]. The coefficients of expansion in equation 3.103 represent the 5HS lamina thermal strain coefficients when the material lamina is *fully* cured. This immediately presented a difficulty since it is well known [73] the the value of b is a function of the HY2954 hardener stoichiometric coefficient $\alpha_2 \approx 0.35$ and the temperature. Using the chemistry data of a typical epoxy resin before the glass transition temperature we were able to determine an approximate value the liquid phase value of $b \approx 50\,\text{ppm}\,\text{K}^{-1}$ which when used

in equation 3.100 delivers a liquid state CTE value of $8.57\,\mathrm{ppm\,K^{-1}}$. The value measured from the data is $8.39\,\mathrm{ppm\,K^{-1}}$. This seeming agreement between the two values may not be accurate however: the effect of the mould could not be included in these calculations due to a lack of experimental data and the experimental value may be offset by the Timoshenko plate formed between the bottom of the laminate gluing to the mould when curing below the glass transition temperature. Experimental evidence of this can be seen in figure 3.26 just beyond the 400 minute mark where the signal becomes noisy, indicating mould interactions between the bottom plate and the steel mould surface [80].

As the temperature approaches the glass transition the resin product has linked up into an infinite molecule for much of $V^{(1)}$ and equation 3.42 that $\langle r \rangle^3 \sim V^{(1)}$. The resin structure begins to harden and solidify and this reduction in mechanical flexibility tends to detach it from the mould [80]. In the same temperature interval, the CTE of the converted resin suddenly rises [73]. Using the data sheet supplied value of $b \approx 75\,\mathrm{ppm\,K^{-1}}$ in equation 3.99 or 3.100 gives a theoretical CTE value for the composite plate of around $12.92\,\mathrm{ppm\,K^{-1}}$ which compares well to the experimental value obtained directly from the optical fibre signal of $12.99\,\mathrm{ppm\,K^{-1}}$. This set of congruences leads one to estimate the glass transition temperature for the LY564/HY2954 epoxy resin system to be the divergence point of the equation 3.100 and the optical fibre signal, which coincide with time when the conversion parameter (figure 3.14) reaches its maximum value of 0.95. This is illustrated in figure 3.26 when $t \sim 300$ min and can be clearly seen in figure 3.27 at $T \approx 395$ K which is $122\,\mathrm{C^{\circ}}$. This compares well with the Huntsman datasheet value of $123 - 127\,\mathrm{C^{\circ}}$ for a similar cure cycle to figure 3.14.

3.5 Conclusions

The use of distributed embedded optical fibre sensing during VARIM panel manufacturing adds an important dimension to the measurement of the internal strains for carbon fibre composite panels. The ability to measure the strain distribution as opposed to strain at a single point provides statistically relevant detail as to the real time performance of high technology materials like carbon fibre weave composites. We have in this article used a single aspect (see figure 3.20) of the information provided by a 2 m long distributed sensor embedded into a composite panel to lead onto a possible hypothesis of the early strain behaviour inside curing panels. Extending that hypothesis to a more general theory of thermo-mechanical substrate curing interactions has provided an explanation of the disparity between the standard viscoelastic solid model CLT and the strain data trends we measured

during manufacturing processes below the glass transition temperature:

$$\mathbf{CTE}_{\text{liquid}} = \mathbf{CTE}_{\text{solid}}\sqrt{\alpha}$$

where α is the cure parameter. There do remain significant unanswered questions however, which will require more work in this area. One of the most unsatisfactory aspects of the article is the natural question of enthalpy changes in a free standing resin as compared to one carrying substrate. This was touched upon in equation 3.56, which is derived for a free standing resin in DSC type experiments, could in fact have missing terms when a substrate is added. Another area of weakness is that the CTE value calculations rely upon a balanced symmetric Ishikawa bridge unit cell [42]. Better models are infact available [24] but it was felt that Ishikawa is quicker and easier to implement as well as being more intuitive. Perhaps the gravest lack of detail was in the contribution of the mold. The experimental data for mold interaction was simply not collected and that has undoubtedly taken away some insight into the process. Lastly, one might ask if the result is of general validity or specific to just this one case - as always, further experimentation must decide. Positively however, the agreement of the CTE equation with experimental data has been encouraging, particularly from the point of view of being an example for what distributed optical measurement techniques can potentially achieve in future. The congruence of data and theory in this paper supports the following conclusions:

(i) The embedded optical fibre measures true strains at all times.

(ii) The close lying high density carbon fibres of the 5HS substrate glued together early on during cure.

(iii) These facts support and imply the “freezing” of the post infusion stress states of both the carbon fibre fabric and the the optical fibre, generating the homogeneous strain shifts seen in figure 3.20.

(iv) The 5HS substrate strain is unit cell surface area dependent (thin laminate) and increases with α.

(v) The mechanical work performed by the expanding resin on the 5HS substrate increases as α

(vi) The mechanical thermal expansion strain of the panel composite below the glass transition temperature increases as $\sqrt{\alpha}$

(vii) For pure epoxy resin the thermal expansion strain of the resin increases as α.

(viii) This fact implies that the VARIM manufacturing process strongly modifies the expansion properties of the resin below the glass transition temperature.

(ix) The thermal expansion strain flow of the composite panel is not viscoelastic but Newtonian.

Chapter 4

Residual strain minimization

4.1 Residual strain

4.1.1 Understand and minimize the residual strain

The study of the residual strain is of great interest to the industries employing composite materials because the presence of such strains can compromise the functionality of the composite material products. Residual strain in the composite laminate are introduced during processing and can have deleterious effects in terms of structural integrity and dimensional stability of composite structures. The different properties of constituent (reinforced fiber and matrix resin), the multi directional layup of the laminate and the elevated fabrication temperature generate the residual strain. Although the residual strain in a complete cured laminate have been characterized, the way in which these stresses develop during processing is still not fully understood. [79] A number of studies have been conducted to optimize the process cycle, to minimize residual strain in specific material systems. However, no matter what the cure cycle residual processing strains seem inevitable as will be shown in this chapter; understanding how they build up can facilitate their reduction through appropriate process control and part design, while estimates of their magnitude can be used to accommodate their in appropriate tool design, allowing the fabrication of a part of net shape and dimensions.[**?**] The prediction of residual strain in composite materials during the curing process was initially carried out through the development of theoretical models to present a multi-physics analysis to investigate the effect of temperature gradients and the degree of cure on residual stresses within the laminated thickness. Models introduced by White and Hahn have added to the kinetics polymerization the study of the viscoelastic behavior of

the material in order to predict historical residual strain in composite materials during the curing process. These first studies were limited to discontinuous analysis, it was not possible to fully monitor the entire cure process and the cooling phase. There were not real-time monitoring systems that allow to get data at any point of processing. In the studies carried out by White and Hahn strain gages have been bonded to ply of a graphite/BMI laminate in order to monitored changes in strain during cure. In these studies the aim of the work was the quantification of residual strains arising from differential thermal expansions and anisotropy of the constituents, during cool-down, after resin solidification was complete through the use of distributed, continuous strain measurements. An intermittent cure technique was used to characterize the development of residual strain during processing. At predetermined points in the manufacturer's recommended cure cycle (MRC) the process cycle was stopped and the specimens cooled at a constant rate (10 °C/min) to room temperature as calculated through minimization of the associated viscoelastic integro differential equations. White and Hahn have found that thermal strains during cool down are dominant in residual strain development in the BMI resin composite investigated, while chemical shrinkage strains are found to be negligible for the processing conditions investigated.[86] They were the first to understand the importance of the cooldown phase in an attempt to minimize residual strain. What has been done through this study is to understand how strains can be *potentially* minimized by modifying the cooling process. It has to be said therefore that the control of strain development through cooling process seems to be a rather large area of study. In that light, more remains to be done than what was possible here, although this study leads to a novel conclusion that could drive research into promising avenues in the future.

4.1.2 Monitoring the residual strain by viscoelastic analysis

In the fabrication of a thermoset composite, the matrix is initially fluid, in the fluid state the resin cannot sustain a stress, and consequently to an approximation, the constituents are initially stress-free. During curing, thermoset resins evolve from liquids of low molecular weight to solids with fully developed 3D cross-linked networks. Cross-links could be formed by chemical reactions that are initiated by curing agents, temperature, pressure or radiation. The cross-linking and branching action results in a loss in the polymers ability to move as individual polymer chains, consequently resulting in an increase in viscosity. The matrix solidifies during the cure process and consequently the stresses build up. During a typical process cycle, initially the resin viscosity drops upon the application of heat, passes through a region of maximum flow and then begins to increase again as the chemical reactions starts and degree of cross-linking between the constituent oligomers increases. This point is known as the gelation point and is characterized by the material transition from a viscous liquid to a

rubbery solid exhibiting viscoelastic type behavior. At this point the viscoelasticity plays a specific role, the high temperature permits and accelerates the relaxation of stresses within the material during the so called mid-curing phase. So much so that when the cooling phase starts the material is usually stress free inside the mold. A linear thermoelastic analysis could be a manner to determinate the residual strain, but it is more significant to use a full viscoelastic analysis when considering that at cooler temperatures the material inhibits relaxation rates and begins once again to store up stress inside its volume. This stress is of course driven by thermal expansion. A viscoelastic analysis with non isothermal conditions in association with the classical lamination theory (as has been employed in earlier chapters) was used to determine the effects of curing temperature history on residual strain of the composite laminate. The time-dependent strains and deformation are functions of the temperature.[79] The residual strains in layer k of the laminate at time t for a temperature variation between $T_{(0)}$ and $T_{(t)}$ were obtained by subtracting the unrestrained thermal strain in layer k from the final strain in that layer within the laminate. This is very similar to the technique used by first used by Hyer, White and Hahn in earlier studies. The main difference arises from the inclusion of full viscoelasticity, first seen in papers by authors such as Weitsmann. A standard equation for the strains in a non isothermal deformation within a composite plate can be written:

$$[\varepsilon^r(t)]^k_{x,y} = [\varepsilon^0(t)]_{x,y} + z_k[\kappa(t)]_{x,y} - \int_{T_{(0)}}^{T_{(t)}} [\alpha(T)]^k_{x,y} dT \tag{4.1}$$

where:
$[\alpha(T)]^k_{x,y}$=temperature dependent coefficients of thermal expansion of layer k;
$[\varepsilon^0(t)]_{x,y}$= midplane strains;
$[\kappa(t)]_{x,y}$= curvatures;
z_k= distance of layer centroid from midplane of laminate.
The midplane strains and curvatures are obtained by using a convolution integral form in the lamination theory expressions for midplane strains and curvatures:[79]

$$[\varepsilon^0(t)] = \int_0^t [a(\xi - \xi')]\frac{\partial}{\partial\tau}[N^T(\tau)]d\tau + \int_0^t [b(\xi - \xi')]\frac{\partial}{\partial\tau}[M^T(\tau)]d\tau \tag{4.2}$$

$$[\kappa(t)] = \int_0^t [c(\xi - \xi')]\frac{\partial}{\partial\tau}[N^T(\tau)]d\tau + \int_0^t [d(\xi - \xi')]\frac{\partial}{\partial\tau}[M^T(\tau)]d\tau \tag{4.3}$$

where $a(\xi)$, $b(\xi)$, $c(\xi)$, $d(\xi)$ are time-temperature dependent compliances where ξ and ξ' are:

$$\xi = \xi(t) = \int_0^t \frac{dt'}{a_T[T(t')]} \tag{4.4}$$

$$\xi^{'} = \xi(\tau) = \int_0^{\tau} \frac{dt'}{a_T[T(t')]} \tag{4.5}$$

where ξ and $\xi^{'}$ are reduced time variables and $a_T(T)$ is the shift function obtained by constructing the master curves for the stiffnesses or compliances of the unidirectional layer.[79] The time-temperature-dependent thermal force and moment resultants were obtained by using the convolution integral form for the standard definition of these quantities in lamination theory.[79]

$$[N^T(t)]_{x,y} = \sum_{k=1}^{n} h_k \int_0^t [\overline{Q}(\xi - \xi^{'})]_{x,y}^k \frac{\partial}{\partial \tau} \left(\int_{T(0)}^{T(\tau)} [\alpha(T)]_{x,y}^k dT \right) d\tau \tag{4.6}$$

$$[M^T(t)]_{x,y} = \sum_{k=1}^{n} h_k z_k \int_0^t [\overline{Q}(\xi - \xi^{'})]_{x,y}^k \frac{\partial}{\partial \tau} \left(\int_{T(0)}^{T(\tau)} [\alpha(T)]_{x,y}^k dT \right) d\tau \tag{4.7}$$

where:
$[\overline{Q}(t)]_{x,y}^k$= layer stiffness matrix referred to the x and y axes
h_k=layer thickness The corresponding residual stresses in layer k along x and y axes are:

$$[\sigma^r(t)]_{x,y}^k = \int_0^t [\overline{Q}(\xi - \xi^{'})]_{x,y}^k \frac{\partial}{\partial \tau} [\varepsilon^r(\tau)]_{x,y}^k dT) d\tau \tag{4.8}$$

The time-temperature-dependent warpage, obtained by integrating the curvature-displacement relations, is:

$$w(t) = -\frac{1}{2}[\kappa_x(t)x^2 + \kappa_y(t)y^2] + \kappa_{xy}(t)xy] + \frac{a}{2}[\kappa_x(t)x + \kappa_y(t)y] \tag{4.9}$$

where the time-dependent curvatures are obtained from the thermoviscoelastic stress-strain relations.The irreversible polymerization shrinkage, or chemical shrinkage, is assumed to occur in full at the peak curing temperature, and is taken as an initial discontinuity at time t = 0. Thus, Equations become:

$$[N^T(t)]_{x,y} = \sum_{k=1}^{n} h_k \int_0^t [\overline{Q}(\xi - \xi^{'})]_{x,y}^k \frac{\partial}{\partial \tau} \left(\int_{T(0)}^{T(\tau)} [\alpha(T)]_{x,y}^k dT \right) d\tau + \overline{Q}(\xi - 0)]_{x,y}^k [e^c]_{x,y}^k \tag{4.10}$$

$$[M^T(t)]_{x,y} = \sum_{k=1}^{n} h_k z_k \int_0^t [\overline{Q}(\xi - \xi^{'})]_{x,y}^k \frac{\partial}{\partial \tau} \left(\int_{T(0)}^{T(\tau)} [\alpha(T)]_{x,y}^k dT \right) d\tau + \overline{Q}(\xi - 0)]_{x,y}^k [e^c]_{x,y}^k \tag{4.11}$$

where $[e^c]^k_{x,y}$ are the chemical shrinkage strains of layer k. Then the residual strains becomes:

$$[\varepsilon^r(t)]^k_{x,y} = [\varepsilon^0(t)]_{x,y} + z_k[\kappa(t)]_{x,y} - \int_{T_{(0)}}^{T_{(t)}} [\alpha(T)]^k_{x,y} dT + [e^c]^k_{x,y} \tag{4.12}$$

Minimizing this last equation with respect to an undetermined temperature profile leads to a difficult mathematical problem. The difficulty lies in the fact that the solution is possible only through certain assumptions and that these assumptions are unphysical (an impossibly rapid decay of temperature). However, it is the only recognized solution possible, and thus it has been used to design an experiment to test its validity here (and by several authors right up to the present, e.g. Gopal). The temperature that solves the last equation is found to be approximately like that used in the experiment (see figure 4.9).

4.1.3 Distributed fiber strain monitoring and Strain-time relation

In light of such unclear circumstances, the real-time monitoring of internal strains is a useful way to clarify the mechanism of residual strain development during cooling. This study focuses on investigating the development of internal strains in woven carbon fabric composites during the curing and cooldown process. It could be possible have a complete knowledge about the entire composite life cycle using embedded fibre bragg grating,FBG,sensors, with limitations. The term life cycle refers to the composite life time from manufacturing and until mechanical testing, as illustrated in Figure 4.1. Fiber optic sensors are considered one of the most recent and promising methods also for the monitoring of the process-induced residual strains. It is important to outline that, in this area, most of the works have been concentrated on global measurements, such as curvature, warpage and spring in at the end of the process cycle, while only more recently sensing techniques, based on Fabry-Perot and Bragg fiber optics have been implemented to get local information about the strain fields during the whole cure stage, allbeit at a single position in the laminate.In this study, on the other hand, embedded distributed optical sensors were employed to determine, in situ, the build up of residual strains in carbon fiber reinforced polymer composites during cure and cooldown phases. The optical sensor was emebedded during the composite layup. Using this facilities it is possible monitoring the development of process induced internal strains and investigate the influence of these strains in the composite during manufacturing and or testing. Such manufacturing control is important if consistency in the quality of the composite is desired. In addition, information of the residual strain in the structure is important if these are to be accounted for the design of a structural component. The importance lies in the continuity of information present along distributed paths inside the composite where strain

symmetries or indeed their absence develops a data rich and complete picture of the *dynamic* of the cooldown process in the manufactured sample. The amount of data obtained is quite substantial and by the end of the doctorate thesis certain things are only just becoming clear. These initial conclusions are however powerful, they serve to eliminate certain ideas about the cooling process and its effect upon residual strain development inside the composite during manufacture. During the cure cycle and cooldown the embedded distributed optical fiber

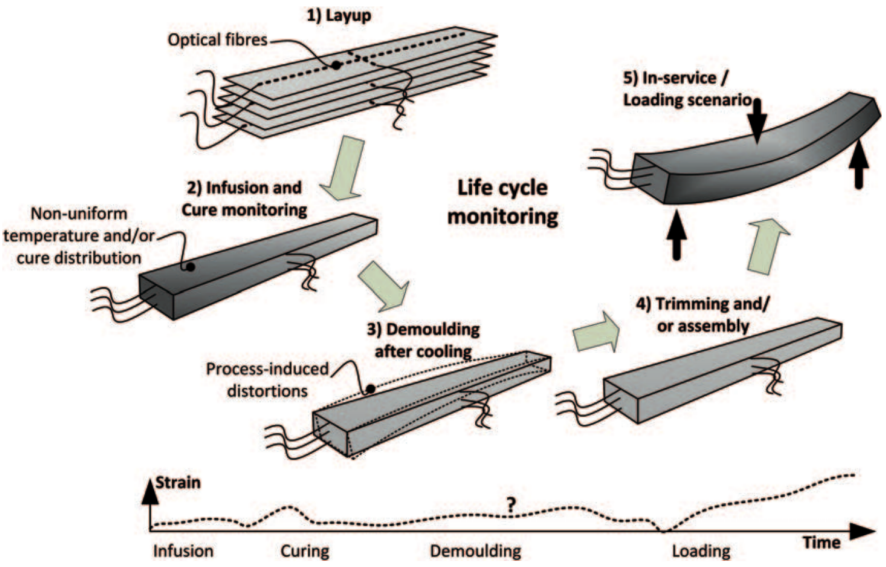

Fig. 4.1 Schematic of life cycle monitoring approach for a laminate[20]

provide information about the strain along the time and the strain along the optical sensor length.As shown in Figure 4.2 the optical sensor measure the microstrains that occur during the entire cure and cooldown phases for our two samples: plates 2 and 3. Figure 4.3 shows the microstrain values in different layers of the second plate, in the same way in figure 4.4 is shown the subdivision between the bottom, middle and top layer of plate 3. The different trend in strain time is strongly associated with the different thermal cycles considered for plates 2 and 3. The thermal cycles used for plate two and for three will be introduced in the next section, along with their impact upon the strain development in the composite. Information about the strain distribution long the optical sensor as shown in Figure 4.5. In Figure 4.5 it is possible to see that the strains have a similar trend at the beginning of the cure and at the end of the cooldown phase, this means that the fiber is surrounding and locked from the beginning by the polymeric resin as was shown in in earlier chapters. When the distributed fibre is embedded in a composite material complete strain transfer is achieved

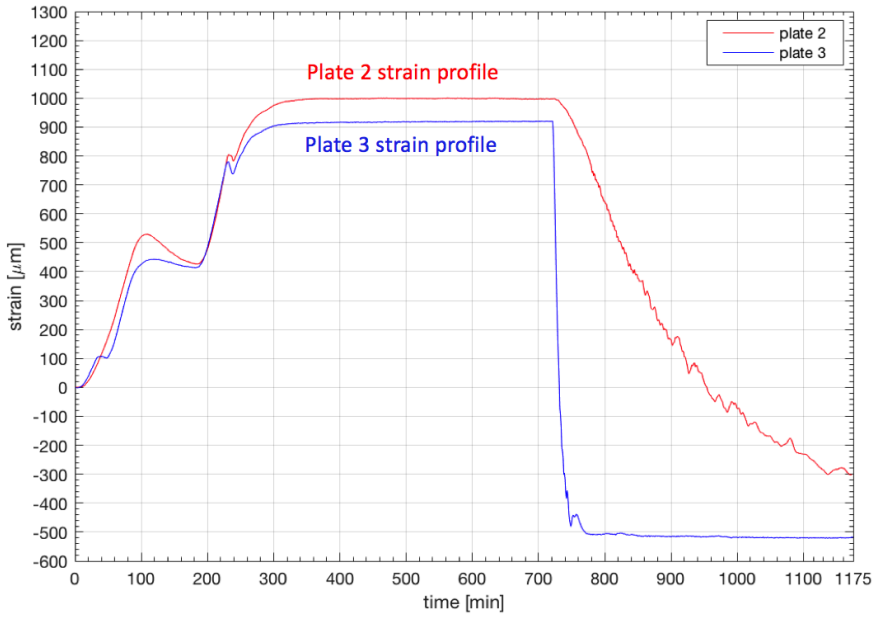

Fig. 4.2 Microstrain compare between the second and third plate.

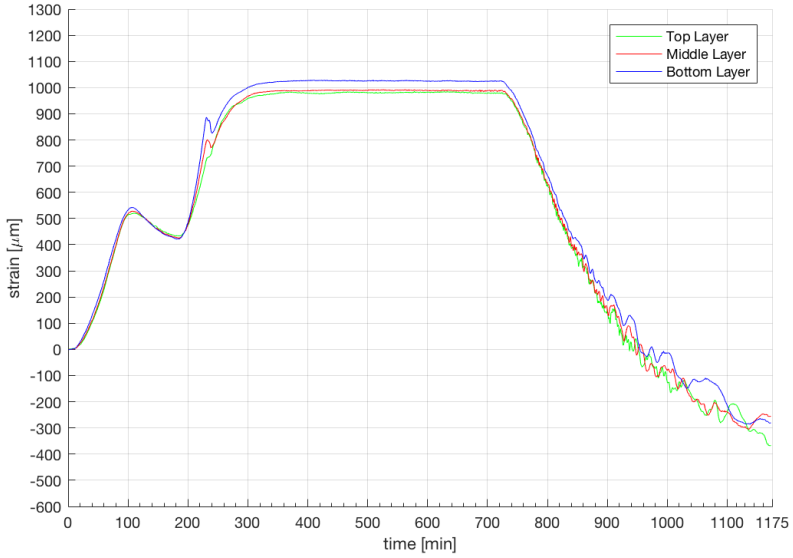

Fig. 4.3 Second plate microstrain in the top(green), middle(red) and bottom(blue) layers.

once bonding between the optical fibre and the substrate material occurs - which is seen to happen right from the start of the cure cycle.

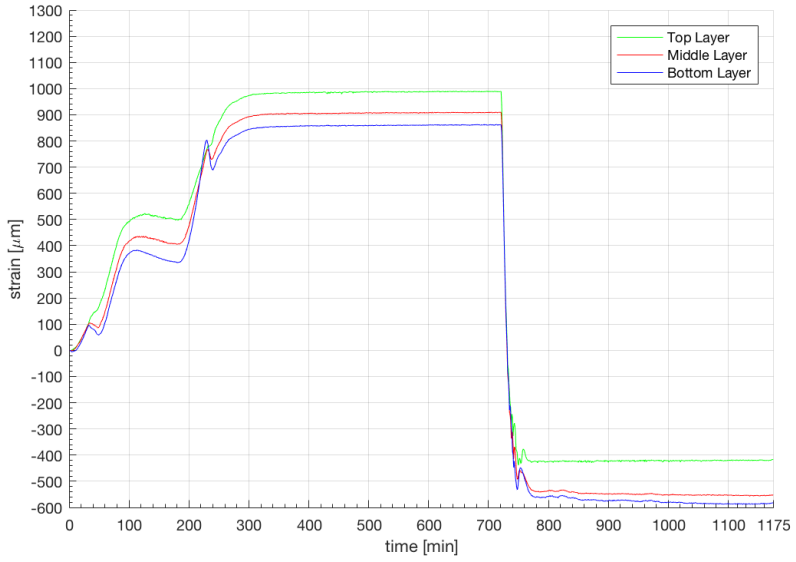

Fig. 4.4 Third plate microstrain in the top(green), middle(red) and bottom(blue) layers.

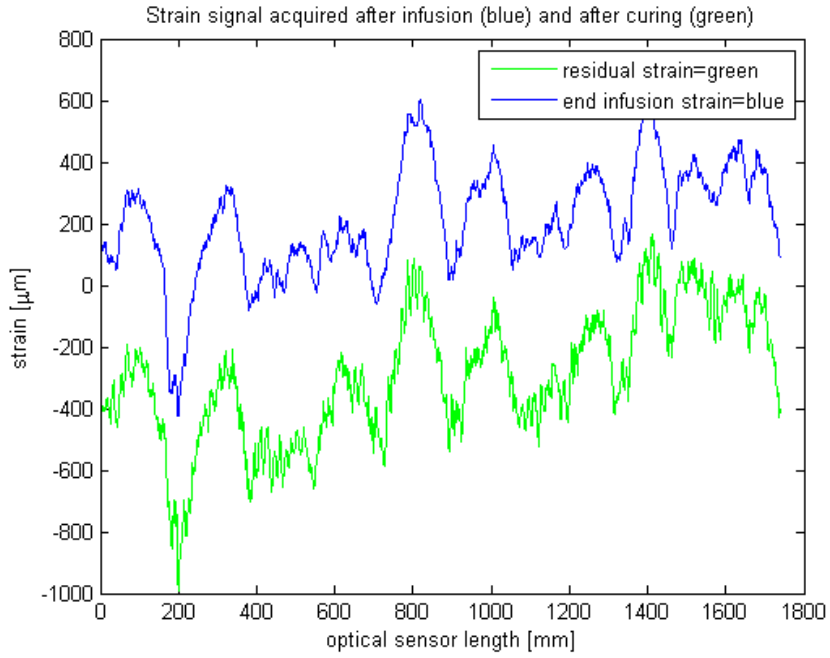

Fig. 4.5 Distributed strain plate 3

4.2 Cure process

The residual strain is generated during the cure process of a composite material. During the curing process, very complex physical phenomena take place that make it difficult to understand the complete nature of the residual strain. Such strains can in fact can be so high as to cause damage or breakage of the lamina in the absence of a load. Once active loads are applied, these can have deleterious effects on the structural integrity and dimensional stability of the composite structure both before and during operation of the composite. A similar situation occurs in residually stressed metallic structures. What is certain is that the effect of the temperature with respect to time plays an important role as the equations of this chapter seem to strongly imply. In fact it would be more precise to say that the involvement of the temperature profile is of great fundamental importance. The temperature rise over time influences the degree of cure, through the so called α parameter, which is connected directly to the chemical and physical process rates occurring within the composite. The degree of cure varies from a zero initial value wherein the resin is a viscous fluid, to an intermediate value when the resin is a gel, up to a value close to unity at the end of the curing process where the matrix is completely polymerized and in a glass state. The standard cure cycle for a particular resin/fibre combination is actually recommended by the manufacturer, this Manufacturer Recommended Cure, MRC usually has two steps, which practically means that there are generally two dwells during the process of cure setting. What needs to be investigated is how to vary the strain by varying the cooling cycle of cure, or to vary the dwell steps to characterise the performance of the strain and obtain an insight into how the resin chemical expansions actually operates inside a composite structure. Several articles [63][84][82][15] demonstrate how certain changes in the cure cycle as opposed to the MRC produce a treatment that can alter the final value of residual strain. Cycle optimization involves the reduction of residual strain keeping final mechanical characteristics of the composite relatively unchanged from the MRC cycle. An optimization of the treatment cycle can be obtained as proposed by Olivier[63] through variations in the temperature and the time or manipulation of the temperature together with the duration of second dwell. The research carried out by Olivier has shown that the cure cycle can be optimized in order to reduce the residual strain going to act not only on the temperature of the treatment and the cure time, but also on possible variations in the rate of cooling or using an multistep process of cure. However, the study is experimentally sound, without clear conclusions towards a quantitative, calculable theory. In the present study in order to analyze the residual strain during cooldown, the cooling cycle recommended by the manufacturer shown in Figure 4.6 is referenced against the fast cooldown treatment cycle shown in Figure 4.7 found by solving the earlier integro differential equations on a computer. Even though the solution has been

highlighted as suspect, studying its practical effect on the composite should and indeed does lead to a positive step forward as to what the best cooling solution for (in this case) composite plate manufacturing should be.

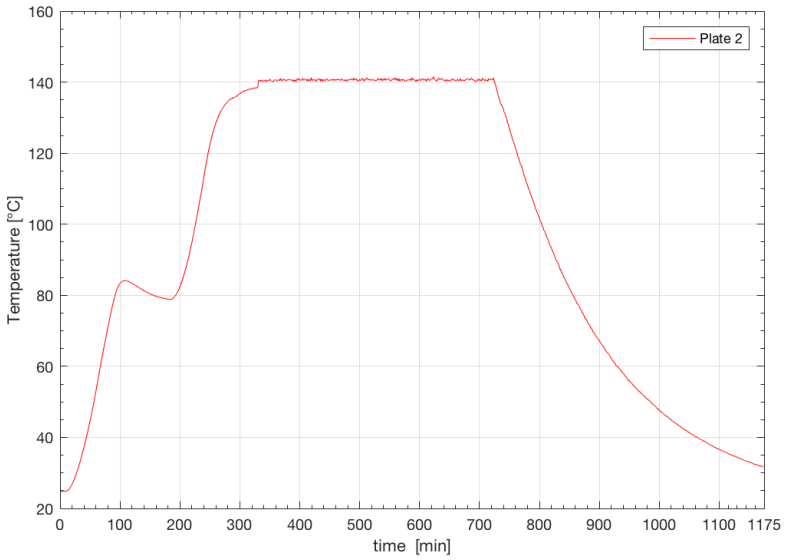

Fig. 4.6 Cure cycle plate 2.

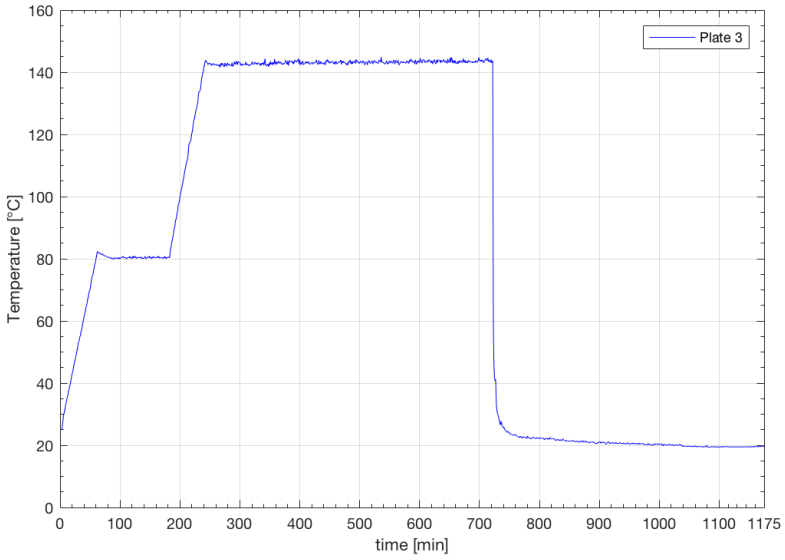

Fig. 4.7 Cure cycle plate 3.

4.2.1 Cure Cycle:cooldown phase plate 2

Residual stresses in composite material evolve during the the curing stage as well as during post-cure cooling from an elevated processing temperature down to the operational temperature [13]. However assuming that a fully relaxed state during the second dwell has been attained will simplify the calculations within a small error. At any rate what is being investigated here at this stage are the *origins* of cooling residual strain and therefore such an assumption may serve as a valid starting position for investigations of greater import. For the production of plate 2 as has been indicated, we used a standard cure cycle. The standard cure process for the polymeric matrices is characterized by two-step of cure. The temperature is changed from room temperature to the temperature of the first dwell, 80°C and is held constant for an hour, then it is raised to the temperature of the second dwell 140°C and held for a period of 8 hours. After the second dwell, the part is cooled to the room temperature when the oven is turned off and the cooling phase follows Newtonś Law of Cooling, which is very slow as shown in Figure 4.8. The first dwell allows the escape of gas trapped inside the matrix and allows the resin to flow, also facilitate the compaction of the composite, the viscosity during the first dwell must be low (as seen in earlier chapters). Initially we have that as the temperature increases the viscosity of the matrix decreases to a minimum value. The second dwell is necessary to complete crosslinking the resin into what is essentially an adhesive around the carbon fibres. At this point the resistance and mechanical properties of the composite are determined. The cure cycle temperature design can also influence residual stress build-up and shape distortions, although as already indicated, we expect this to be minimal because of the relaxed stresses inside the material at that curing region. During curing, temperature dwells are normally used in order to obtain uniform temperatures in the part after the initial heating stage where these serve to allow the resin time to set or relax the material.

4.2.2 Cure Cycle:cooldown phase plate 3

By contrast, again as previously indicated, the production of plate 3 has not been subject to a standard cure cycle. The cure process modification is also extended to the two-step curing phases - though this is minimal with respect to the change made to the temperature profile upon cooling: The modification in these regions is thus kept to a minimum and the temperature change from room temperature to the temperature of the first dwell, 80°C and is held constant for an hour, then it is raised to the temperature of the second dwell 140°C and held for a period of 8 hours. After the second dwell, the part is cooled to the room temperature, at the end of the cure process, the cooling phase is different, the oven is opened

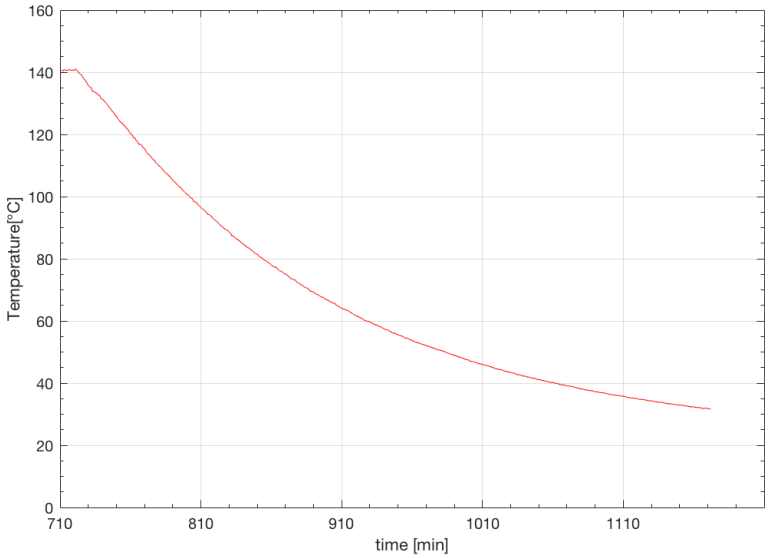

Fig. 4.8 Cooldown phase for the second plate laminate

and the hot air is expelled out of the oven at a given rate to ensure approximately the correct cooling profile. The third panel cooldown phase is shown in Figure 4.9. In Figure 4.10 is

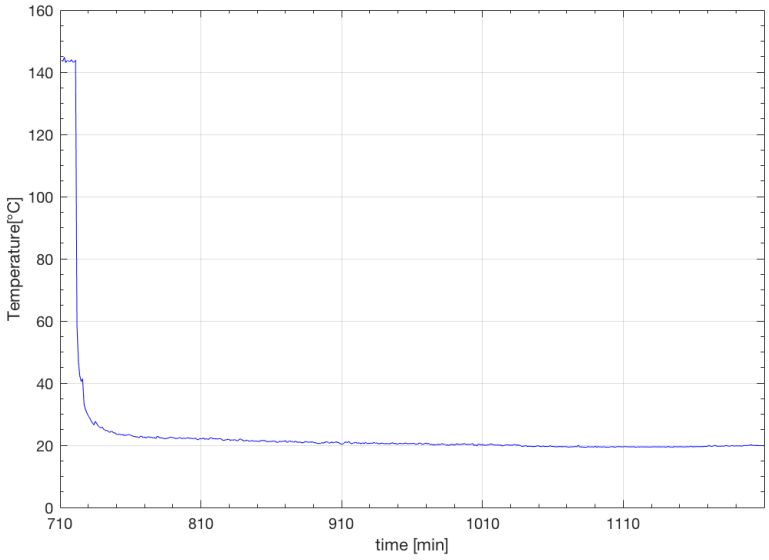

Fig. 4.9 Cooldown phase for the third plate laminate

shown a compare between cooldown phases about plate 2 and 3.

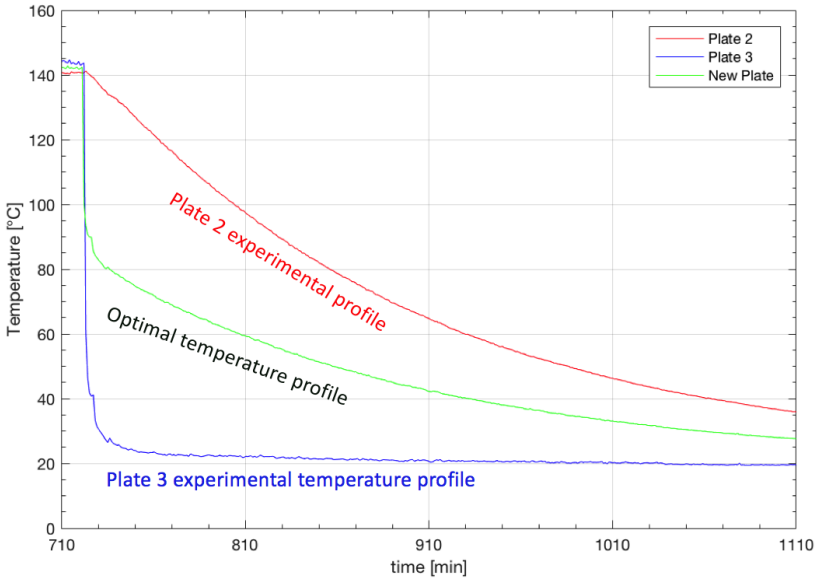

Fig. 4.10 The cooldown phase compare between the second and third plate laminate

4.2.3 Strain vs Temperature:Hysterisis on the thermal plane

On the thermal plane is rappresented the microstrain variation as function of Temperature for the second and third plate, see Figure 4.11. The red line is rappresentative of plate two, while the blue one is rappresentative of plate three. For both plates the relationship exhibits a hysteresis on the thermodynamic plane. As Figure 4.11 shows, the width of the hysterisis loop is different for plate two and three.In order to understand how the plates are characterized in detail it is possible refer to the Figure 4.12 and 4.13 to obtain the microstrain variation as function of Temperature for the bottom layer, the middle layer and the top layer. Figure 4.12 and Figure 4.13 shows respectively inside plate 2 and inside plate 3 that the trends between the different layers are constant, and that plate 3 has a large hysterisis, while plate 2 have a small hysterisis by comparison. The area enclose inside the hysterisis is the same for the bottom, middle and top layer. The initial value for plate two and three is zero, the last values one after the cooldown are respectively -300μm and -525μm.Figure 4.13 shows during the cooldown phase a costant microstrain values between 140°C and 40°C, these microstrain values during this Temperature range are locked which is a remarkable phenomenon. This is because it is this effect that leads to plate 3 having a significantly higher final CTE value with respect to that obtained by plate 2. Therefore a variation in the cooling cycle produces its first major measurable change : the thermal stiffness of the two plates and their hysterises are significantly different. As predicted by Hahn et al we

also see that the net result is that plate 3 obtain a much greater residual strain endpoint - which is somewhat contradictory to Gopal et al and their (and other authors) results: the massive change in thermal stiffness together with a large observable experimental difference in hysterisis implies a large difference in internal material state upon cooldown that is not merely explained by a mathematical theory. The hysterisis is also significant from a different point of view : the strain versus temperature plane for the composites could be likened to a force versus extension curve for a metal: The significant conclusion is this; a metal hysterisis measures the energy used to return material to zero extension. By comparison, here, we have a thermodynamically *irreversible* change that exhibits energetic characteristics in its behaviour. If the strain axis were squared, then indeed thermodynamic expansion energy stored in the material might become associated to the area of the hysterisis in some sense. What is clear is that 1) plate 3 is of much higher thermal stiffness than plate 2, 2) that the rapid cooling may optimise the earlier viscoelastic equations using a temperature profile that we and other authors report to be more like a thermal shock or *quenching* of the composite, but it remains far from clear what the structural condition of the material volume inside plate 3 is when compared to plate 2. That aside, a further point 3) can be made: the linear optical fibre strains are large for plate 3 when compared to plate 2 while both plates maintain opposite but relatively similar bending curvatures (see below), leading to a simple conclusion that the bending moment in both plates upon cooling is similar, *but not the internal stress state*.

4.3 Curvature

Thus it is well known that during the processing of composite laminates, laminate distortions of different kinds may occur. The laminate can take different configurations than those provided for in the design phase, as has always been emphasized. In particular, the laminates can assume a curved configuration, and such curves are due to several physical parameters, the most that affect the composite are the thickness of the laminate, the properties of the individual constituents that characterize the composite fiber and matrix, and on the thermal history, then the cure cycle set to processing the composite. At a structural level the thickness and type of material are design constraints that must be respected, it follows that to limit the curvatures of the composite plate the parameter on which we can act is the thermal cure cycle. So the goal is to identify the thermal cure cycle can minimize the residual stress *and* minimize the final curvature assumed by a laminate, which are not necessarily one and the same thing. During cooling from curing temperature to the room temperature within a laminate, the deformation of one ply is constrained by the other plies with different fiber

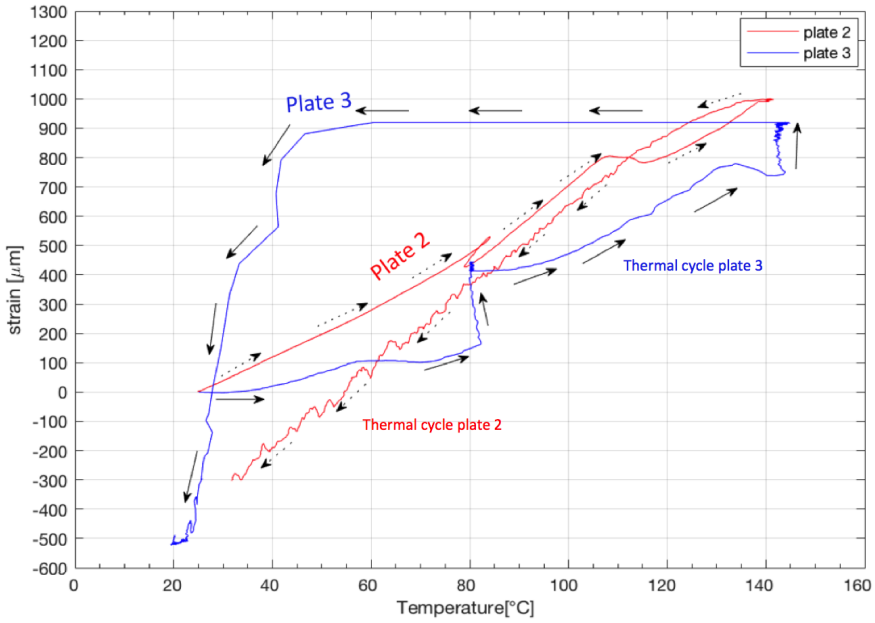

Fig. 4.11 Second and third plate microstrain variation with Temperature.

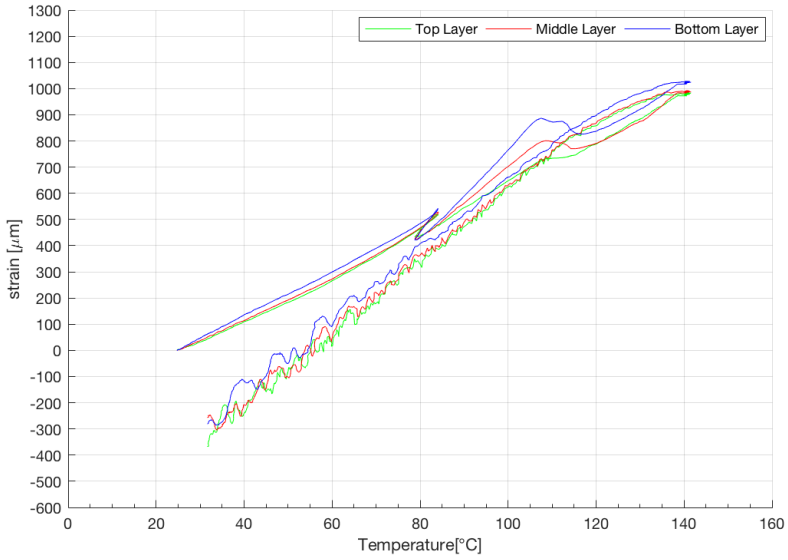

Fig. 4.12 Second plate microstrain variation with Temperature in the top(green), middle(red) and bottom(blue) layers.

orientations. Hence, residual stresses are built up in each ply. Consequently, the layers are under tension and compression and therefore thermal loads are induced leading to curving

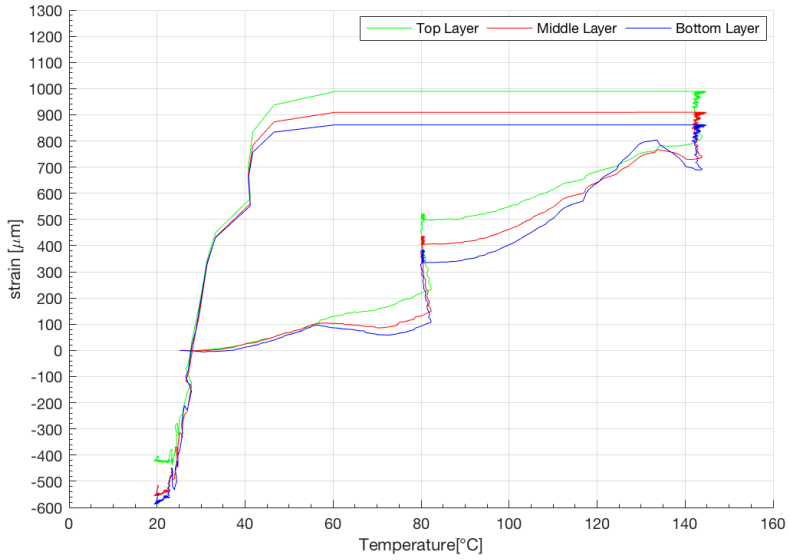

Fig. 4.13 Third plate microstrain variation with Temperature in the top(green), middle(red) and bottom(blue) layers.

during cooldown. It must also be noted that the plates are not subject to isotropic cooling - the mold inhibits the cooling of the bottom plate with respect to the top plate for both experiments.

4.3.1 Inversion of curvatures

The data gathered from the experiments is usefully depicted if one plots strain with depth as in Figure 4.14 where the final cooled strain data points are shown about the mean values of the bottom, middle and top layers for the plate two and the mean values of the bottom, middle and top layers for the plate three. In this way it has been possible find the six data points. The fitting of the data points was of course made with the aim of detecting the plate curvatures. The plot shows that the two curvatures are opposite but of similar size, one curvature is positive, the other one is negative. This strongly suggests that through means of what is essentially a thermal shock or quench which the equations at the beginning of this chapter imply are a viscoelastic strain minimization, it is not possible to avoid linear residual strain, but it is possible to alter the *curvature* of the plates significantly. That in turn is suggestive of the fact that if the material state changes are quasi static, then there must exist a set of continuous thermodynamic temperature profiles that join them: naturally, one cannot expect to minimize linear strain, but it is feasible to minimize curvatures. Mathematically, it

must therefore be possible to conjecture a temperature profile, that is *not* a solution of the Weitsmann equations that *will produce an average zero curvature plate*. If such a temperature profile can be found (see figures below) then it would be a step that progresses to eliminating the *springback* effect as is so very sought after by industrial clients. Unfortunately, what successful theory would provide such a result is far from clear at this time. However the experimental results do provide some clues as to where to look: a mean field theory involving curvature through all lamina sections using the Weitsmann theory would be a place to start. Specifically the mean field curvature vanishes and the resulting quantites diseminate the temperature profile through calculus. Thus the experimental steps sight the next horizon to make physical the solution to the Weitsmann et al class of theories.

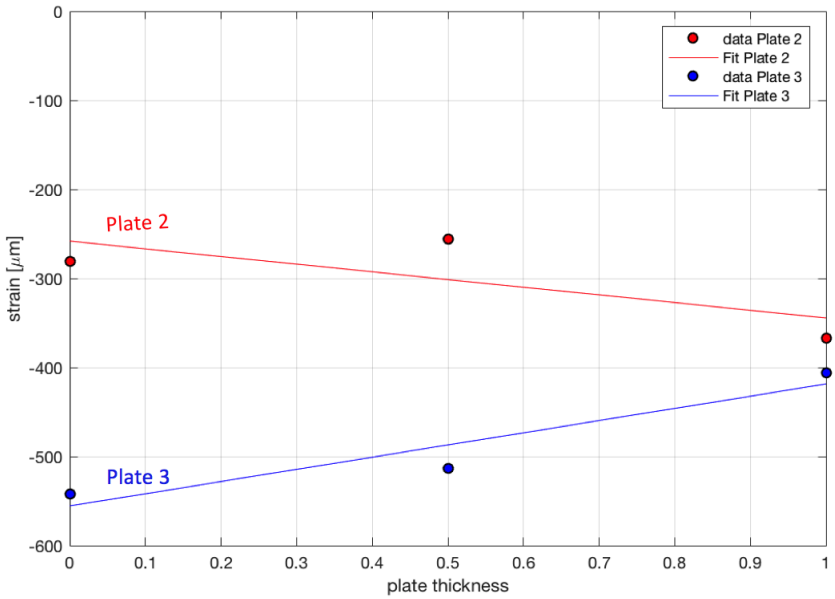

Fig. 4.14 Mean values strain (top, middle and bottom layers) in Second and Third plate

4.3.2 Slow rate cooldown reduction of curvature

As anticipated in the introduction to the chapter the control and reduction of processing-induced residual stresses has been investigated by modifying processing conditions for a graphite/BMI composite material by White and Hahn. The effects of dwell temperature, dwell time, cool-down rate, cool-down pressure, and postcure on residual stresses were investigates. Experimental results have shown that residual strain can be reduced. To reduce the processing-induced residual stresses in composites, modifications of the MRC cycle were investigated both experimentally and analytically. The viscoelastic nature of polymer

composite systems can be used during and after processing to relax residual stresses. The viscoelastic relaxation of BMI was investigated by monitoring changes in the dimensionless curvature when the cool-down rate was changed from 5.6°C/mm to 0.56°C/mm. *Slower* cooldown rates can be used to enhance the strain relaxation effects during cool down and results of experiments indicated a reduction in curvature, [85]. Again this is in interesting contrast to recent theoretical developments in the field.

4.4 Influence of tool/part interaction

The mismatch of coefficient of thermal expansion (CTE) between tool and part is one of the known causes of residual stress during cure of composites. As a consequence, geometrical distortion of the part will be induced. Process induced stresses can develop during VARTM where thermal and mechanical driven effects play a role. The main driving factor behind stress development are the differential strains between the mould and part due to differences in material thermal expansion behaviour and shrinkage. The difference in tool/part expansion can result in shear interaction along the contact interface. This is known to induce residual stresses in the part if a stiff mould tool is used, which can lead to warpage after demoulding. While these stresses are partly avoided in the manufacture of large composite structures by use of less stiff composite moulds, geometry, thickness and fibre volume fraction, can vary within the part, making stress development during processing inevitable.

4.5 Conclusions

The quality of composite components is largely affected by the cure cycle that must be designed and optimized: the common problem in the cure cycle design of a thermoset composite material manufacturing is how to set-up the time-temperature-pressure profile in such a way that certain criteria are fulfilled and the result is optimal.[74] This is exactly what is suggested by the results for plate 3. Indeed one way to reduce the residual stress is to act on the cooling rate and it should be considered as an evolution of the reduction of residual strain, instead of removing the linear residual strains which it has to be said can be compensated for through raw material volume considerations. Indeed as has been shown by previous studies, and also from the present results, *it is not possible to zero the linear CTE induced strains*. Looking at the Figure 4.14 it is clear that opposite curvatures have been obtained by making a composite with the same material and the same dimensions. The objective that could be set is to make the curvature zero, the aim is have little curvature strain variation within the thickness of the composite. This does not mean that there are no residual

strain in the composite but there are constant strains along the thickness so that the curvature is zero, which is progress towards solving the industrial problems with springback effects especially in thin composite plates. A possible configuration of a zero curvature plate is shown in figure5.1 and the cooldown phase associated with possible zero curvature is shown in figure 5.2. The strain Temperature profile could be the profile shown in figure 5.3 where the new plate profile is the green one.

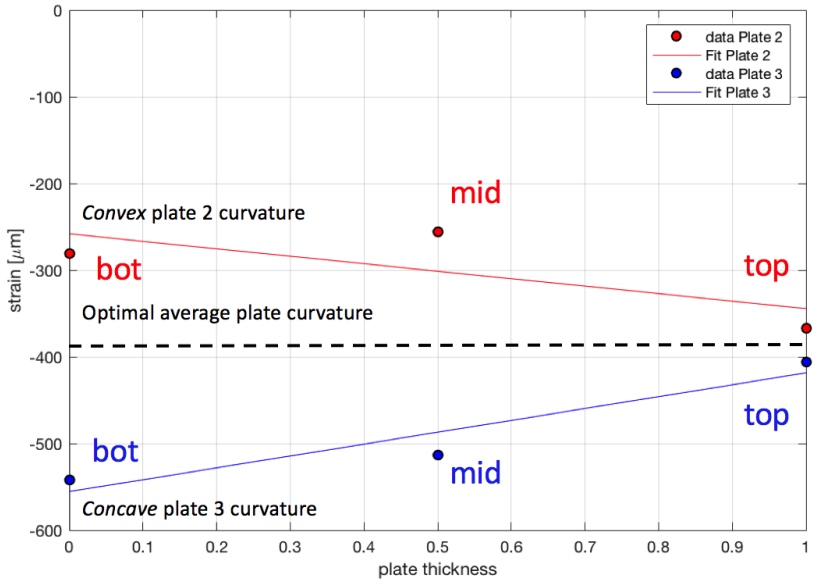

Fig. 4.15 Mean values strain (top, middle and bottom layers) in Second and Third plate compare with an ideal new plate

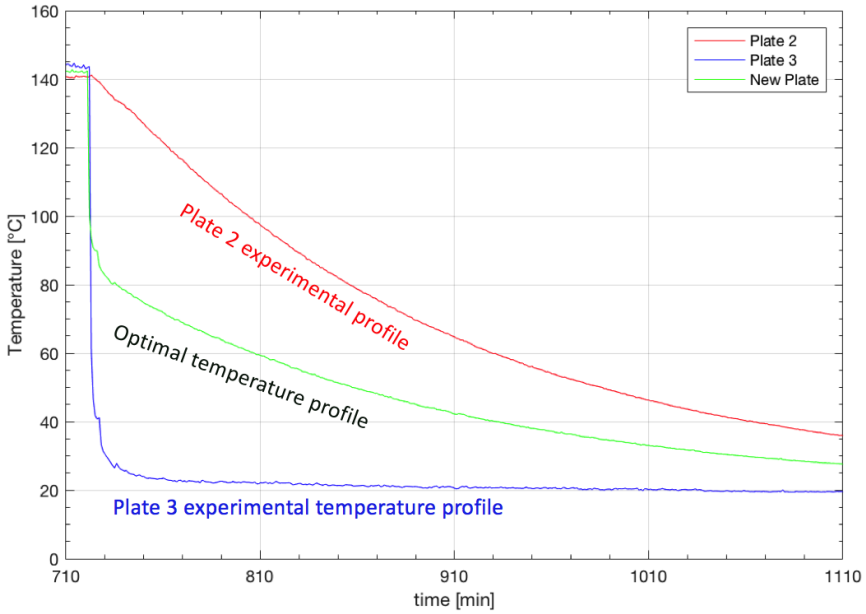

Fig. 4.16 The cooldown phase compare between the second and third plate and an ideal New plate laminate

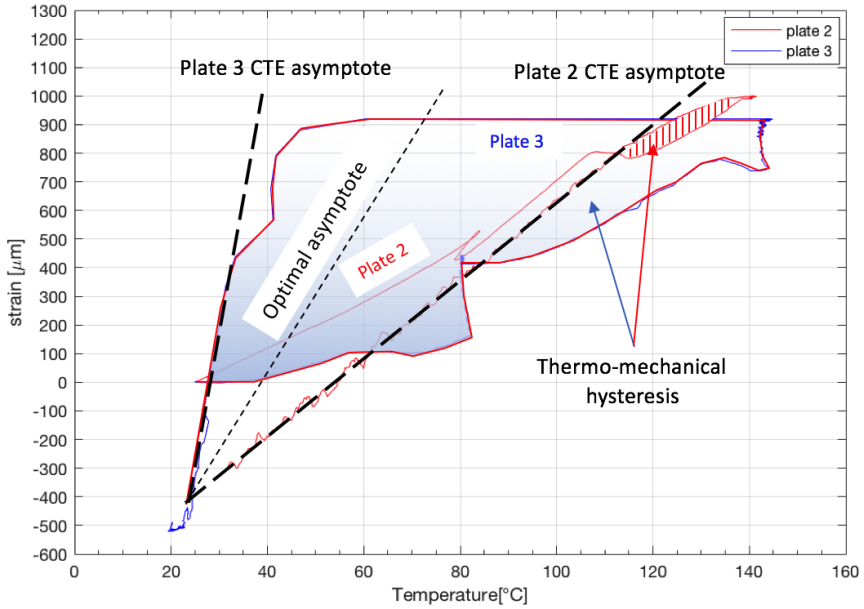

Fig. 4.17 The cooldown phase compare between the second and third plate and an ideal New plate laminate

Chapter 5

Conclusions and Future Work

5.1 Conclusions

The use of distributed embedded optical fibre sensing during VARIM panel manufacturing adds an important dimension to the measurement of the internal strains for carbon fibre composite panels. The ability to measure the strain distribution as opposed to strain at a single point provides statistically relevant detail as to the real time performance of high technology materials like carbon fibre weave composites. We have in this article used a single aspect (see figure 3.20) of the information provided by a 2 m long distributed sensor embedded into a composite panel to lead onto a possible hypothesis of the early strain behaviour inside curing panels. Extending that hypothesis to a more general theory of thermo-mechanical substrate curing interactions has provided an explanation of the disparity between the standard viscoelastic solid model CLT and the strain data trends we measured during manufacturing processes below the glass transition temperature:

$$\mathbf{CTE}_{\text{liquid}} = \mathbf{CTE}_{\text{solid}}\sqrt{\alpha}$$

where α is the cure parameter. There do remain significant unanswered questions however, which will require more work in this area. One of the most unsatisfactory aspects of the article is the natural question of enthalpy changes in a free standing resin as compared to one carrying substrate. This was touched upon in equation 3.56, which is derived for a free standing resin in DSC type experiments, could in fact have missing terms when a substrate is added. Another area of weakness is that the CTE value calculations rely upon a balanced symmetric Ishikawa bridge unit cell [42]. Better models are infact available [24] but it was

felt that Ishikawa is quicker and easier to implement as well as being more intuitive. Perhaps the gravest lack of detail was in the contribution of the mold. The experimental data for mold interaction was simply not collected and that has undoubtedly taken away some insight into the process. Lastly, one might ask if the result is of general validity or specific to just this one case - as always, further experimentation must decide.

Positively however, the agreement of the CTE equation[1] with experimental data has been encouraging, particularly from the point of view of being an example for what distributed optical measurement techniques can potentially achieve in future. The congruence of data and theory in this paper supports the following conclusions:

(i) The embedded optical fibre measures true strains at all times.

(ii) The close lying high density carbon fibres of the 5HS substrate glued together early on during cure.

(iii) These facts support and imply the freezing of the post infusion stress states of both the carbon fibre fabric and the the optical fibre, generating the homogeneous strain shifts seen in figure 3.20.

(iv) The 5HS substrate strain is unit cell surface area dependent (thin laminate) and increases with α.

(v) The mechanical work performed by the expanding resin on the 5HS substrate increases as α

(vi) The mechanical thermal expansion strain of the panel composite below the glass transition temperature increases as $\sqrt{\alpha}$

(vii) For pure epoxy resin the thermal expansion strain of the resin increases as α.

(viii) This fact implies that the VARIM manufacturing process strongly modifies the expansion properties of the resin below the glass transition temperature.

(ix) The thermal expansion strain flow of the composite panel is not viscoelastic but Newtonian.

The usefulness of this study links to the present day fabrication challenges through greater use of automation, out-of-autoclave tooling, ceramic matrix composites and processing for structures - plus more integration of natural fibers, bio-resins, and other “green” materials and

[1] Now accepted for publication by SAGE in The Journal of Composite Materials

processes – are among the main trends projected to dominate the composites manufacturing landscape in the future. Other emerging trends coming in the next three to five years include steady growth in aerospace and engine manufacturing, particularly with more advanced composites going into aircraft primary structures and next-generation engine and duct and cowl designs.

In the automotive, aircraft engine, wind, and aerospace industries, lighter weight parts result in more fuel efficient, lower carbon footprint products. Industries that are set to benefit from more efficient manufacturing processes include:

- Aerospace;
- Automotive;
- Defense;
- Recreational and sporting goods;
- Wind and alternative energy.

Composites manufacturing is the production of parts or components made of materials consisting of at least two primary constituents. Typical composite materials consist of fiber, carbon, glass, or ceramic material, and a resin. There are many ways to manufacture composite parts across several major industries. In manufacturing processes, like Resin Transfer Molding (RTM) the fiber and resin are combined while enclosed in a mold. Successful applications of parts consisting of composite materials often contain one or more of the following traits:

- Lighter in weight: Designers have the ability to design parts where the direction of the fiber corresponds to the loads seen by the part, therefore allowing more fiber to match orientations of high loads, and less fiber in directions that see lower loads;
- Higher strength: This is in comparison to the same parts made of traditional materials like steel, titanium, aluminum, or plastic; Unitized part designs: These models combine several parts into a single component. This unitized part design reduces overall part count, thereby reducing assembly costs;
- Longer fatigue life: This is in contrast to parts not made of composite materials;
- Higher heat tolerance: This is especially true in ceramic matrix composites, which allows higher operating engine temperatures, for improved fuel efficiency in aircraft engines;

- Overall, costs are lower than rival products made of traditional materials. Typically, some of the above advantages are leveraged into a superior product at a competitive cost.

One of the major challenges for composite manufacturing is the cost of the material is often higher than traditional materials, like aluminum and plastic. Despite the increased use of composite materials, many parts are still manually made, and these obstacles, while somewhat formidable, have done little to derail or dampen composite manufacturing's growth in industry. What is required are new publishable and applicable results to meet those challenges for composites to be better manufactured and be more widely distributed.

For about thirty years the precise effect of the liquid state resin upon optical fiber or other methods of measurement has been subject to speculation for example, and in this study we attempt to provide a simple model and experimental evidence to come the conclusion that in fabrication processes for composite materials it is highly likely that the optical fiber always measure the true strain. Embedded optical fibers can be used when a component is subjected to mechanical loading, a concept that can be exploited in the design of composite structures and components when in service, assisting with real time structural health monitoring.

The present study therefore contributes to a better understanding of the physics of resin rheology by proposing a simple physical theory that could lead to improved composites design. A better model of resin rheology leads one directly to a precise understanding of the gellation process during the second dwell of the curing cycle and the glass transition temperature. Subsequently this may have a significant impact upon the way the cooling cycle operates on the stresses in the relaxed structure. Furthermore, and perhaps more significantly, we observe and explain that the presence of carbon fiber structures within a resin matrix strongly modify the rheology and hence the residual strain behaviour. In particular we precisely identify how this new rheology operates in terms of a physical mechanical mechanism. The originality of the substrate strain model proposed lies in the fluid-chemical action of the curing resin when it is considered as a distributed adhesive. This simple fact leads directly to a thermodynamic non extensive modification of the strain response of the composite material which is encapsulated in the pseudo-liquid state equation for connecting the solid state and liquid-state composite coefficients of thermal expansion.

5.2 Future Work

The quality of composite components is largely affected by the cure cycle that must be designed and optimized: the common problem in the cure cycle design of a thermoset composite material manufacturing is how to set-up the time-temperature-pressure profile

in such a way that certain criteria are fulfilled and the result is optimal.[74] This is exactly what is suggested by the results for plate 3. Indeed one way to reduce the residual stress is to act on the cooling rate and it should be considered as an evolution of the reduction of residual strain, instead of removing the linear residual strains which it has to be said can be compensated for through raw material volume considerations. Indeed as has been shown by previous studies, and also from the present results, *it is not possible to zero the linear CTE induced strains*. Looking at the Figure 5.1 it is clear that opposite curvatures have been obtained by making a composite with the same material and the same dimensions. The objective that could be set is to make the curvature zero, the aim is have little curvature strain variation within the thickness of the composite. This does not mean that there are no residual strain in the composite but there are constant strains along the thickness so that the curvature is zero, which is progress towards solving the industrial problems with springback effects especially in thin composite plates. A possible configuration of a zero curvature plate is shown in figure5.1 and the cooldown phase associated with possible zero curvature is shown in figure 5.2. The strain Temperature profile could be the profile shown in figure 5.3 where the new plate profile is the green one.

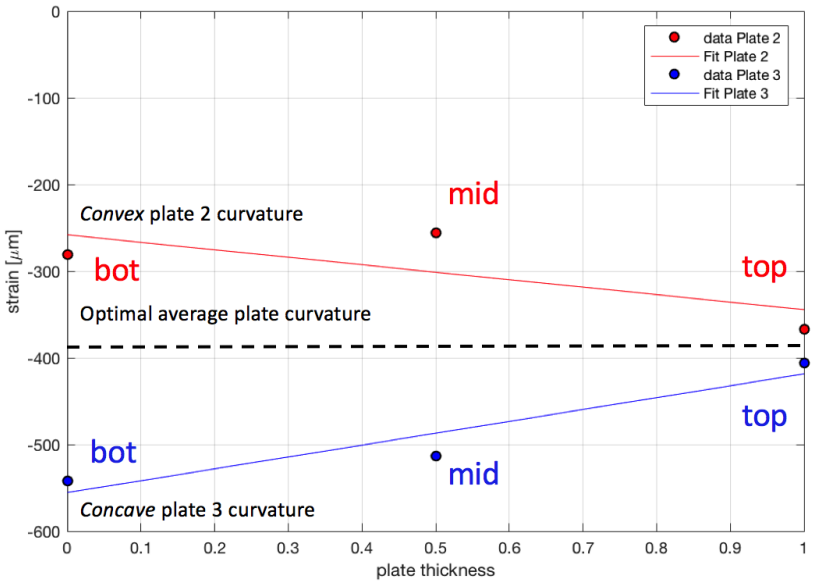

Fig. 5.1 Mean values strain (top, middle and bottom layers) in Second and Third plate compare with an ideal new plate

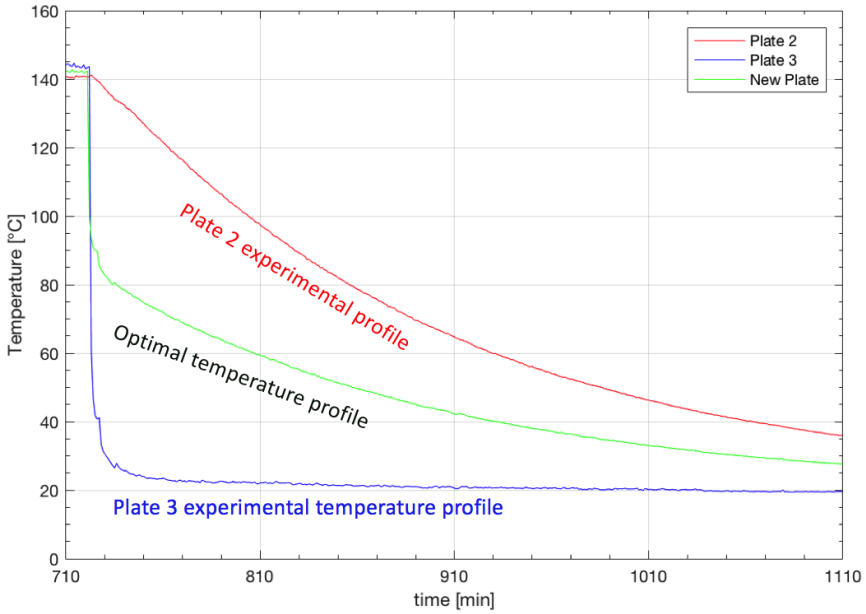

Fig. 5.2 The cooldown phase compare between the second and third plate and an ideal New plate laminate

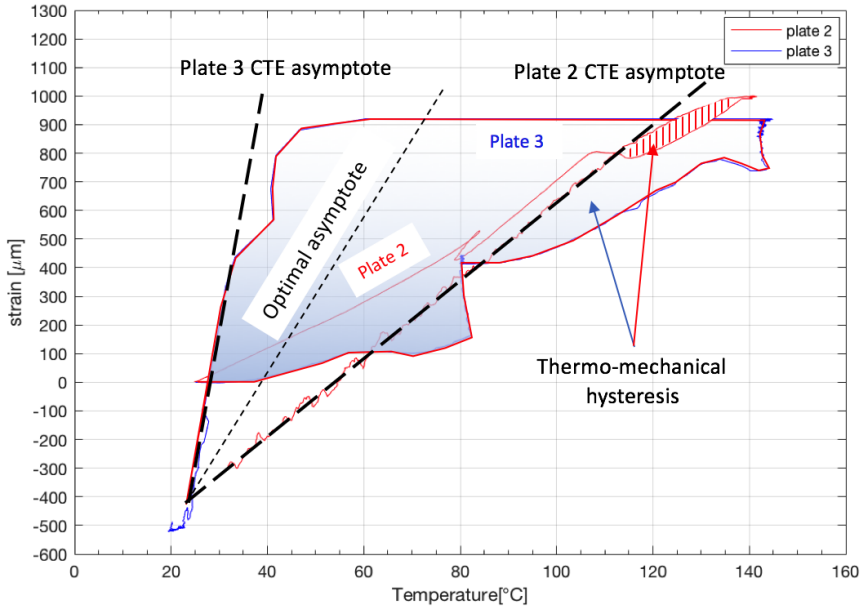

Fig. 5.3 The cooldown phase compare between the second and third plate and an ideal New plate laminate

References

[1] A, K. L., K, C., and H, P. (2012). Thermo-mechanical properties of 5-harness satin fabric composites. *Journal of Composite Materials*, 46(25):3121–3136.

[2] Abusrea, M. R. and Arakawa, K. (2016). Improvement of an adhesive joint constructed from carbon fiber-reinforced plastic and dry carbon fiber laminates. *Composites Part B: Engineering*, 97(Supplement C):368 – 373.

[3] Aris, R. (1963). Vectors, Tensors and the Basic Equations of Fluid Mechanics. 5:165–165.

[4] Aronhime, M. T. and Gillham, J. K. (1986). Time-temperature-transformation (ttt) cure diagram of thermosetting polymeric systems. pages 83–113.

[5] Baker, A., Dutton, S., Kelly, D., and Kelly, D. (2004). *Composite materials for aircraft structures*. AIAA education series. American Institute of Aeronautics and Astronautics.

[6] Balasubramanian, M. (2013). *Composite Materials and Processing*. CRC Press.

[7] Berthelot, J. and Cole, J. (2012). *Composite Materials: Mechanical Behavior and Structural Analysis*. Mechanical Engineering Series. Springer New York.

[8] Bianchini, G. and Oldring, P. (1997). *Waterborne & Solvent Based Epoxies and Their End User Applications*. Waterborne & solvent based surface coatings & their applications. John Wiley.

[9] Bos, J., Klein, J., Froggatt, M., Sanborn, E., and Gifford, D. (2013). Fiber optic strain, temperature and shape sensing via OFDR for ground, air and space applications. *Proc. SPIE - Int. Soc. Opt. Eng.*, 8876:1–15.

[10] Brown, M. and Gallagher, P. (2011). *Handbook of Thermal Analysis and Calorimetry: Recent Advances, Techniques and Applications*. Handbook of Thermal Analysis and Calorimetry. Elsevier Science.

[11] Carothers, W. (1938). Trans. Faraday Soc. 34:49–57.

[12] Cha, K. (2013). *Composite Materials: Science and Engineering*. MATERIALS RESEARCH AND ENGINEERING. Springer New York.

[13] Chen, L., Cao, J., and J. Weitsman, Y. (2006). Optimal cool-down in linear and nonlinear thermoviscoelasticity and the effects of initial stress. 128.

[14] Chou, T. (2005). *Microstructural Design of Fiber Composites*. Cambridge University Press.

[15] Crasto, A. S., Kim, R. Y., and Russell, J. D. (2002a). In situ monitoring of residual strain development during composite cure. *Polymer Composites*, 23(3):454–463.

[16] Crasto, A. S., Kim, R. Y., and Russell, J. D. (2002b). In situ monitoring of residual strain development during composite cure. *Polym. Compos.*, 23(3):454–463.

[17] de Oliveira, R., Lavanchy, S., Chatton, R., Costantini, D., Michaud, V., Salathé, R., and Månson, J. A. E. (2008). Experimental investigation of the effect of the mould thermal expansion on the development of internal stresses during carbon fibre composite processing. *Compos. Part A Appl. Sci. Manuf.*, 39(7):1083–1090.

[18] Dhotkar, B., Chhabra, R., and Eswaran, V. (2000). Flow of Non-Newtonian Polymeric Solutions Through Fibrous Media. *J. Appl. Polym. Sci.*, 76(7):1171–1185.

[19] Ellis, B. (1993). *Chemistry and technology of epoxy resins*. Blackie Academic Professional.

[20] et al., M. W. N. (2014). Life cycle strain monitoring in glass fibre reinforced polymer laminates using embedded fibre bragg grating sensors from manufacturing to failure. *Journal of Composite Materials*, 48(3):365–381.

[21] Flory, P. (1953). *Principles of Polymer Chemistry*. Baker lectures 1948. Cornell University Press.

[22] Gabbott, P. (2008). *Principles and Applications of Thermal Analysis*. Wiley.

[23] Gaisford, S., Kett, V., and Haines, P., editors (2016). *Principles of Thermal Analysis and Calorimetry*. The Royal Society of Chemistry.

[24] Ganesh, V. K. and Naik, N. K. (1994). Thermal expansion coefficients of plain-weave fabric laminates. 51:387–408.

[25] Gillham, J. K. (1986). Formation and properties of thermosetting and high tg polymeric materials. *Polymer Engineering Science*, 26(20):1429–1433.

[26] Gopal, A. K., Adali, S., and Verijenko, V. E. (2000). Optimal temperature profiles for minimum residual stress in the cure process of polymer composites. *Compos. Struct.*, 48(1):99–106.

[27] Gorbacheva, V. and Mikhailov, N. (1965). Differential thermal analysis of polymers. *Polymer Science U.S.S.R.*, 7(1):28 – 32.

[28] Goren, A. and Atas, C. (2008a). Manufacturing of polymer matrix composites using vacuum assisted resin infusion molding. *Archives of Materials Science and Engineering*, Vol. 34, nr 2:117–120.

[29] Goren, A. and Atas, C. (2008b). Manufacturing of polymer matrix composites using vacuum assisted resin infusion molding. *Arch. Mater. Sci. Eng.*, 34(2):117–120.

[30] Govignon, Q., Bickerton, S., and Kelly, P. (2010). Simulation of the reinforcement compaction and resin flow during the complete resin infusion process. *Composites Part A: Applied Science and Manufacturing*, 41(1):45 – 57. Special Issue: Flow Processes in Composite Materials.

[31] Guemes, A., Fernandez-Lopez, A., and Soller, B. (2010). Optical fiber distributed sensing - physical principles and applications. *Struct. Heal. Monit.*, 9(3):233–245.

[32] Guo, Q. (2012). *Thermosets: Structure, Properties and Applications*. Woodhead Publishing in Materials. Elsevier Science.

[33] Halley, P. J. and Mackay, M. E. (1996). Chemorheology of Thermosets - An Overview. *Polym. Eng. Sci.*, 36(5):593 – 609.

[34] Happel, J. and Brenner, H. (1983). *Low Reynolds Number Hydrodynamics*, volume 21.

[35] Her, S.-C. and Huang, C.-Y. (2013). Thermal strain analysis of optic fiber sensors. *Sensors*, 13(2):1846–1855.

[36] Hill, R. R., Muzumdar, S. V., and Lee, L. J. (1995). Analysis of volumetric changes of unsaturated polyester resins during curing. *Polym. Eng. Sci.*, 35(10):852–859.

[37] Hosur, M., Vaidya, U., Jones, S., Eduljee, R., and Gillespie, J. (1999). Activity-based cost modeling of liquid molding process techniques for thick-section composites. In *American Society for Composites, Technical Conference, 14 th, Fairborn, OH*, pages 968–977.

[Huang et al.] Huang, C., Bao, X., Zeng, X., Arcand, A., and Lee-sullivan, P. Simultaneous Temperature and Strain Monitoring of Composite Cure using a Brillouin-Scattering-Based Distributed Fiber Optic Sensor. 4328(2001):70–78.

[39] Hull, D. (1981). *An Introduction to Composite Materials*. Cambridge Solid State Science Series. Cambridge University Press.

[40] Hyer, M. and White, S. (1998a). *Stress Analysis of Fiber-reinforced Composite Materials*. Mechanical engineering series. WCB McGraw-Hill.

[41] Hyer, M. and White, S. (1998b). *Stress Analysis of Fiber-reinforced Composite Materials*. Mechanical engineering series. WCB McGraw-Hill.

[42] Ishikawa, T. and Chou, T. (1982a). Stiffness and strength behaviour of woven fabric composites. *J. Mater. Sci.*, 17(11):3211–3220.

[43] Ishikawa, T. and Chou, T. W. (1982b). Stiffness and strength behaviour of woven fabric composites. *Journal of Materials Science*, 17(11):3211–3220.

[44] Jain, P., Choudhary, V., and Varma, I. (2003). Effect of structure on thermal behaviour of epoxy resins. *European Polymer Journal*, 39(1):181–187.

[45] Kamal, K. (2016). *Composite Materials: Processing, Applications, Characterizations*. Springer Berlin Heidelberg.

[46] Kamal, M. R., Sourour, S., and Ryan, M. (1973). Integrated thermorheological analysis of the cure of thermosets. *SPE Tech. Pap.*, 19:187–191.

[47] Kang, H.-K., Kang, D.-H., Bang, H.-J., Hong, C.-S., and Kim, C.-G. (2002a). Cure monitoring of composite laminates using fiber optic sensors. *Smart Materials and Structures*, 11(2):279–287.

[48] Kang, H.-K., Kang, D.-H., Bang, H.-J., Hong, C.-S., and Kim, C.-G. (2002b). Cure monitoring of composite laminates using fiber optic sensors. *Smart Mater. Struct.*, 11(2):279–287.

[49] Kang, H.-K., Kang, D.-H., Hong, C.-S., and Kim, C.-G. (2003). Simultaneous monitoring of strain and temperature during and after cure of unsymmetric composite laminate using fibre-optic sensors. *Smart Mater. Struct.*, 12(1):29–35.

[50] Karbhari, V. (2013a). *Non-Destructive Evaluation (NDE) of Polymer Matrix Composites*. Woodhead Publishing Series in Composites Science and Engineering. Elsevier Science.

[51] Karbhari, V. (2013b). *Non-Destructive Evalutation(NDE) of Polymer Matrix Composites*. Woodhead Publish Series in Composite Science and Engineering. Elsevier Science.

[52] Kaw, A. (2005). *Mechanics of Composite Materials, Second Edition*. Mechanical and Aerospace Engineering Series. CRC Press.

[53] Kim, K. and Hahn, H. (1989). Residual stress development during processing of graphite/epoxy composites. 36:121–132.

[54] Lawrence, C. M., Nelson, D. V., Bennett, T. E., and Spingarn, J. R. (1998). An embedded fiber optic sensor method for determining residual stresses in fiber-reinforced composite materials. *Journal of intelligent material systems and structures*, 9(10):788–799.

[55] Lee, C. L. and Wei, K. H. (2000). Curing kinetics and viscosity change of a two-part epoxy resin during mold filling in resin-transfer molding process. *J. Appl. Polym. Sci.*, 77(10):2139–2148.

[56] Leng, J. and Asundi, A. (2003). Structural health monitoring of smart composite materials by using EFPI and FBG sensors. *Sensors Actuators, A Phys.*, 103(3):330–340.

[57] Lu, C., Cui, Z., Yang, B., Su, X., Huo, C., and Shen, J. (2002). Polymerization mechanisms and curing kinetics of novel polymercaptan curing system containing epoxy/nitrogen. *Journal of Applied Polymer Science*, 86(3):589–595.

[58] Mahnken, R. and Dammann, C. (2016). Effective meso and macro properties for fibre-reinforced-polymer curing coupled to visco-elasticity. pages 2398–2416.

[59] Mallick, P. (1993). *Fiber-Reinforced Composites: Materials, Manufacturing, and Design, Second Edition*. Dekker Mechanical Engineering. Taylor & Francis.

[60] Montserrat, S. and Martín, J. G. (2002). Non-isothermal curing of a diepoxide-cycloaliphatic diamine system by temperature modulated differential scanning calorimetry. *Thermochim. Acta*, 388(1-2):343–354.

[61] Murukeshan, V. M., Chan, P. Y., Ong, L. S., and Seah, L. K. (2000). Cure monitoring of smart composites using Fiber Bragg Grating based embedded sensors. *Sensors Actuators, A Phys.*, 79(2):153–161.

[62] Naik, N. and Ganesh, V. (1992). Prediction of on-axes elastic properties of plain weave fabric composites. 45:135–152.

[63] Olivier, P. and Cottu, J. (1998). Optimisation of the co-curing of two different composites with the aim of minimising residual curing stress levels. *Composites Science and Technology*, 58(5):645 – 651.

[64] Pedemonte, E. (2011). Fondamenti di struttura, propriet tecnologia dei polimeri.

[65] R, A. and R.S, D. V. (1998). *Thermomechanical properties of woven fabric composites*. International Conference on Fibre Reinforced Composites FRC'98.

[66] Rajan, G. and Prusty, G. (2016). *Structural Health Monitoring of Composite Structures Using Fibre Optic Methods*.

[Robinson] Robinson, A.T.C.; Marks, R. *TWoven cloth construction*.

[68] Rohr, D. F. and Klein, M. T. (1990). Modeling diffusion and reaction in crosslinking epoxy-amine cure kinetics: a dynamic percolation approach. *Ind. Eng. Chem. Res.*, 29(7):1210–1218.

[69] Samira, G. (2016). A review of non-destructive testing methods of composite materials.

[70] Sánchez, D. M., Gresil, M., and Soutis, C. (2015). Distributed internal strain measurement during composite manufacturing using optical fibre sensors. *Compos. Sci. Technol.*, 120:49–57.

[71] Sawyer, L. (2012). *Polymer Microscopy*. Springer Netherlands.

[72] Sepe, M. and Limited, R. T. (1997). *Thermal Analysis of Polymers*. RAPRA Technology Limited Shawbury: Rapra review reports. Rapra Technology Limited.

[73] Skourlis, P. (1971). An Experimental Investigation of the Effect of Prepolymer Molecular Weight and Stoichiometry on Thermal and Tensile Properties of Epoxy Resins.

[74] Sorrentino, L., Polini, W., and Bellini, C. (2014). To design the cure process of thick composite parts: experimental and numerical results. *Advanced Composite Materials*, 23(3):225–238.

[75] Takagaki, Hisada, S., Minakuchi, S., and Takeda, N. (2017). Process improvement for out-of-autoclave prepreg curing supported by in-situ strain monitoring. *Journal of Composite Materials*, 51(9):1225–1237.

[76] Turi, E. (2012). *Thermal Characterization of Polymeric Materials*. Elsevier Science.

[77] Varma, I., Gupta, V., and K, S. (2000). *Thermosetting Resin Properties*, volume 2.

[78] Wang, R.-M., Zheng, S.-R., and Zheng, Y. G. (2011). *Polymer matrix composites and technology*. Elsevier.

[79] Wang, T.-M., Daniel, I., and Gotro, J. (1992). Thermoviscoelastic analysis of residual stresses and warpage in composite laminates. *Journal of Composite Materials*, 26(6):883–899.

[80] Waris, M., Liotier, P.-J., and Drapier, S. (2013). Effect of the mold on the residual strain field monitored with optical fibers sensors in resin transfer molding processes. *J. Compos. Mater.*, 48(21):2589–2601.

[81] Weitsman, Y. (1979). Residual Thermal Stresses Due to Cool-Down of Epoxy-Resin Composites. *J. Appl. Mech.*, 46(3):563–567.

[82] White, S. and Hahn, H. (1992a). Process modeling of composite materials: Residual stress development during cure. part i. model formulation. *Journal of Composite Materials*, 26(16):2402–2422.

[83] White, S. and Hahn, H. (1992b). Process Modeling of Composite Materials: Residual Stress Development during Cure. Part II. Experimental Validation. *J. Compos. Mater.*, 26(16):2423–2453.

[84] White, S. and Hahn, H. (1993a). Cure cycle optimization for the reduction of processing-induced residual stresses in composite materials. *Journal of Composite Materials*, 27(14):1352–1378.

[85] White, S. and Hahn, H. (1993b). Cure cycle optimization for the reduction of processing-induced residual stresses in composite materials. *Journal of Composite Materials*, 27(14):1352–1378.

[86] White, S. R. and Hahn, H. T. (1990). Mechanical property and residual stress development during cure of a graphite/bmi composite. *Polymer Engineering Science*, 30(22):1465–1473.

[87] White, S. R. and Hahn, H. T. (1992c). Process Modeling of Composite Materials: Residual Stress Development during Cure. Part I. Model Formulation. *J. Compos. Mater.*, 26(16):2402–2422.

[88] Wisnom, M., Gigliotti, M., Ersoy, N., Campbell, M., and Potter, K. (2006). Mechanisms generating residual stresses and distortion during manufacture of polymer–matrix composite structures. *Composites Part A: Applied Science and Manufacturing*, 37(4):522 – 529. Internal Stresses in Polymer Composites.

[89] Yoo, S. H., Han, M. G., Hong, J. H., and Chang, S. H. (2015). Simulation of curing process of carbon/epoxy composite during autoclave degassing molding by considering phase changes of epoxy resin. *Compos. Part B Eng.*, 77:257–267.

[90] Yoon, S.-J., Arakawa, K., Han, S.-W., Chen, D., and Choi, N.-S. (2017). Effect of compaction treatment on laminated cfrp composites fabricated by vacuum-assisted resin-transfer molding. *Polymer Composites*, 38(2):217–226.

[91] Young, W.-b. (2013). A Two-layer Model for the Simulation of the VARTM Process with Resin Distribution Layer. pages 1305–1319.